UNIVERSITEIT VAN PRETORIA
UNIVERSITY OF PRETORIA
YUNIBESITHI YA PRETORIA

Department of Mechanical and Aeronautical Engineering

AUTHOR:

Jacobus Christiaan Smit

11013258

Supervisor: Prof PS Heyns

Development of a compensated capacitance sensor for solid mass flow measurement in pneumatic conveying systems

2017/02/02

Development of a compensated capacitance sensor for solid mass flow measurement in pneumatic conveying systems

Author: JC Smit

Supervisor: Professor P.S. Heyns

Degree: Masters in Mechanical Engineering

Summary

This dissertation describes research and experimental work done to improve the accuracy and applicability of capacitive sensors which are used to evaluate the mass flow rate of solid material within pneumatic conveying environments in power plant engineering applications. The research is focused on creating a measurement methodology on which solid mass flow rate can be evaluated without being dependent on variable flow regimes. The proposed research investigates the process of identifying four different types of flow regimes using a decision tree that utilises support vector machines and cut off values. During the study an investigation was also made into what electrode setup would provide proficient information regarding the flow distribution and orientation. Compensation according to the identified regime is then proposed by means of using a nonlinear fraction curves determined through calibration experiments.

Acknowledgements

I would like to thank the following persons for their contributions and support throughout the project:

1. Prof P.S. Heyns as academic supervisor (University of Pretoria)
2. Mr H. Fourie as Industrial Mentor (Eskom)
3. Mr G. Breytenbach as lab assistant (University of Pretoria)
4. Mr H Booysen as lab assistant (University of Pretoria)
5. Mr J Brand for the Auger feeder (Shosalowe)
6. Texas Instruments for the supply of capacitance modules

I also greatly acknowledge the financial support provided by Eskom Power Plant Engineering Institute (EPPEI) in the execution of this project

Table of Contents

Nomenclature

Symbol	Description
$\dot{m}$	Mass flow rate $\left(\frac{kg}{s}\right)$
ρ	Bulk density $\left(\frac{kg}{m^3}\right)$
A	Area (m^2)
V	Velocity $\left(\frac{m}{s}\right)$
$\emptyset$	Volume fraction
R_1	Internal pipe radius (m)
R_2	External pipe radius (m)
R_3	Shield radius (m)
C	Capacitance (F)
ε_0	Permittivity of free space
ε_s	Effective permittivity of sample
A_p	Area of plate (m^2)
d	Distance between electrodes (m)
α or $\emptyset$	Volume fraction
α_1	Volume fraction solids
α_2	Volume fraction air
L	Length between electrodes (m)
τ	Transit time (s)
R_{xy}	Cross correlation function
f	Sampling frequency (Hz)
f_c	Sampling frequency concentration electrodes (Hz)
f_v	Sampling frequency velocity electrodes (Hz)

Δt_i	Time increment (s)
V_{EI}	Velocity estimate due to gravity $\left(\frac{m}{s}\right)$
d_i	Distance travelled by solids (m)
m_{tot}	Total mass conveyed (kg)
ΔT	Conveyed time (s)
Cal_{chang}	Change in capacitance due to filled pipe (F)
Δc	Change in capacitance with regard to initial capacitance (F)
$Var()$	Variance of evaluated data set
$w( )$	Constants for calibration curves
E_{bin}	Energy associated frequency bin
$H_h(s)$	High pass filter
$H_l(s)$	low pass filter
$H_b(s)$	band pass filter
ω_n	Rotational frequency
f_1	Cut off frequency for low pass filter (Hz)
f_2	Cut off frequency for high pass filter (Hz)

1. Introduction

1.1 Problem statement and back ground

The dynamics of spent fuel handling within all power stations situated in South Africa are changing drastically as old technologies are replaced by new and upcoming handling techniques such as pneumatic conveying systems. The implementation of new techniques increases the overall plant efficiency and decrease running cost but also creates new uncertainties in the form of quantification of the actual handling plant's performance. Multiple implications then arise around the implementation of these new systems that influence factors like capacity planning and the limitations set by the capacity of the system and the effect it will have on the overall electricity supply. The investments in used material handling systems often accumulate to large capital expenses that could lead to significant losses if these systems are not built to correct specification.

To quantify the performance of such a pneumatic system, one is required to validate the actual mass flow rate with the system specified solid flow rate which in return will provide an indication of the build quality. Although the measurement sounds simple in concept multiple factors constrain the measurement of the conveyed material, for instance the use of load cells in storage facilities seems the like the best option at first but due to sheer size of silos and storage bunkers would be nearly impossible to implement. The alternative would be to use a measurement technique that concentrates on determining the mass flow rate through the system itself rather than measuring the accumulation of material at the collection bin.

Due to the nature of power stations the evaluation technique is subject to multiple restrictions ranging from safety of employees to limiting the influence of the measurement technique on the actual conveying system. The nature of the project then causes multiple difficulties in terms of safety applicability and flow regime sensitivity, which need to be overcome to ensure that an improved and more accurate sensor is developed. The developed sensor should then be able to evaluate not only used fuel conveying systems but also in a variation of solid conveying systems.

These conveying systems also show minimal information regarding their actual operating conditions, for instance the actual flow regime present in the system. These conditions have a significant influence on the accuracy of the chosen flow rate monitors and without any viable identification system could lead to large scale errors. To fully rectify the lack of flow rate monitors in pneumatic systems the flow monitoring sensor /system should be able not only to evaluate the flow rate but also provide additional information regarding the flow circumstances in the control volume.

Multiple methods of determining the mass flow rate of solids are found in the literature. These range from techniques that exploit the measurement changes in the flow caused by mechanisms such as coriolis and gyroscopic effects (Zheng & Liu 2011; Yan 1996), to sensors that can be used without change to the conveying system. These include ultrasonic techniques (Szebeszczyk 1994), radiometric techniques (Barratt et al. 2000) and laser techniques (Zheng et al. 2007). As part of preparation for the work a comprehensive study was done to investigate the applicability of the above stated methods to

pneumatic conveying systems within a power station environment. During this study it was concluded that the use of concave capacitive sensors would be best suited for the measurement of solid flow in power station environments (see paragraph 2 and Appendix 1 for more details)

This research therefore aims to reduce the largest limitation associated with capacitive flow measurements namely flow dependency (Williams et al. 1991). Support vector machines and energy methods are investigated as viable methods for the identification of flow regimes. This is done by means of using data from a compounded electrode setup capable of identifying changes in solid distribution due to variable orientations. Experimental calibration of flow dependent fraction curves can then be used to determine the fraction of the volume occupied by solids in order to determine the flow rate of solids passing through the measurement environment instead of assuming a linear relationship. During the study the above stated method is tested and verified as possible improvement to difficulties faced in industry today.

1.2 Scope of research

This study focuses on the development of a concave capacitive sensor capable of measuring the solid mass flow rate of pneumatically conveyed solids over a variety of flow regimes while being able to firstly identify the induced flow regime and then compensate for the flow regime using a non-linear fraction curve. The study is limited with respect to a number of aspects that can be broadly characterised as follows:

- Safety
- Capital cost
- Investigation range
- Instrumentation

The implementation and use of the proposed system should not pose any safety hazard to the operator or staff working in the vicinity of the system itself. The sensor should also not cause health hazards via the transported solids.

The experimental setup was limited to constructing a scaled pneumatic conveying system due to the sheer cost and complexity involved in building a test setup that simulates exact industrial conditions. The investigation was divided into two primary experimental setups namely:

- Auger fed experimental setup that induces a flow regime similar to systems that are representative of feeders with a periodic nature (refer to paragraph 2 for types of feeders).
- Gravity fed experimental setup with fitted nozzle to induce the 3 primary types of solid flow (Annular, rope and stratified flow regimes)

The range of investigation was limited to finish the research within the given time scale of one year. The boundaries that were set are as follow:

- The number of flow regimes investigated was limited to stratified, rope and annular for constant distribution regimes and an auger fed system for variable flow regimes.

- The solid medium was chosen to be silica sand as spilled fly ash would have caused multiple inconveniences when spilled in the laboratory.
- The effect of moisture content was neglected as little to no moisture would be found in the experimental setup as well as the spent fuel station.

The use of the evaluation modules supplied by Texas Instruments had a number of limitations that required additional attention regarding the signal processing and velocity measurements.

- The chosen electrode setup required the use of two evaluation modules that required two separate computers to run on, due to the GUI only being able to run a single evaluation module at a time. This meant that the two modules were not started exactly at the same time and required alteration of data set to show only systems where solid flow is present in the system.
- The sample rate and the associated resolution of measurements caused difficulties in terms of having data that is representative of actual flow velocity of solids resulting velocity estimations done in terms of gravity (discussed in more depth later).

1.3. Introduction to Pneumatic conveying

Pneumatic conveying systems of solids (like fly ash or pulverised coal) are viewed as an alternative technique to convey solids for long distances within a facility. This technique provides a cleaner and more effective method for convening ash produced within coal fire power stations when compared with open conveying systems. Pneumatic conveying is also preferred when compared to other closed systems like slurry pumps. The main idea of a pneumatic conveying system is to transport solid particles from a discharge hopper (that feeds the material into the system) by means of compressed or blown air from one point to the discharge hopper or storage facility via pipe system. A typical setup can be seen in figure 1.

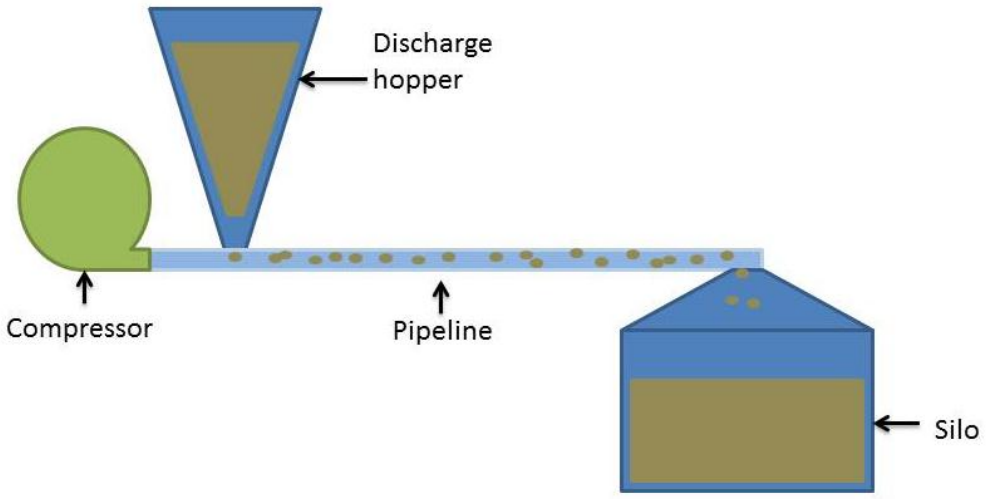

Figure 1: Basic pneumatic conveying

1.3.1. Flow patterns

According to (Konrad 1986) multiple flow patterns or regimes occur in horizontal flow pipes when carrier gas' velocity is altered. These patterns can be described as:

- Fully suspended flow: All the solids are fully airborne with no material being conveyed on the surface of the pipe. The technique of transport comprises the support of particles by means of turbulent eddies where the remainder of the particles are simply flowing from the top surface to the bottom surface of the pipe. This flow pattern occurs in conveying systems where flow is conducted at high velocities.
- Stratified flow: This flow pattern is similar to suspended flow but in the case of stratified flow the majority of particles are situated in the bottom half of the pipe. These flows also contain particles that are transported by the technique of rolling on the bottom surface of the pipe.
- Dune conveying: This technique of conveying shows three different flow regimes within the pipe. The entails a layer of gas that is almost particle free at the top section of the pipe. The second regime consists out of a few particles moving at relatively high velocities in the top section of the pipe, while the third regime comprises slow moving particles with a density close to the bulk density of the particle. This flow technique simulates the transitional phase to dense phase conveying.
- Plug or slug conveying: This represents the conveying of particles in the form of a slug that fills the pipe from the bottom to the top reaching close to the packaging density. The interval between slugs consists of a pocket of moving gas at the top and a stationary slab of particles at the bottom.
- Moving bed flow: This comprises the conveying of particles that fill the whole pipe without causing the slug or plug effect described earlier.
- Rope flow: Bulk of the solid material is concentrated at the centre of the pipe with little to no material at the circumference of the pipe. This flow regime is more likely to occur at vertical sections.
- Annular flow: Comprises the opposite of the rope flow phenomenon where all the material are concentrated around the circumference of the pipe.

These conveying flow patterns are schematically presented in figure2

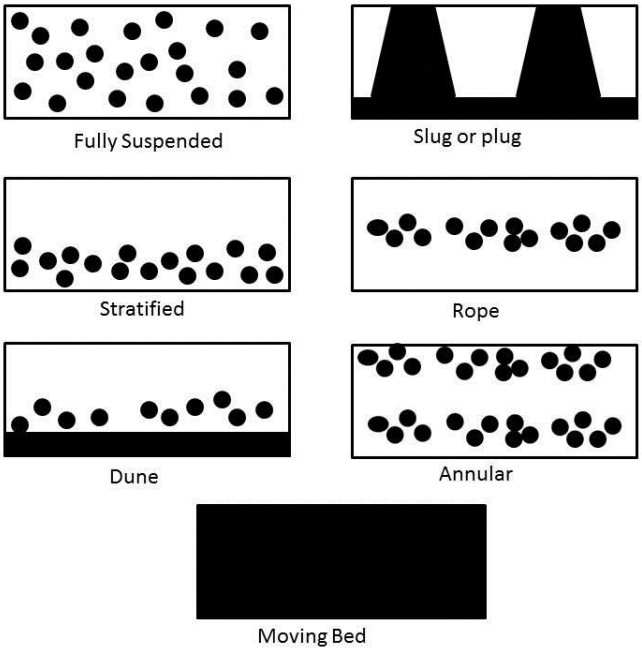

Figure 2: Pneumatic flow regimes(adapted from (Konrad 1986)**)**

1.3.2. Pneumatic feeding systems

Pneumatic systems are highly reliant on the feeding system installed to control the mass flow rate of the conveyed solids. Feeding systems can be divided into eight main types that will briefly be described below with accompanying illustrations (figures 3 to 5) (Mills 2004).

a. Rotary systems: These feeding techniques consist of a rotary valve below a material hopper (see figure 3a). The valve commonly consists of a rotor with blades that have variable shapes and sizes in order to control the amount of material fed into the pipeline. These feeding systems are renowned for high velocity flow rates, caused by the pressure difference from the blade tip clearances, and therefore can suffer from erosive effects. These techniques are used in positive and negative feeding systems but have the disadvantage of air leakage. The material fed into the conveying system with a pulsating action that can cause loss of energy along with turbulent flow.(Mills 2004)

b. Screw feeders: Screw feeding devices are similar to rotary systems (see figure 3b) but in this case the feed rate can be varied by changing the rotary speed of the feeder. These feeders are commonly used in positive pressure and vacuum systems but have the disadvantage of being prone to the abrasive effects of coarse material. The rotation of the screw delivers material into the conveying system and has the advantage that there is a linear relationship between the rotational speed and material feed rate giving the operator a technique to control the mass flow rate.

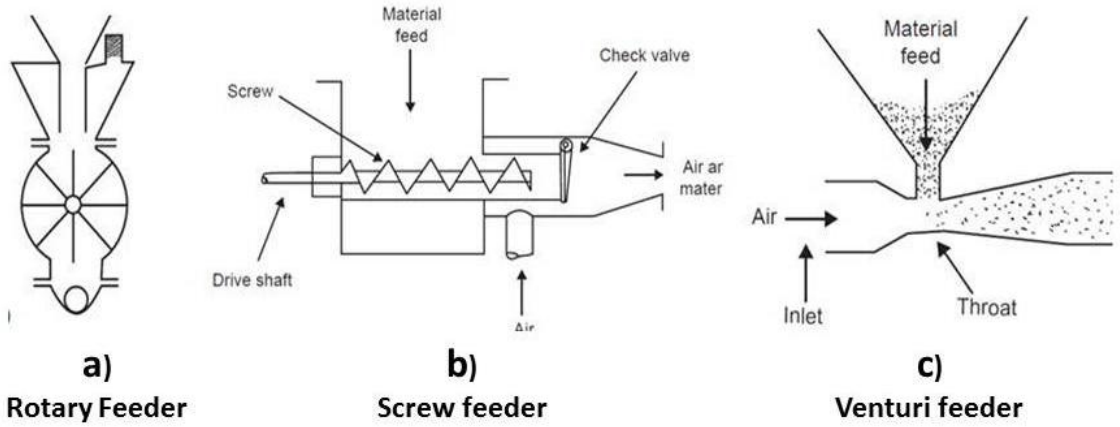

Figure 3: Feeder types (Image adapted from(Mills 2004))

c. Venturi feeders: These systems work on the principle of reduction of the pipe cross section at the outlet of the material feeder but a main characteristic is the disadvantage that the material flow rate cannot be controlled (see figure 3c). Due to venturi feeders having no moving parts an inherent advantage is that they are less prone to wear. The feeders also occupy smaller volume than other feeders, but are commercially only used in conveying systems that have low flow rate and short distance requirements. Variations in feeder specifications do occur and allows the control of material flow in terms of the addition of certain gates or valves.

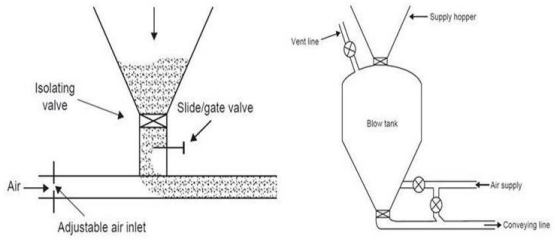

Figure 4: Feeder types 2 (Images adapted from (Mills 2004))

d. Trickle feeder: This feeder is commonly used in vacuum systems but suffer the disadvantage of improper flow rate control. It is however considered inexpensive compared to other vacuum feeders and is therefore commonly used. The mass flow rate within trickle valves is controlled by means of a sliding gate and an isolating valve (see figure 4a).

5. Blow tanks: These feeders are generally used for systems which include abrasive materials, that are required to be conveyed either at high or low pressures. The mass flow rate is controlled by means of air proportioning in terms of having some air pressurizing the blow tank while the bypassed air is used to dilute the material to the required solid loading ratio. Blow tanks are commonly used within coal-fired

power stations as a conveying technique for either pulverised fuel or ash conveying purposes (see figure 4b).

e. Suction nozzle: These applications mainly focus on plants where open piles of materials are required to be transported to a different location. The mass flow rate of vacuumed material is controlled using an additional air inlet apart from the suction point that reduces occurrences like pulsated flow or blockages (see figure 5a).

f. Gate valves: Gate valves represent feeders that are operated by means of a flap valve that can be opened or closed to control material feed and are controlled by means of a motor or gravity. The use of gate valves should be carefully monitored to prevent blockages that might occur. These valves are not commonly used in the industrial environments (see figure 5b).

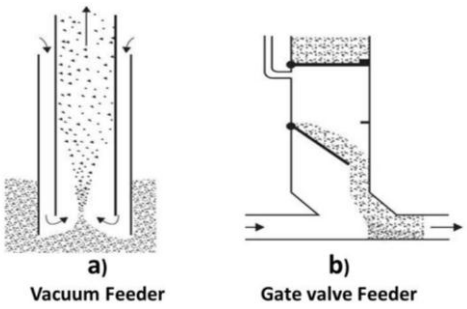

Figure 5: Feeder types 3(Images adapted from (Mills 2004))

2. Literature study

2.1. Mass flow monitoring

Currently mass flow measurements of solids can be done in multiple ways witch each method having its own pros and cons associated with sensitivity, accuracy and limitations. The use and selection of these techniques are based on the requirements of the specific project and should be carefully selected in order to obtain the optimal sensoring unit that will provide results within the scope of the system or project.

Broadly these methods can be categorised into two main groups namely direct and indirect methods. Direct mass flow methods consist out of sensoring systems that obtain the mass flow rate by means of a single measurement, where indirect methods require additional measurements or readings For instance Indirect methods require a concentration/volume fraction measurement along with a velocity reading in order to determine the mass flow rate. This study focuses more on an indirect method which will be elaborated further on in the dissertation. Equation 1 illustrates how mass flow rates can be determined using the density ρ, velocity V and area of the pipe A. where equation 2 focuses on more dynamic systems where the velocity $V(t)$ and concentration $\emptyset(t)$ of material flowing through the pipe change constantly.

$$\dot{m} = \rho A V \quad [1]$$

$$\dot{m}(t) = \rho A \times V(t) \times \emptyset(t) \quad [2]$$

A summary of some of the techniques can be seen table 1.

Table 1: Types of sensing methods

Direct Methods	**Indirect methods**
• Thermal detection technique	Velocity Methods:
• Active charge techniques	• Doppler methods (Microwaves, Laser and sound)
• Passive charge techniques	• Cross correlation methods
• Particles least square techniques	• Electrodynamics techniques
• Coriolis force technique	• Spatial filtering
• Gyroscopic techniques	Concentration methods:
	• Capacitive techniques
	• Microwave techniques
	• Radiometric techniques
	• Laser sensing
	• Magnetic Resonance sensors
	• Tomography techniques

Further details regarding the accuracies, limitations and applicability of these methods can be found in Appendix A.

Following a comprehensive literature review, the use of capacitance sensors are believed to be superior to other techniques in power plant engineering applications due to the simplicity of the sensor, the low cost associated with construction and low risk associated with health factors such as radiation when compared to other sensors. It enables the use of the cross correlation principle for calculating the solid particle velocity, through comparison of output signals to determine changes in time.

Capacitive techniques are not only used in pneumatic ash conveying systems but have been widely prescribed and used in the literature and were used to determine multiple concentration readings that vary from moisture content in soil, void fractions in fluids (Das et al. 2014), water fractions in crude oil (Aslam & Tang 2014) and solids concentration (Sun et al. 2008; Arko et al. 1999). The use of capacitance sensors is also suggested by Sen et al. and Xie et al. (Xie et al. 1990; Sen et al. 2000) because of the advantages associated with them. They are listed below:

- Simple structure
- Free of maintenance
- No interference of the flow field
- Output is directly available in the form of an electric signal.

2.1.1. Capacitive Technique overview

The concept works in terms of the relative permittivity (ε) changing within the cross section of a pipe due to the presence of solids within the carrier gas. Thus when the concentration of solids changes within the control volume (increases or decreases), it will change the effective capacitance measured by instrument.

There are also multiple capacitive designs that differ in effectiveness, cost and sensitivity. An investigation into six different capacitive sensors was done by (Abouelwafa & Kendall 1980) in order to determine the most effective one for evaluating the phase percentage in multiphase pipelines. The sensors investigated can be seen in figure 6 and consist of: Parallel Plate Capacitors, Concave Plate Capacitors, Stagger Concave Plates, Double Helix Capacitors, Multiple Helix Capacitors and a Four Plate Concave Capacitor. During the investigation the authors found that the most effective technique was the double helix capacitor and also suggested that the concave plate setup was used in systems where high sensitivity is required (Abouelwafa & Kendall 1980). The use of the concave plate setup also allows easy manufacturing and enables the use of the sensor sensitivity to identify the flow regime that is currently present in the system through the difference in electrode readings (The concept is elaborated on in later paragraphs).

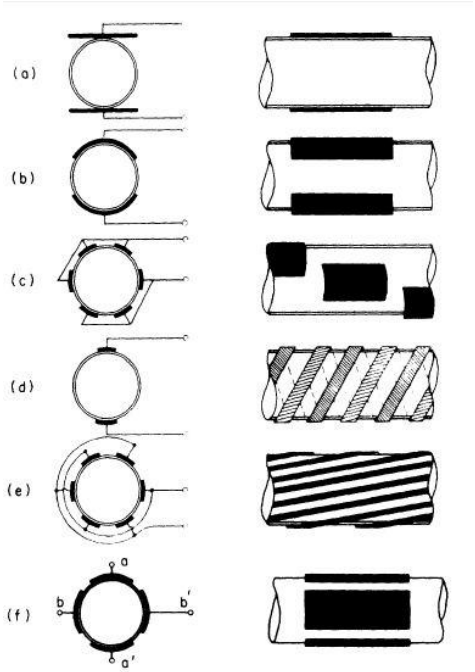

Figure 6: Capacitive techniques (Abouelwafa & Kendall 1980)

2.2. Review of existing capacitive methods for determining the mass flow rate

Capacitive sensors have been widely used over the last 35 years in order to determine the particle concentration and velocity of solids in pneumatically conveyed systems. This section of the study presents a literature review on what has been done in the past and highlights the lessons have been learned from conducting experiments on the sensors and their associated experimental setups.

2.2.1. Strip vs. ring capacitors

Irons and Chang (Irons & Chang 1982) conducted experiments in a static and dynamic environment on two different types of capacitive electrodes namely strip and ring type capacitors. This is shown in figure 7.

During their study stationary experiments were conducted in order to evaluate the effects on the capacitive readings when a specified flow regime (stratified) and electrode geometry (Ring or strip type) was used. During these experiments they found that the strip type electrodes showed increased sensitivity towards and induced flow regime when compared to ring type electrodes. Although the strip type electrode poses the problem that it is more useful when the flow regime is known, it provides the required sensitivity for an accurate measurement.

In order to determine the particle concentration Irons and Chang used the change in capacitance over the electrodes to determine the particle concentration (due to change in the effective permittivity between the plates). Furthermore a high speed camera was used to determine the general velocity of particles, the determination of these instantaneous properties allows the calculation of the flow rate of the solid material and can then be compared with a measured value. Figure 7 illustrates the experimental setup used.

During their investigation they were able to identify multiple flow regimes by means of visual observation, the flow regimes tested were stratified, annular and core for the static analysis and rope, dispersed and slug flow for the dynamic analysis. The identification of the flow regime in industry would prove to be difficult and would require an alternative method of identification to that of a visual approach. This leads to one of the project aims that entail the successful identification of variable flow regimes with the addition of a correction factor to increase the accuracy of the sensing unit.

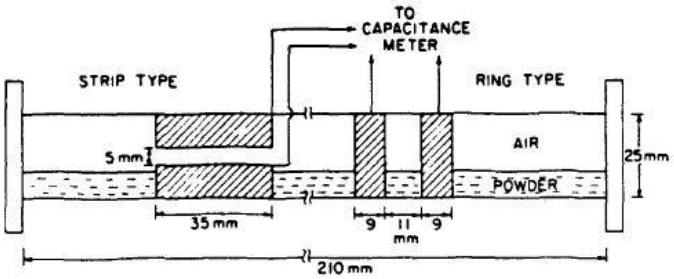

Figure 7: Strip and ring type electrodes (Irons & Chang 1982)

Irons and Chang claim that an error smaller than 8%, with regards to particle concentration and velocity, has been achieved when the solid flow rate is known.

2.2.2 Capacitive and electrodynamic sensors combination

Xie et al. (Xie et al. 1989) proposed a sensoring system consisting out a capacitor sensor combined with two separate electrodynamic sensors. The experimental setup can be seen in figure 8.They encountered multiple problems regarding the accuracy of the velocity measurement done by means of a cross correlation technique between the 2 electrodynamic sensors. The main reason for the error in measurement can be due to the dependence of the sensor reading on the flow's Reynolds number, particle size and velocity which are not all constant and precisely predetermined.

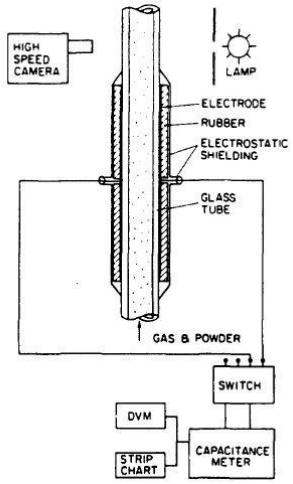

Figure 8: Experimental setup (Irons & Chang 1982)

Similar to Irons and Chang, Xie et al. conducted the concentration measurement by means of strip capacitive sensor with two plates around the conveying pipe. During their investigations Xie et al found that the capacitance measurements for stratified flow vary when the sensors are orientated differently with regards to one another and therefor suggests that the sensors will be sensitive towards varying flow patterns that are not homogeneously spaced. Xie et al. proposes that in practice during installation a suitable orientation of the sensor should be selected in order to compensate for the type of flow experienced. This further indicates the possibility of a flow regime identification correction method that could be employed to improve the accuracies of such systems. The use of a transformer arm bridge principle was used to minimise the effects of base line drift along with filters to reduce the noise level within the signal and will be discussed at a later stage in the dissertation.

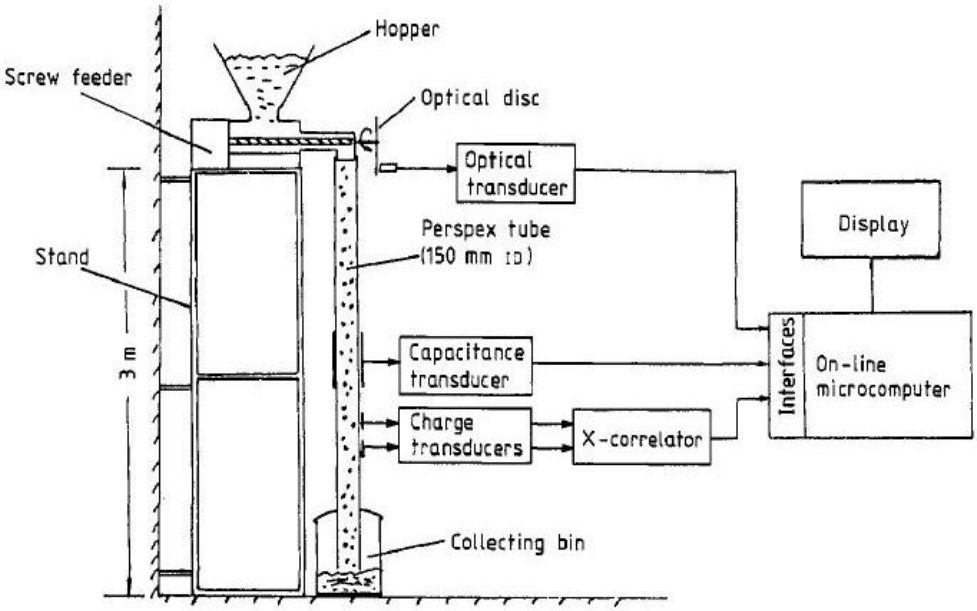

Figure 9: Experimental setup (Xie et al. 1989)

Xie et al later investigated the influence of the sensor geometry on the sensitivity field of a strip capacitor and what the optimal design ratios would be in order to have a sensor with a higher sensitivity as well as a good uniform sensitivity field. It should be noted that for his research the assumption was made that the plate lengths were long enough to minimize the fringe effect (length is 2 times the pipe diameter).

The results of their studies identified the optimal sensor geometry factors that can be seen in table 2 with the geometrical explanations in figure 10.

Table 2: Optimal sensor size

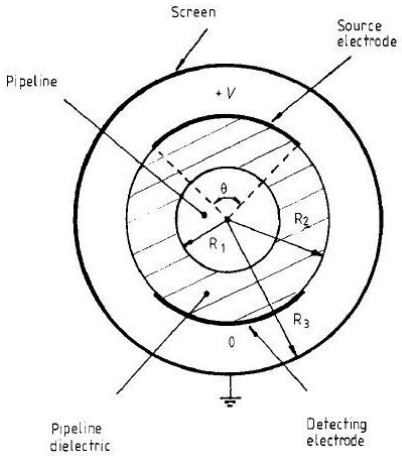

Figure 10: Capacitance sensor layout (Xie et al. 1990)

$$R_3 - R_2 = (0.2 \rightarrow 0.5)R_1$$

$$\varepsilon_{wall} \approx 1 \rightarrow 2$$

$$R_2 - R_1 = (0.5 \rightarrow 1.5)R_1$$

$$\theta \ dependent \ on \ wall \ thickness$$

$$R_2 - R_1 = (0.5)R_1 \rightarrow 130° < \theta < 140°$$

$$R_2 - R_1 = (1)R_1 \rightarrow 120° < \theta < 130°$$

$$R_2 - R_1 = (1.5)R_1 \rightarrow 110° < \theta < 120°$$

* Note that R_1 is given as a unit length in the literature

Although the values given by Xie et al. are the optimal values for obtaining the best sensitivity the actual implementation of a sensor that has a wall thickness as thick as its inner radius will not be efficient or compact and will lead to a bulky and oversized sensor. Therefore an objective decision should be made in terms of what would be possible in practice and how the guidelines given can still be partially followed to get the best possible result. The practicality of the optimal values for the walls emissivity should also take into consideration. The material should be able to withstand the environmental effects observed within a pneumatic conveying environment such as corrosion, temperature, abrasion and pipeline pressure (Yan et al. 1995).

2.2.3. Compounded capacitive electrode sensors

Shao et al.(Shao et al. 2000) conducted a study that evaluates the mass flow rate of a pneumatic ash conveying system on an iron making plant, using compounded capacitance electrodes and a time difference method for the velocity component. The addition of another capacitance plate serves as a compensation sensor by having a better sensitivity field on the parts where the first sensor lacks good sensitivity.

The use of multiple plates in order to compensate for sensitivity towards different flow regimes can be used in a further evaluation by adding a third plate for the additional compensation of the sensor sensitivity as well as having an additional set to calculate the solid particle velocity. Further evaluation can also be done to determine if the addition of a third plate (or two thin plates) would enable or improve the identification of flow regimes in order to improve measuring accuracies with regards to variable flow regimes

The experiments were conducted over a mass flow range of 0.49-1.98 t/h in 60 different sets of data and resulted in an error range of ∓5% with the largest difference being 5.68% at an mass flow rate of 11.06 t/h showing that a large improvement have been made. The experimental setup along with the sensor arrangement can be seen in figures 11 and 12.

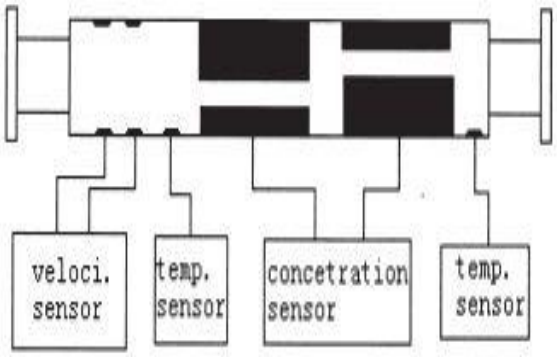

Figure 11: Sensor setup (Shao et al. 2000)

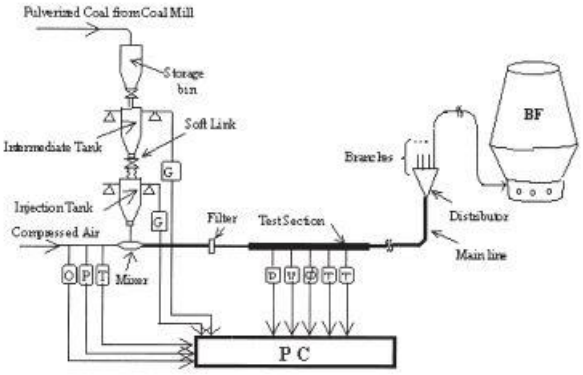

Figure 12: Experimental Setup (Shao et al. 2000)

Sen et al. (Sen et al. 2000) used a similar setup as Xie et al. (Xie et al. 1989) consisting out of a capacitive sensor (for concentration) combined with 2 electrodynamic sensors for particle velocity measurement. The research proposed a novel PC based system that uses the rms of the fluctuations of the voltage output from the concentration sensor in order to reduce baseline drift as well as compensating for a constantly changing environment. The use of a PC based analysis enabled the analysis and interpretation of multiple systems and aspects of the sensoring unit in itself and would prove to be useful in order to evaluate the properties allowing possible flow regime identification.

When considering the size of the capacitance sensors Sen et al. used a relatively short capacitance sensor, 15 mm long when compared to the pipe diameter of 12.7 mm (resulting in 1.18D) which is not the recommended two times the diameter. This shows that reliable results can still be obtained although the required sensor length may not be used. The application of the transformer arm principle was also used during the design of the capacitance sensor (which will be explained later on).

Although the results showed are not as accurate as previous methods the use of the PC system will contribute significantly toward the scope identified in this work.

2.2.4. Capacitive dummy sensor

Hu et al. (Hu et al. 2006) propose a novel method for concentration measurement of pulverised fuel for fossil power stations by means of an CDS capacitance circuit that eliminates the effects of capacitance drift along with low temperature drift and noise. For the experiments Hu et al. proposed a dual sensor design that consisted out of an actual sensor combined with a dummy sensor exposed to the same temperatures (in this case 40°C and 100°C°). The circuit described will be discussed in a later paragraph dedicated to the reduction and elimination of negative effects associated with capacitance sensors. These implementations can lead to an improvement of overall accuracy and sensitivity of the sensors.

The proposed sensor design strays from the proposed optimal sensor as prescribed by Xie et al (Xie et al. 1990) and uses a source grid electrode as a means of measuring the capacitance for concentration purposes. The experimental setup along with the sensor setup can be seen in figure 13 and 14. The proposed system proved to have a linearity of about 5% when compared to the actual measured

concentration, which is done by measuring the average concentration collected by a mesh. No observations were recorded in conjunction with the flow regime variation.

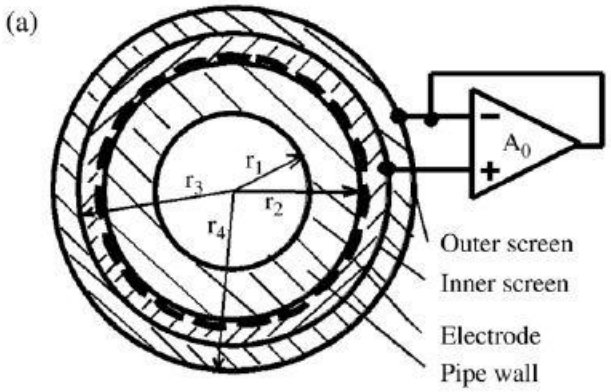

Figure 13: Sensor setup (Hu et al. 2006)

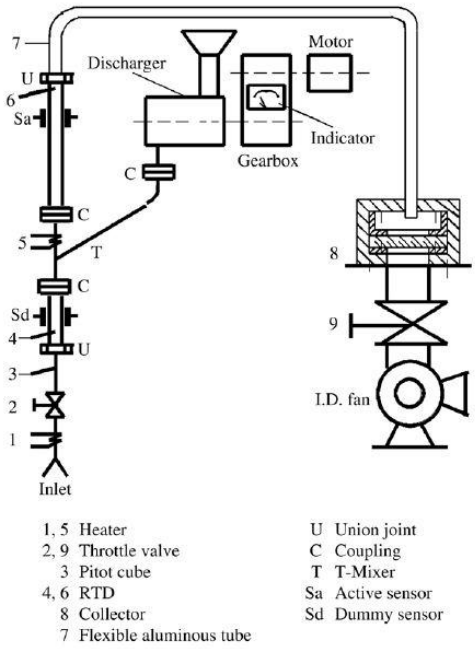

Figure 14: Experimental setup (Hu et al. 2006)

2.2.5. Regime identification through frequency analysis techniques

Zhang et al (Zhang et al. 2012) conducted experiments to determine the concentration fractions of three phase flow within a pulverised fuel plant by means of using a Hilbert transform and a combination of two signals, one for a capacitance reading and one for an electrostatic reading for calibration of the solid concentration components. Zhang et al. used the same capacitive electrode configuration and experimental setup as Sen et al. (Sen et al. 2000) and may be seen in figures 13 and 14.

The energies of each sub-band (obtained by the Hilbert transform) of the electrostatic meter (along with the specified operating conditions) are then fed into a neural network (back propagating neural network) which determines the corresponding flow regime. Zhang et al. then use a dual regression method to determine the calibration coefficients for determining the concentration of the bio mass and the pulverised coal.

The use of similar technique as prescribed by Zhang et al. can be used to improve the accuracy a mass flow rate system by first identifying the flow pattern by means of comparing the outputs of variable sensors orientated differently and then determining a coefficient that serves as a correction factor to improve the original capacitance measurement reducing the sensitivity with regard to flow regime and improving the application of capacitance sensors with regards to variable flow regimes. The investigation can also be extended by identifying more than two types of flow regimes in order to improve from the progress made by Zhang et al

2.3. Review of existing methods for evaluating volumetric concentration

The concentration calculation was done in terms of measuring the change in capacitance reading, which reflects a in change in permittivity within the control volume. This variation in permittivity is caused by the variation in volumetric concentration of both air and sand. During the research two methods were found that was used to determine the solid concentration. They can be summarised to be as follows:

1. Change in capacitance in terms of permittivity ratio.

As explained earlier the change in relative permittivity is observed when additional particles are situated within the control volume. The change in permittivity is measured would then be measured by means of observing a change in the capacitance (C) as shown in equation 3.

$$C = \varepsilon_0 \varepsilon A_p / d \quad [3]$$

In the above equation A_p is the area of overlap of the electrode plate, ε_0 is equal to the permittivity of free space and d the separation between the two plates.

The concept is better explained by (Shao et al. 2000) who states that the capacitance of a fixed geometry can be written as equation 4:

$$C = K\, \varepsilon_{eq} \quad [4]$$

$$\varepsilon_{eq} = \frac{V_1}{V_s}\varepsilon_1 + \frac{V_2}{V_s}\varepsilon_2 \quad [5]$$

For the above equation [4] K is determined by fixed geometry properties and ε_0, that is equal to the permittivity of free space as in equation 3. The equivalent permittivity can then be determined by using equation 5 (Abouelwafa & Kendall 1980) that takes into consideration the permittivity of both the solid and the air ($\varepsilon_1 and\ \varepsilon_2$). If only the 2 materials are present in the system their volume fractions can be related to one another by using equations 6 and 7. Where V_1 and V_2 represent the volume fraction occupied by material 1 and 2 with their associated permittivity's $\varepsilon_1$and ε_2.

$$\alpha_1 = \frac{V_1}{V_1 + V_2} \quad [6]$$

$$\alpha_2 = \frac{V_2}{V_1 + V_2} = 1 - \alpha_1 \quad [7]$$

With these equations the relationship between the volumetric fraction of solids and capacitance can be determined. The measured capacitance can then be compared with the predetermined values of capacitance in order to find the actual solid volume fraction within the system. This relationship can be established by combining equations 3 to 7 as shown in equation 8 to 10.

$$\varepsilon_{eq} = \alpha_1\varepsilon_1 + \alpha_2\varepsilon_2 \quad [8]$$

$$C = K\,(\alpha_1\varepsilon_1 + \alpha_2\varepsilon_2) = K\,(\alpha_1\varepsilon_1 + (1-\alpha_1)(C)) \quad [9]$$

$$\alpha_1 = \frac{\frac{C}{K} - \varepsilon_2}{\varepsilon_1 - \varepsilon_2} \quad [10]$$

2. Change in capacitance in terms of volume fraction

The principle of change in volume fraction can be explained in the following manner: The sensor capacitance can be measured by means of using an LCR (inductance, capacitance and resistance) analyser. The total sensor capacitance (C_{tot}) can be written as a function of the sample capacitance (C_s) and the capacitance of the wall (C_w). The sample and wall capacitance act as capacitances in series leading to equation 11 as given by (Aslam & Tang 2014)

$$C_{tot} = \frac{C_s C_w}{C_s + C_w} \quad [11]$$

The effective permittivity of the sample (ε_s) can be given as a function of the volume that each component represents (V_{fa} and V_{air}) within the control volume (V_s) and their associated permittivity (ε_{fa} and ε_{air}) and can be seen in equation 12.

$$\varepsilon_s = \frac{V_{fa}\varepsilon_{fa} + V_{air}\varepsilon_{air}}{V_s} \quad [12]$$

Aslam and Thang (Aslam & Tang 2014) then give a relationship that describes the effective capacitance of an concave semi cylindrical capacitor having two plates as equation 13, where ε_0 relates to the dielectric permittivity of free space and d to the minimum distance between the two opposite electrodes.

$$C_s = \sum_{i=0}^{n} 2\,\varepsilon_0 \varepsilon_s A_e \times \left[\frac{1}{d + (i-1)\Delta d}\right] + \frac{\varepsilon_0 \varepsilon_s A_e}{2R} \quad [13]$$

These relationships given in equations 11 to 13 can be used to determine the volume occupied by the solids.

These methods will not be used to determine the volumetric concentration due to the fact that they all represent a theoretically based analysis where the orientation of solids with regard to the electrode sensitivity field is known. Though they form a critical part in understanding previous work done by researchers they are only approximations to systems where the distribution and volumetric concentrations are known. The lack of knowledge regarding the exact position of solids and their associated concentration makes these methods near impossible to implement in practice, instead experiments will be conducted where the volumetric concentration and flow regime will be altered within a controlled environment. The alteration to these properties will lead to different responses of the individual electrode pairs, the results will then be used to create a concentration to change in capacitance curve (calibration curve) for each individual flow regime or flow instance. (Note that the same flow regime can have different capacitive measurements due to its orientation with regards to the electrode orientation.) This method will be greatly elaborated on in later chapters.

2.4. Review of existing methods for evaluating particle velocity

Multiple cross correlation methods can be found in literature that provide viable means for evaluating the velocity of flowing particles within a pneumatic conveying environment, and they are as follow:

1. Peak vs. Peak time.
2. Area under the graph.
3. Passing time method
4. Pattern recognition methods
5. Option 1 or 2 with a specified grace period grace or fault margins.

The capacitive cross correlation technique is explained and used by Shao et al. (Shao et al. 2000) who utilises the concept of clouds of particles that form within the pipeline, each of these clouds having their own properties that result in unique forms that appear when looking at the output signal of the capacitor. The output signal of two identical sensors is then compared (as seen in figure 15) in order to find the change in time τ.

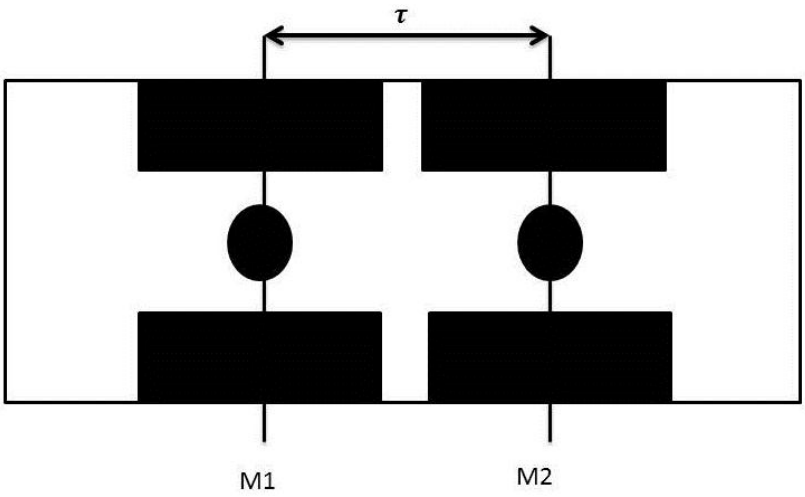

Figure 15: Compounded capacitive sensor adapted

The velocity can then be determined by dividing the length between the capacitive sensors by the transit time (τ). This is shown mathematically in equation 14.

$$v = \frac{L}{\tau} \quad [14]$$

The determination of the transit time (τ) was done by finding the difference in time for a certain peak occurring on both sensors. Shao et al. (Shao et al. 2000) use the manipulation of the output signal to a square wave in order to determine distinct intervals that can be tracked. This is shown in figures 16 and 17, and will also be discussed in a mathematical equation further on.

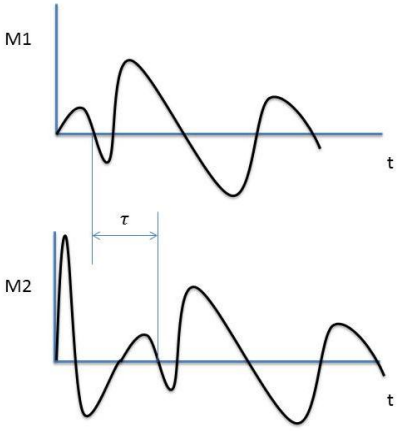

Figure 16: Capacitance signals

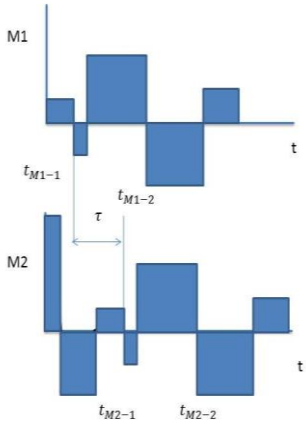

Figure 17: Simplified block wave signal

M1 and M2 represent separate capacitance measurements of which square wave representation can be seen in figure 17. The transportation time τ is observed where the same pattern occurs at measurement point two (M2). The transportation time can then be expressed as:

$$\tau = t_{M2-1} - t_{M1-1} \; or \; \tau = t_{M2-2} - t_{M1-2} \quad [15]$$

If the response stays constant between two points the transit time between each wave should be the same resulting in equation 16.

$$\tau - \tau = (t_{M2-1} - t_{M2-2}) - (t_{M1-1} - t_{M1-2}) = 0 \quad [16]$$

This is not completely realistic and therefore Shao adds a factor that takes into consideration small variations that might occur in terms of a tolerance period δ.

$$(t_{M2-1} - t_{M2-2}) - (t_{M1-1} - t_{M1-2}) \leq \delta \quad [17]$$

Shao (Shao et al. 2000) also reduce false identification of clouds, due to the same time period occurring multiple times, by adding additional requirements in terms of the previous and sequential wave times as shown in equation 18.

$$\begin{aligned} (t_{M2-1} - t_{M2-2}) - (t_{M1-1} - t_{M1-2}) &\leq \delta \cap \\ (t_{M2-1} - t_{M2-0}) - (t_{M1-1} - t_{M1-0}) &\leq \delta \cap \\ (t_{M2-3} - t_{M2-3}) - (t_{M1-3} - t_{M1-2}) &\leq \delta \end{aligned} \quad [18]$$

Sun et al. (Sun et al. 2008) use a different approach to that of Shao by comparing the upstream and downstream signals. The technique is based on searching for the peak of the cross correlation function to determine the time delay. The formulation can be seen in equation 19.

$$R_{xy}(j) = \frac{1}{N}\sum_{j=0}^{M}\sum_{i=1}^{N} x(i)y(i+j) \quad [19]$$

$$j = 0,1,2,3,\ldots\ldots,M$$

$$i = 1,2,3,\ldots\ldots,N$$

In the above equation $\boldsymbol{x(i)}$ and $\boldsymbol{y(i)}$ represent the upstream and downstream data of the produced capacitance signal along with the number of samples N. j represents the number of the delayed sample and M the number of samples in the cross correlation calculation. The time delay can then be calculated by looking for the maximum in the cross correlation function. If the maximum is found the index is used for determining the time delay(τ_m) by using the sampling frequency ($\Delta t = \frac{1}{f}$) as is shown in equation 20.

$$\tau_m = k \times \Delta t \quad [20]$$

2.5. Regime compensation

The flow dependence of capacitance sensors are well known and was noted as early as the 1980s (Irons & Chang 1982) where researchers have shown that the measurement of strip like electrodes show different capacitance readings for the same volume fraction depending on the type of flow regime experienced. Strizollo and Converti (Strizzolo & Converti 1993) emphasized in their findings that the effect of phase distribution or flow regimes cannot be neglected and should be compensated for . The principle is shown in figure 18 where the solid material used was silica sand.

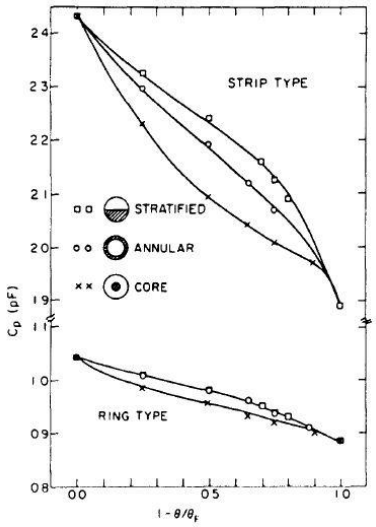

Figure 18: Flow regime dependence of strip sensors (Irons & Chang 1982)

The concept is further illustrated by Tollefsen and Hammer (Tollefsen & Hammer 1998) where significant tests were done on strip plate electrodes as well as helical plates. In the research they show

that for strip plate electrodes, the results for each volume fraction the capacitance reading differs significantly with regards to the flow regime experienced (figure 18). It should be noted that the results tabulated by Tollefsen were only done in terms of a theoretical approach and were not validated by means of an experimental setup. Although not explicitly done previously these properties can be used to find a line of best fit to a standard equation (exponential, log, quadratic or even linear). The experimental capacitance can then be compared with the calibrated curve for a specific flow regime to determine the corresponding volume fraction.

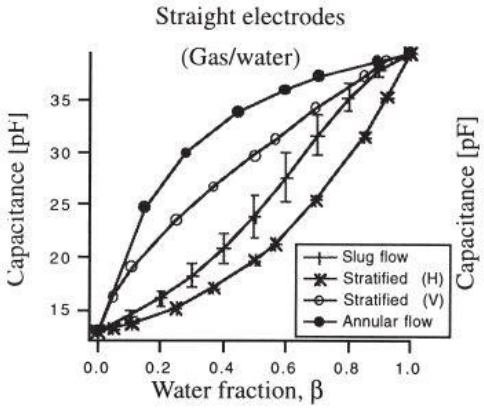

Figure 19: Flow regime dependency (Tollefsen & Hammer 1998)

The work of Geraets and Borst (Geraets & Borst 1988) show an interesting approach towards identification of flow patterns for pulsating flows like slug and plug flow by using the results of the capacitance readings in the time and frequency domains. The pulsating flow regime is then identified by measuring the frequency of the capacitance peaks providing a positive identification technique. From the results shown in their work (figure 20) there is a clear difference in peak frequencies between the flow regimes increasing the probability that full flow regime identification could be conducted.

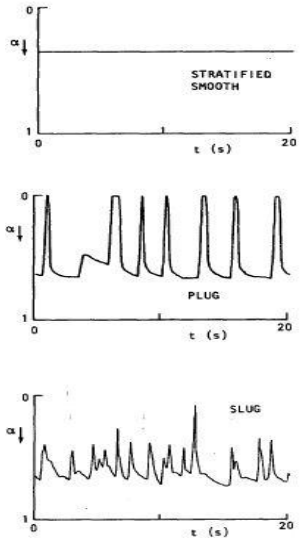

Figure 20: Capacitive sensor results for different flow regimes (Geraets & Borst 1988)

From the above the flow identification and correction factors can be done in the following manner:

1. The identification of all orientated stratified flow regimes can be identified by comparing the results from the compounded electrode sensors. Compensation can then be done by means of a calibration curve corresponding to an induced flow regime.
2. The identification of core and annular flow by comparing statistical results.
3. Slug and plug flow identification through a frequency measurement.

The coupling of this idea with a compounded electrode setup compensating for different stratified flow or non-homogeneous flow regimes will most likely improve accuracy of strip electrode flow sensors and will result in a less flow regime dependent system.

2.6. Review of existing methods for minimizing the external effects.

According to Hu et al. capacitive sensors are sensitive to multiple factors that can cause deviations in the accuracy of these sensors. The factors that affect the sensor accuracy are as follows:

1. Base line drift: Xie et al.(Xie et al. 1989) propose an transformer-ratio arm bridge to minimize base line drift, The principle measures the difference in current flowing through the sensors capacitor and a balance capacitor (C_x and C_b).
2. Difference in nominal capacitance.
3. Noise on signal due to static charge.
4. Large cable capacitance
5. Stray capacitance: (Huang et al. 1988) states that stray capacitance can be eliminated by using an intrinsically stray-immune circuit (figure 14) which can be constructed by having an one of the electrode plates connected to an voltage source and the other connected to the input of a current detector with a very low impedance connected to earth. The stray capacitance is then in parallel with the voltage source and the current detector and will result in a system having no effect on the current measurement moving through the capacitor.

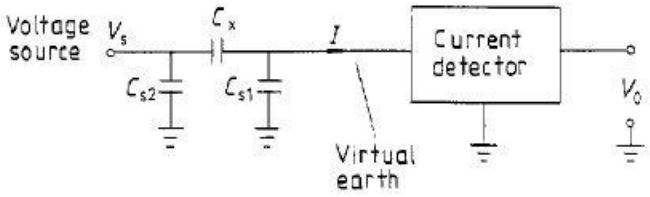

Figure 21: Intrinsically stray-immune circuit (Huang et al. 1988)

Zhang et al. (Zhang et al. 2012) also state that the use of a differential capacitor can minimize the effect temperature, stray parameters and electromagnetic interference while increasing detection sensitivity. They also prescribe the use of shielded twisted pair cables with identical lengths to produce the same nominal capacitance over the 2 plates.

2.7. Factors to take into consideration during experimental setup and design

According to Terzic et al. (Terzic et al. 2012) capacitance sensors may be affected by multiple factors that can negatively influence the accuracy and validity of the sensors. The factors require adequate planning and consideration in order to supply the required accuracy specified by Eskom.

The factors that will influence the sensor accuracy are as follow:

1. Environmental factors: Factors like temperature, moisture content, humidity and pressure will influence the material between the effective dielectric permittivity in the sense that they change material properties. Experimental conduction in extreme temperature conditions will cause expansion and shrinkage of capacitor plates. The physical change in plate size will lead to the change in geometrical constants and gap sizes. These changes have an adverse effect on the accuracy of measurements. The effect of these factors can be limited by means of using a temperature gauge in order to compensate for dielectric emissivity changes, or keeping temperatures constant in the testing environment. Sensors can also be shielded from the environmental effects by means of an isolation layer that minimize the temperature changes observed by the plates.
2. Contamination: The inclusion of different materials (other than fly ash) will change the material composition between capacitor plates. Unanticipated material changes will lead to inaccurate capacitance measurement on the concentration side of the calculation.
3. Sensitivity to stray capacitance and Noise: The effect of noise and stray capacitance can be minimised by means of using electrical shielding on cables as well as capacitive plates.

2.8. Conclusion on Literature review

Paragraph 2.1 to 2.7 shows the importance of correct implementation of capacitive flow meters from all perspectives; concentration, velocity, orientation and external effects. From the investigation the conclusion can be drawn that a compensation method for variable flow regimes, specifically non-periodic flow regimes, is required in industry in order to improve the accuracy of these type of sensors. The compensation can be done in two separate parts namely identification and flow compensation (addressed in paragraph 4.2 and 4.3) as both would be required in an industrial environment.

The effect of external factors will also be minimised in the experimental setup by conducting the experiment in a lab where the temperature is kept constant. The conveyed material will also be protected from environmental effects such as moisture that could affect the permittivity drastically by isolating the experimental setup from rain and other environmental effects. The effect of moisture content is also neglected in the experiments as they were done in a control environment as is the case for the industrial circumstances for which the instrumentation is intended.

3. Experimental Setup

As required a given requirement the sensor should be able to operate in a system where there are no prior knowledge of the experienced flow rate or the actual flow regime as well as conveying method. The experimental setup should therefore be versatile to simulate variable flow regimes along with the ability to change the flow rate of material through the system. Therefore 2 experimental test setups were used, namely an auger fed test rig and a gravity chute system with interchangeable nozzles as seen in figures 22 and 23.

3.1 Auger fed test rig

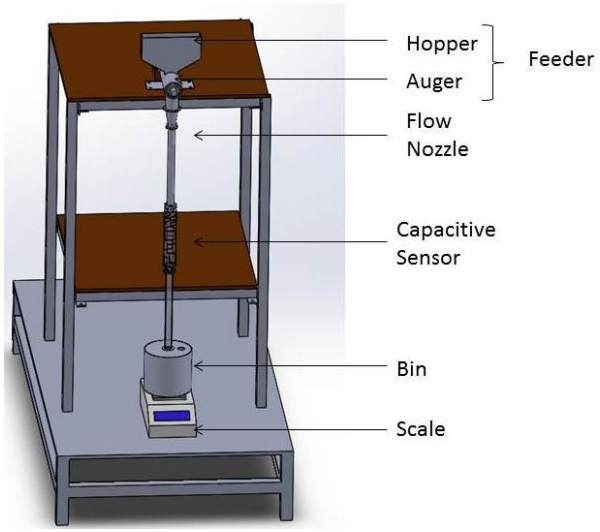

Figure 22: Auger fed experimental setup

Figure 22 illustrates a conveying system based on an auger fed system coupled to a gravity tube that enables the simulation of material being fed through a piping system at periodic intervals representative of the screw feeding rate. The stored solids are fed into the vertical conveying system by means of a screw feeder that ensures that a constant mass flow rate of solids representative of the controlled rotational speed of the electrical motor. A more in depth discussion of the setup will be done in paragraph 3.1.

The associated advantages of the Auger fed setup are as follows:

1. The setup allows the measurement, calibration and comparison of the capacitive sensor with the actual mass flow rate measured by the load cell or scale.
2. Material flow rate can be altered by means of the proposed feeder that allows for multiple evaluation experiments.
3. No external flow propulsion is required.
4. The setup will have a lower cost than alternative options.
5. The setup requires a smaller experimental area.
6. The use of a vertical gravity system will reduce the amount of solid accumulation drastically on the surface of the pipe, thus increasing the accuracy and ability to simulate certain flow regimes.

System components and functions

1. **Hopper:** The hopper: serves as a temporary storing facility for material that is being fed into the conveying system as seen in figures 22 and 24.
2. **Feeder:** The feeder serves as main supply gate to the pipeline and should be able to manipulate the solid material in a certain manner in order to create a wanted flow environment (periodic flow similar to slug or plug flow). The feeder should also be able to increase or decrease the amount of ash supplied in order to simulate a variation in conveying flow rates.

   An investigation was conducted into the types of valves and feeders commercially available and can be seen in paragraph 2.1.4 for more information. After careful consideration the following valves can be considered applicable to an experiment similar to the proposed:

   a. Gate valves: Because they are relatively inexpensive.
   b. Trickle valves: Simple and relatively inexpensive.
   c. Screw feeder: Can control the mass flow rate (relatively).
   d. Rotary Feeders: Can control the mass flow rate (relatively).

   The choice was then made to use a screw feeder as it would allow the required behaviour and was also sponsored to the University of Pretoria by a private company Shosalowe, as a contribution towards research in the field of solid flow measurement.

3. **Capacitance sensor:** the capacitance sensors are used to determine the particle concentration along with the velocity associated with the solids by means of measuring the change in permittivity and using a cross correlation technique.
4. **Collection Bin:** The collection bin is used as storage facility in order to measure the conveyed solids by comparing the start and end mass of the collection bin
5. **Filter:** A filter is used on top of a breathing hole of the collection bin in order to improve pressure distribution and minimization of the influence of pressure build up on the flow regime. The filter will ensure the entrapment of material leading to minimal release of solids out into the environment.
6. **Scale:** The scale is used to monitor the actual mass flow rate of material into the bin by means of measuring the mass change of accumulated solid material in the collection bin. The mass conveyed will also serve as a verification method in terms of the actual mass conveyed versus the sensor estimated conveyed ash.

3.2 Gravity fed experimental setup

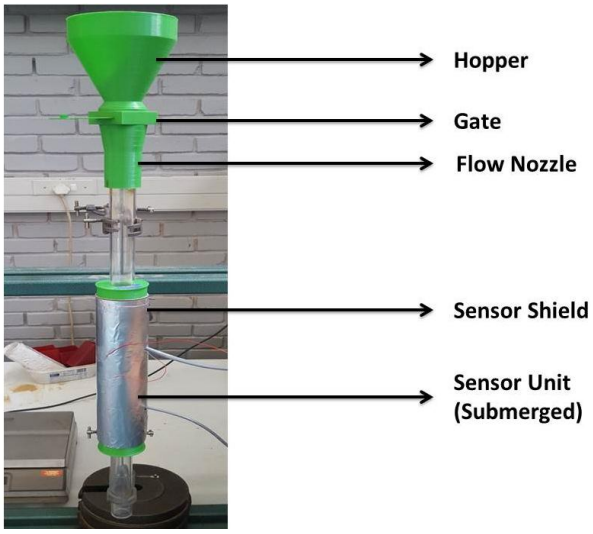

Figure 23: Actual experimental setup

The gravity fed system is proposed to induce constant (non-periodical patters) flow regimes into a vertical gravity fed system by means of using a flow inducing nozzle. As stated the investigation of the flow regimes were limited to three constant regimes and one periodic flow regime.

Components and their functions:

1. Hopper: Serves as loading bay to feed the system sand.
2. Gate: Serves as mechanism to increase or decrease the amount of sand that flows through the nozzle. This increases or decreases the volumetric fraction of solids flowing through the control volume.
3. Flow nozzle: Employed to induce variable flow regimes into a gravity fed chute by means of a 3D printed nozzle (shown in figures 35 to 37). The variety of nozzle geometries were used in order to simulate varies volume fractions for the same type of flow regime.
4. Sensor shield: The external shield is used to minimize all external noise that can be induced to the system as the experiments require the experimentalist to work in close proximity to the sensors and when working with such small capacitance all possible measures should be taken to minimize the influence of outside noise.
5. Sensor unit: Measures the mass flow rate experienced by each of the concentration electrode units to estimate the actual capacitance to concentration relationship.

Similar to the auger fed system the experimental setup would use a collection bin used in combination with a scale to validate and evaluate the error of the estimated conveyed solids.

3.3. Experimental Component Discussion

In terms of storage and feeding the auger fed experimental rig feeds material into the vertical conveying system by means of a screw feeder and hopper assemble (shown in figure 24). This setup ensures a constant feed rate, with a variation in flow regime throughout each of the conveying periods. In addition to the periodic flow regime the operator can also change the flow rate by means of increasing/decreasing the motor rotational speed.

Unlike the auger fed experimental setup the gravitational fed experimental setup uses a flow nozzle to alter the flow regime before entering the conveying system as required. The nozzles used manipulated flow into either a stratified, annular or roping regime. The solid material feed was done by means of using a funnel shaped hoper connected to a gate valve, the gate valve can be used to increase or decrease the amount of solids entering the flow altering system.

The material then passes through the capacitive sensor where the concentration electrodes are used to determine the volume fraction of material that occupies the control volume between each electrode by means of measuring a capacitive difference (discussed in more detail within paragraph 4.2). Compounded velocity electrodes are then used to determine the average solid velocity by means of using a cross correlation method (discussed in more detail within paragraph 4.4).

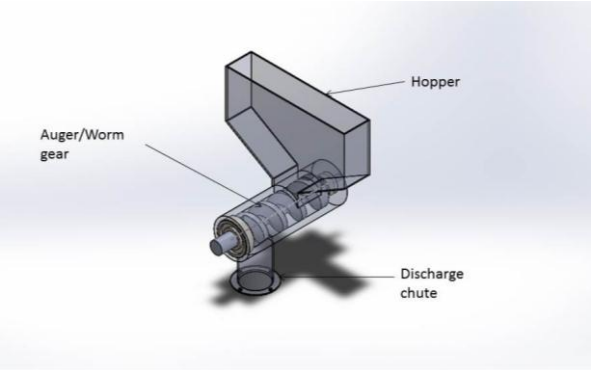

Figure 24: Auger Feeder

3.3.1 Electrode and sensor setup

Currently multiple capacitive sensors can be used to determine solid flow rate for curved surface as shown and briefly discussed in paragraph 2.2.1. The sensor design considered multiple factors that were seen as important to the research, such as:

- Size of total system
- Sensitivity towards variation in flow regimes.
- Manufacturability
- Knowledge of type of electrodes.

The decision to use a curved plate setup was based on their high sensitivity (Abouelwafa & Kendall 1980). The use of other sensors (like the helix) would also prove to be difficult to manufacture and understand completely given the facilities available and knowledge of the manufacturing crew (The

experiments were conducted and manufactured in a mechanical engineering lab). The sensitivity of concave plate capacitors can be used to investigate the probability of detection for a variation in flow regimes by using the change in capacitance when more than one electrode pairs are used.

Shao et al. (Shao et al. 2000) concluded in their study in 2000 that the use of compounded electrodes orientated differently have an higher sensing performance than the simple single plate capacitors, from the conclusion given by Shao the addition of a compounded electrode design will have an improved measurement accuracy and will also supply additional information required to identify the flow regime within the system that will aid in the improvement of sensitivity towards a variety of flow regimes.

During the experimental procedure the instantaneous concentration calculation is done using 3 electrode pairs that are rotated with regard to one another in order to provide an improved estimation of the actual volumetric concentration (see figure 30). The decision of using 3 electrodes are based on the non-uniform sensitivity field of a concave electrode as shown (figure 25) and explained by Shao et al. (Shao et al. 2000). Figures 26 and 27 illustrate this concept by showing that the sensitivity of the capacitor will contribute to a higher capacitive change at the edges of the electrode rather than at the centre of the electrode. This might lead to over or under estimation of the actual volumetric concentration due to a non-homogeneous distribution of particles as shown in figure 27. The implication of non-homogeneous flow is that the linearity of capacitance to volumetric fraction will be lost. This will be discussed further in paragraph 4.2.1.

Figure 25: Concave Capacitive Sensitivity (Shao et al. 2000)

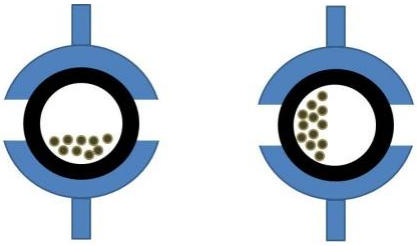

Figure 26: Non- Homogeneous flow regime

Taking into consideration the guidelines given by Xie et al. and the discussion of literature in section 2.3 the concentration sensor was designed to work in an industrial environment where the size of the measuring equipment needed to be minimal while being able to evaluate not only homogeneous flow regimes but other that might also be applicable (Rope, Annular and Stratified) to the environment faced in a pneumatically ash conveying system.

Figure 27 shows the actual electrode configuration as fixed to a Plexiglass pipe (30mm OD and 3mm wall thickness). Details of the electrode dimensions and orientation can be seen in table 3. An important assumption made for the research is that the fringe effect on the electrodes can be neglected for all the experiments as there is no quantifiable method of determining what the effect will be on the actual capacitance measurement. As mentioned previously the pipewall material was made of Plexiglass due to the availability thereof and its relatively good machining properties.

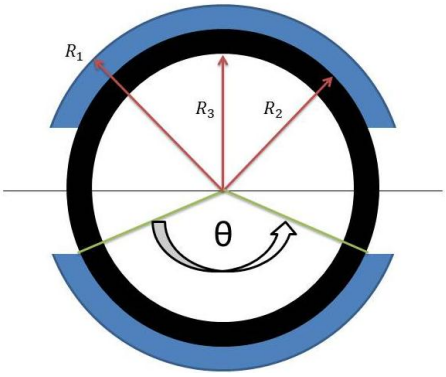

Figure 27: Capacitor Geometry 1

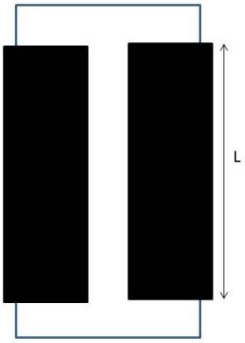

Figure 28: Capacitor geometry 2

The chosen sensor geometries, for each of three concentration electrode pairs and two Velocity electrode pairs, according to figures 28 and 29 are shown in table 3.

Table 3: Concentration electrodes information

Property	Electrode 1 to 3	Electrode 4 to 5
Theta (θ)	135°	135°
R_1(mm)	15.1mm	15.1mm
R_2(mm)	15mm	15mm
R_3(mm)	12mm	12mm
L(mm)	40mm	15mm

Figure 29 shows the variation in electrode orientation that is used to evaluate the induced flow regime by means of having different sensitivity field orientations which will have different capacitive readings when the an induced regime flows through the system.

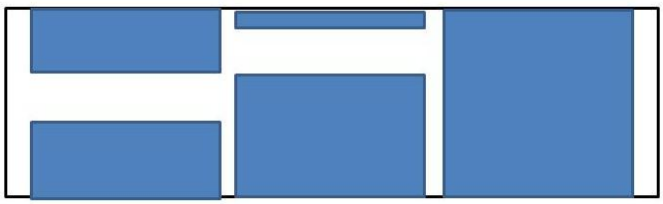

Figure 29: Concentration Electrode Setup

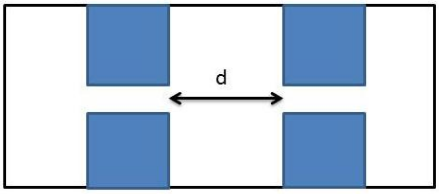

Figure 30: Velocity electrode setup

The distance between the velocity electrodes (**d** as shown in figure 30) was also increased to 40 mm (inner edge to inner edge) to enable the system to be evaluated over a wider variety of velocities. The upper limit of sampling rate achieved with the EVM was in the range of 182Hz meaning that a maximum velocity of 10.01 m/s could be evlauated. There is still a limit in terms of the velocity resolution that can be evaluated, due to the limitation in sampling frequency the concept is illustrated in table 4. Changes in the indices represent the transit time in terms of the time taken for a cloud to move from electrode M1

to M2 in terms of sample rate. For example the difference in indices for a peak in the capacitance signal will represent the time taken for a cloud to move from M1 to M2, if the indices change is one the solid velocity will be 10.01 m/s for (refer to figure 15).

Table 4: Indices Change vs. Measurable velocity

Indices Change	Velocity (m/s)
1	10.01
2	5.01
3	3.34
4	2.50
5	2.00
6	1.67
7	1.43
8	1.25
9	1.11
10	1.00
11	0.91
12	0.83
13	0.77

3.3.2. Material feeding system

Auger fed

The method of conveying and feeding material into the system was chosen to have a constant mass flow rate as it would have been experienced in practice with a blow tank, but cost and space limitations were major constraints that lead to the elimination of building a fully functional pneumatic conveying system. The gravity system enables the conveying of material without the additional requirement of an air propulsion system (which was not readily available for this study).

The only problem with a gravity feeding system is that it requires a feeding system that supplies the material into the chute with a constant and homogeneous feed rate. All the feeders that were discussed in paragraph 1.3.2 have the ability to feed the material continuously when the pressure and material level are kept constant within the material hopper, this type of system would not be achievable during the research but led to the decision of using a motor powered screw feeder system. A graphical representation of a screw feeder can be seen in figure 24.

The motor powered screw feeder enables the following features of the system:

1. The use of an adjustable speed motor will enable the manipulation of particle flow by means of increasing and decreasing the motor speed. The use of valve methods will limit the material flow by being dependent on valve opening and the amount of material still in the hopper above the feeder.

2. The pulsating action of a worm feeder will to some extent emulate industrial circumstances. The pulsating action will help in the identification of the particle velocity, which is dependent on a change in volumetric particle density moving through the sensor.

Gravity fed setup

As described above gravity fed system requires a feeding system. For the gravity fed system the silica sand was poured into the hopper (which is funnel shaped). The funnel feeds the flow induced nozzle like an hour glass. The result is a uniform induced solid flow regime for the time period where the height of material in the hopper is significantly larger than the nozzle size or diameter. The only period of instability was during the first and last moments where the hopper is not filled significantly with regard to the nozzle size (discussed later in the paragraph 4.2). The use of a nozzle enables assessment of regimes caused by anomalies or pipe positions resulting in regimes similar to stratified, rope or annular.

3.3.3. Material Collection and solid measurement

After the material has been conveyed through the pipe section they are collected in cylindrical collection bin capable of holding 8 kg of sand before being filled. The collection bin also had a blow hole to enable airflow out of the system. The hole was also covered with a cloth to prevent any sand from being spilled into the lab.

Before and after each test the collection bin was weighed in order to determine the actual mass conveyed throughout the test. The measurement was done by means of using a scale capable of a measuring resolution of 1 gram. The small resolution enables good accuracy for means of validating the estimated conveyed mass.

3.3.4. Data logging and acquisitioning

A Texas Instruments FDC2114EVM was used to measure capacitance in the femto farad range with high accuracy and sample rate (figure 32) for a multi-channel configuration setup. The evaluation modules came with compatible software in the form of a graphical user interface (GUI) that enables alteration of the modules properties such as:

- Number of active ports.
- Sampling frequency of module.
- Writing frequency.
- Optimal parameters according to electrode size.

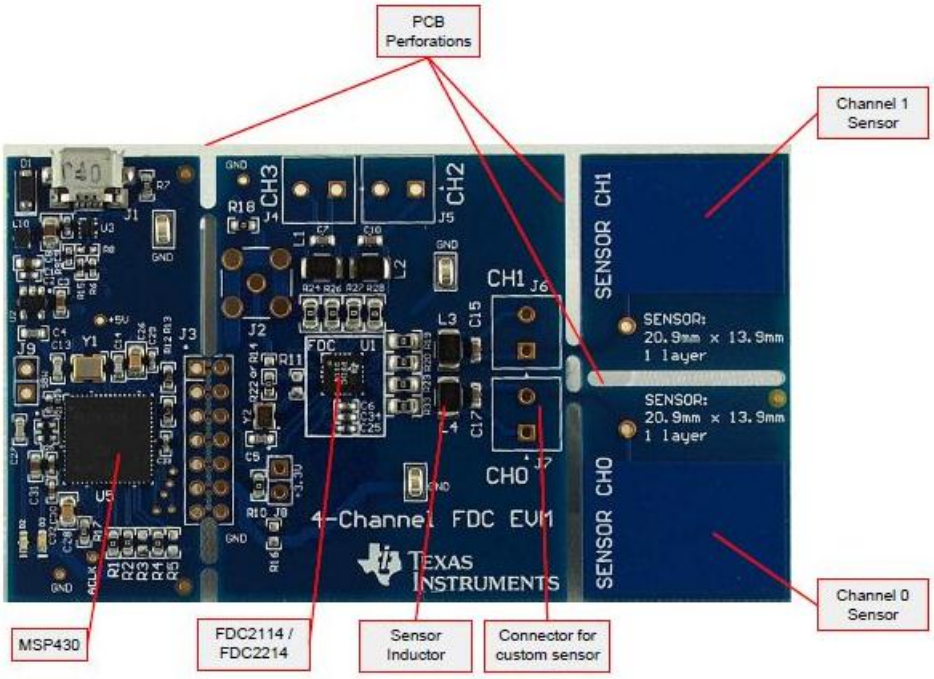

Figure 31: FDC2114EVM module(Texas Instruments 2015)

The amount of adjustability causes high levels of variability in results but also enables the improvement of measurements by giving the designer a large operating range in which he can alter the module to suit his individual needs. The following settings were adjusted as described by (Texas Instruments 2015).

1. The number of sensors used was changed in the configuration settings from 2 to 3 for the concentration module, where for the velocity module the number of sensors was left at 2.
2. The second step was to change the sensor current by means of detecting the optimal prescribed current using the “IDetect” button.
3. The sampling rate of the module was then adjusted to conform to the requirements of the test, by means of altering the Reference Count used in the “RCount” column. The choice of Rcount was based on the requirements of each group of sensing electrodes, for instance the concentration electrodes require high resolution rather that a fast sample rate that would result in very low resolution signal. On the other hand the velocity sample rate should be high in order

to calculate a more accurate velocity (dependent on the distance between the electrodes and sampling frequency see paragraph 3.3.1). The chosen RCount values and their applicable influences on the module sample rate are given in table 5.

4. The data writing rate was altered by changing the plotting option in the live streaming tab to 4.098 ms for the velocity module and 40.55ms for the capacitance module.
5. The data was then written into comma delimited file as specified by the selected directory of the data saving option.

Table 5: Influence of RCount on sample rate and resolution

	RCount	Max Sample Frequency	Max Logging rate (ms)	Number of effective Bits (Resolution)
Concentration Electrodes	32768	24.659Hz	40.55	19
Velocity Electrodes	4098	182Hz	4.098	13

It should be noted that the specified data logging rate will not be the actual data logging rate and should be determined using the reference time specified by the data file. There should also be a play off between the sample rate and the required resolution of the signal as the degradation of the resolution will lead to decreased efficiency in velocity identification by means of peak cross correlation.

The GUI setup is currently only programmed to support single module evaluation, leading to the use of two different computer systems for data acquisitioning. The problem arises that the time vectors of the concentration do not link up precisely with the time vector of the velocity electrodes, this will not influence the results due to the assumption that the flow velocity (in terms of a time constant) will remain constant throughout the experimental procedure, the velocity electrodes were also not be used in the experiments as for reasons explained at a later stage in the dissertation.

4. Experimental method and Explanation

Paragraph 4 covers the method used to determine the mass flow rate by means of using volumetric concentration and particle velocity. The computation of these properties was done using Matlab as basis for programming and can be broken into 6 stages that will be elaborated on in the paragraphs to follow. The stages are characterised as follows:

1. Data collection and manipulation.
2. Flow regime, Identification.
3. Concentration, Estimation.
4. Velocity, Estimation.
5. Calculation of mass flow rate.
6. Error estimation.

The hierarchy of relations between the categories can be seen in figure 33 which also indicates the logic of the approach followed to complete the whole process of calculating the mass flow rate.

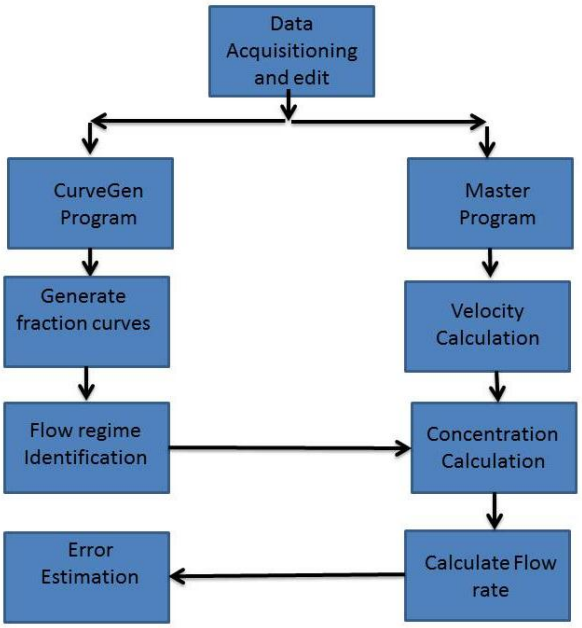

Figure 32: Program flow diagram

4.1. Data Acquisitioning and manipulation

As explained in paragraph 3.3.4 the raw data obtained from the evaluation module would be unsuitable for use without the manipulation thereof. The manipulation of the data is required due to the following data characteristics.

1. The data contained both numbers and strings within the same matrices.
2. The file contained multiple non-essential data elements.
3. The time vector was in the form of time increments and not a continuous time signal.

DataEditor.m was written to fix these problems by extracting only the capacitance and time signals from the data set using the xlsread.m function. The strings were then removed by means of assigning each columns (starting at the second entry) to a variable representing its property. After extracting the applicable data the time vector could be formed using the cumsum.m function to add up the individual time increments resulting in the applicable time signal.

The Concentration (C) and velocity (V) vectors are then written into csv files that contain only the required information. The naming of these files was also done according to their specific date and flow details. The raw data can then be used as an input into the master program with the advantage of having a more user friendly format and an improved processing time.

The master code is mainly used to extract the data from csv files (discussed above) that contain applicable data for the vectors corresponding to a 5 electrode setup (will be discussed in paragraph 4.2). The time vector was then evaluated to determine the applicable sampling frequency for both the velocity and concentration electrodes. The sampling frequency was calculated using the total number of samples taken over the time period and dividing them by the cumulative sum of all the individual sample time increments. The sampling frequency is critical in calculating the velocity of passing particle (discussed in paragraph 4.4) and will also be used in the frequency analysis..

$$f_{c\ or\ v} = \frac{N}{\sum \Delta t_i} \qquad [21]$$

Figures 33 and 34 represent samples of how the capacitance versus time signals would be represented when sand flows through the system. The figures also illustrates that the actual changes in capacitance are extremely small when compared to their baseline value and would require further signal processing in order to have signals that are comparable to each other(explained later). The large period of time that elapses before material starts to flow through the sensor is due to the delay in the system start up where the sampling should be started followed by the initiation of the electrical motor and thereafter material addition to the hopper.

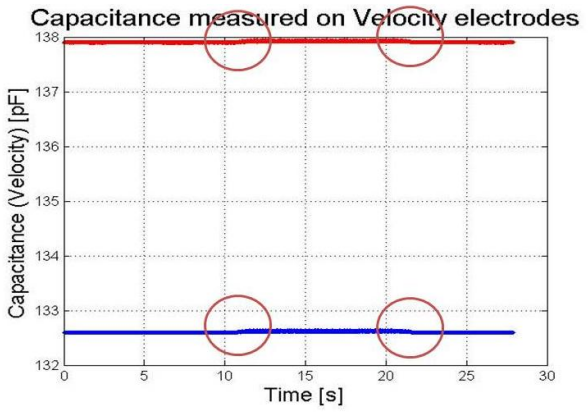

Figure 33: Raw data for the velocity electrodes

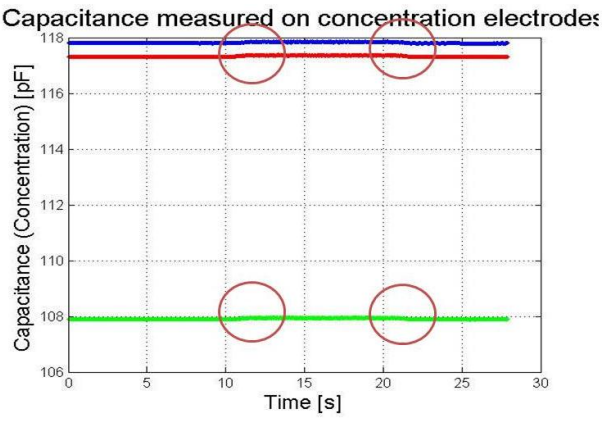

Figure 34: Raw data for the concentration electrodes

4.2 Flow Identification

4.2.1. Regime dependent experiments

The evaluation of the electrode system with induced flow regimes at a constant feeding rate resulted in the ability to evaluate the response of electrodes when variable flow regimes are induced into the control volume. This can be used as a basis for the estimation of flow rate or mass flow rate when the induced flow regime is known. If a flow regime identification technique is constructed it would lead to the possible reduction of the flow dependence for capacitive concentration measurements.

With this as the aim, a flow regime dependent experimental setup was constructed as seen in figure 23 and discussed in paragraph 3.2. For the evaluation of the three variable flow regimes multiple nozzles were created by means of using a 3D printer. The nozzles, as seen in figures 35 to 37, were printed to represent rope, annular and stratified flow regimes, and were also altered to resemble variance in the individual flow regimes by means of changing the geometrical properties of the nozzles (Increase or decrease flow rate by means of increasing inlet area).

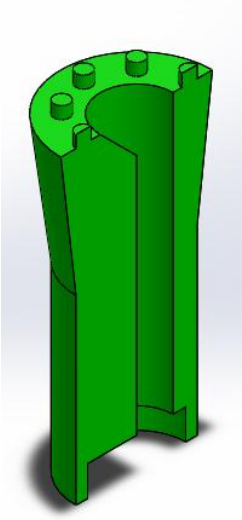

Figure 35: Stratified flow nozzle

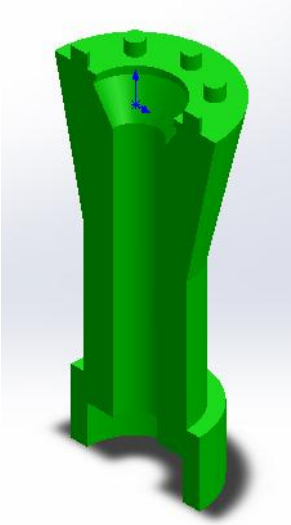

Figure 36: Rope Flow nozzle

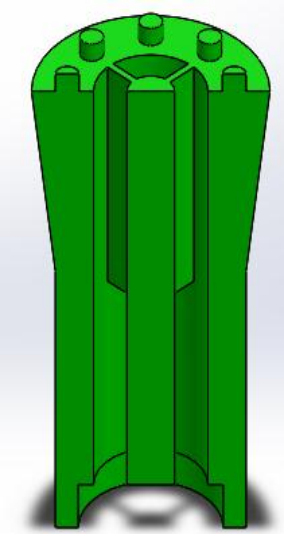

Figure 37: Annular flow nozzle

Experimental Procedure:

- Nozzle selection and rotation: Before the actual experiment the flow nozzle was selected and fixed to the pipe and sensors by means of a plastic overlap at the end of the nozzle. When testing stratified flow regimes the orientation of the actual stratified flow to the sensors was manipulated by means of rotation. After the completion of five tests at a certain angle the angle would be changed by 22.5 degrees in order to gain a more reliable representation of the effect of flow regime sensitivity with regards to sensitivity on the inside of the electrode when the stratified flow is rotated around the circumference of the pipe.(discussed in paragraph 4.3).

- GUI settings and measurement: Before the start of the experimental procedure steps were taken to ensure that the correct evaluation setting is selected and then ensures that the correct data storage path and names were selected.
- The two GUIs (due to program not able to evaluate multiple modules as explained in paragraph 3.2.3) are then started. Note although they are started separately the signal of both the sensors are edited to only use the applicable data (where solids are present in the control volume) in order to minimize the effect of small capacitance instability to add to the overall mass conveyed (concept is shown in figures 38 The reduction of the inapplicable signal was done by means of setting a signal applicability condition which reduces the signal to start at the first point where the signal rises above a specified percentage with regards to the maximum and minimum capacitance change values. Capacitive change (ΔC) refers to the change in capacitance from its base capacitance where no solid material is present in the control volume.
- Sand is then added to the hopper to enable material conveying through the nozzle which alters the flow regime through the sensors.

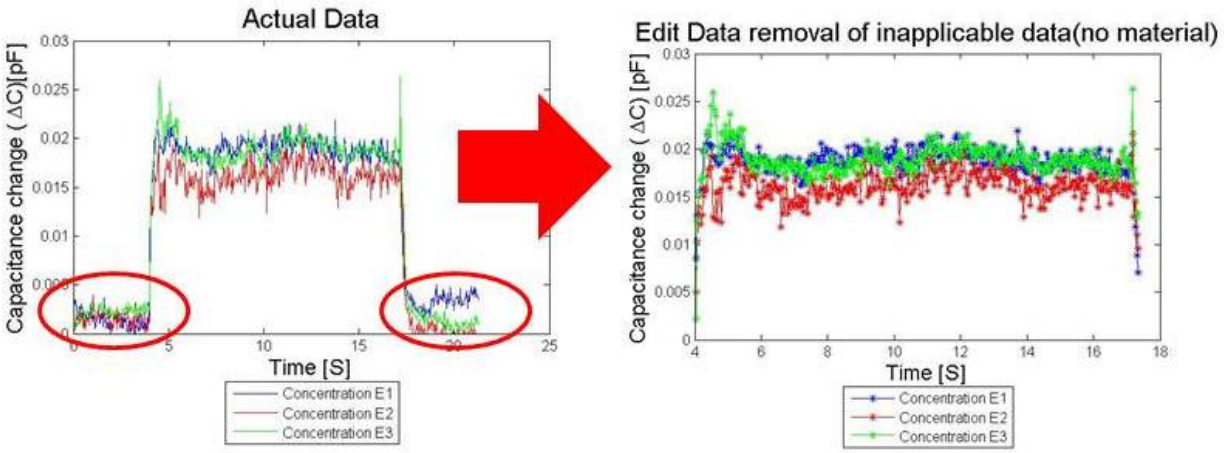

Figure 38: Removal of inapplicable data

- Further signal processing is required in terms of removing outliers from the data assuming a Gaussian proses. The applicable data string is then analysed by means of removing data points that fall outside the two standard deviation mark This means that 95% of the data remain the same while outliers with values larger than the mean plus two standard deviations are removed. The removed points are then replaced by the mean value. The process is then repeated till the difference in mean values, before the current alteration and after current alteration, is less than ten per cent. A representation of peak removal can be seen in figure 39. The decision was made to decrease the effect of a different flow regime (not representative of the calibration curve), representative of the short instance at the start and the end of the analysis where the system is not stabilized yet.
- The conveyed mass is then measured by means of a scale.

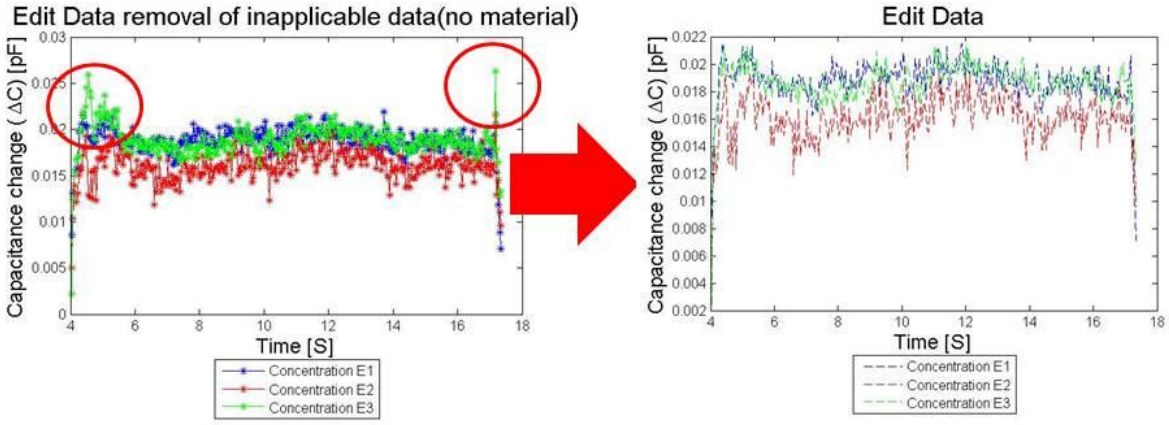

Figure 39: Removal of outliers from applicable data

- From there the data is converted to the required format and analysed by means of calculating what the theoretical volume fraction should be at the average capacitance values during the induced flow regime. The assumption of constant acceleration (because of gravity) is made and the velocity (V_{ei}) is then determined by means of using gravity and the distance that the solids have travelled from the inlet of the nozzle to each of the measuring electrode (d_i) as seen in equation 22.

$$V_{ei} = \sqrt{2(9.81)(d_i)} \quad [22]$$

$$\emptyset_i = \frac{m_{tot}}{\rho A V_{ei} \Delta T} \quad [23]$$

- The volume fraction which is then derived from the total mass conveyed (m_{tot}), material bulk density (ρ), flow area (A), solid particle velocity (V_{ei}) and the time taken to convey the material (ΔT) is shown in equation 23. After the completion of the volume fraction calculation the corresponding capacitance change would then be used to plot a capacitance change vs. volume fraction curve that can be used to determine the optimal equation representing a certain flow regime. The curve generation process was conducted multiple times at different volume fraction and flow regimes to have a valid representation of the actual effect of an induced flow regime on the capacitance reading.
- The data analysis was done by means of fitting the flow induced data to a "guessed" curve that is representative of the phenomenon of flow dependency described in paragraph 2.3.These flow curves can be characterised representing them with a linear (equation [26]) or exponential (positive equation [25] and negative equation[24]) approximation. The curves were purely used as a method of comparison to curves that represent differ types of flow regimes, which can be used as indication towards the initial guess for curve estimation. In equations 24 to 26 the change in capacitance from an empty to filled control volume is referred to as $\mathrm{Cal}_{\mathrm{Change}}$. and $\emptyset$ refers to the volume fraction.

$$f_{neg}(\emptyset) = \text{Cal}_{\text{Change}}(i) \times \frac{1 - 1.35^{-\emptyset}}{\max\left((1 - 1.35^{-\emptyset})\right)} \quad [24]$$

$$f_{pos}(\emptyset) = \text{Cal}_{\text{Change}}(i) \times \frac{1.45^{\emptyset} - 1}{\max\left((1 - 1.45^{\emptyset})\right)} \quad [25]$$

$$f_{lin}(\emptyset) = \text{Cal}_{\text{Change}}(i) \times \emptyset \quad [26]$$

- The fit is then analysed by means of evaluating 3 parameters namely the mean error, R^2 and the normalised cross correlation. The approximation of these parameters can be seen in Equations [27] to [29].where $\Delta C(\emptyset)$is representative of the capacitance change at the specified volume fractions. $\Delta C_{Est}(\emptyset)$ on the other hand represents the estimated capacitance for the specified volume fraction

$$\text{Mean Error}(\%) = \frac{abs\left(\Delta C(\emptyset) - \Delta C_{Est}(\emptyset)\right)}{\Delta C(\emptyset)}(100) \quad [27]$$

$$R^2 = 1 - \frac{\sum\left(\Delta C(\emptyset) - \Delta C_{Est}(\emptyset)\right)^2}{length\left(\Delta C(\emptyset)\right) \times var(\Delta C(\emptyset))} \quad [28]$$

$$NCC = 2 \times \frac{\sum(\Delta C_{Est}(\emptyset) \times \Delta C(\emptyset))}{\sum \Delta C_{Est}(\emptyset)^2 + \sum \Delta C(\emptyset)^2} \quad [29]$$

- The curve with the best error parameters was then used as basis for determining the applicable shape for the fraction to capacitance for that associated flow regime. From there the optimal equation for the fraction to capacitance curve was generated using an optimization method. The cases were the curve equation is dependent on flow orientation with regards to electrode position will be investigated by means of rotation the induced flow around the circumference of the pipe in an 22.5° interval sequence resulting in curves representing each electrode pair for intervals of 22.5° rotation.

Statistical Analysis

To determine the number of tests that was required for establishing the flow regime dependent curves. A statistical analysis was done. During this analysis 17 consecutive tests were done using the smaller rope inducing nozzle. The aim of the experiment was to determine if the use of five data sets were sufficient to make a viable representation of the actual capacitance change when a certain flow regime is induced.

The statistical analysis was done using data as described above after it has been edited as explained in the experimental procedure section of paragraph 4.2.1. The average capacitance for each electrode during each experiment was then used as basis for comparison with other 16 tests.

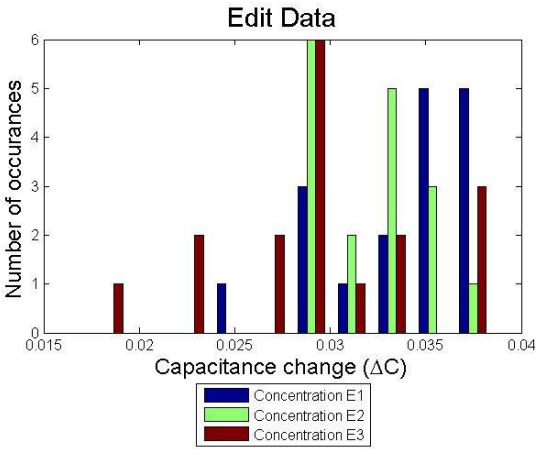

Figure 40: Histogram of data distribution

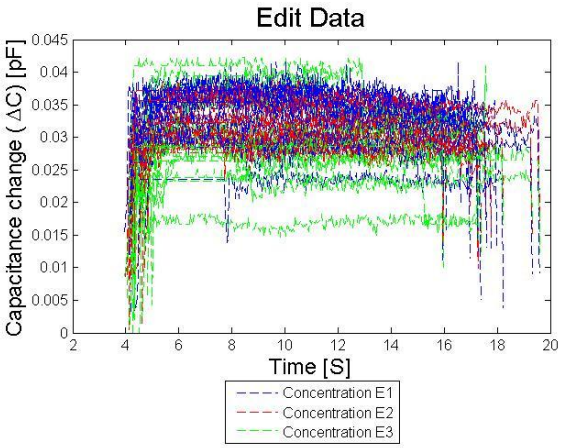

Figure 41: Data used for statistical analysis

The result showed that the data are roughly spread in a normal distribution fashion (showed in figure 40) with the corresponding capacitance signals showed in figure 41. The results show that some outliers do occur within the data sets. Even though there are outliers small standard deviations show that the variation in data is small and would provide reliable data. The standard deviation for each of the electrodes can be seen in table 6.

Table 6: Standard deviation of statistical analysis

Standard deviation		
Electrode 1	**Electrode 2**	**Electrode 3**
0.0037	0.0025	0.0053

From the above experiments it is clear that the assumption of using 5 experiments for the calculation of a flow regime dependent calibration curve would be viable and would also provide a sufficient representation of the effect of a change in the flow regime.

Discussion and results

The following section cowers the preliminary results of the curve based experiments and show the logic used in determining the input parameters for curve optimization.

Rope flow

The rope flow experimental procedure followed was as follows:

1. Attach the applicable flow nozzle according to previous experiments (increasing rope diameter).
2. Conduct the experiment 5 times to increase reliability (showed in statistical analysis section).

3. Proceed to the next nozzle diameter to simulate an increase in the volumetric fraction.

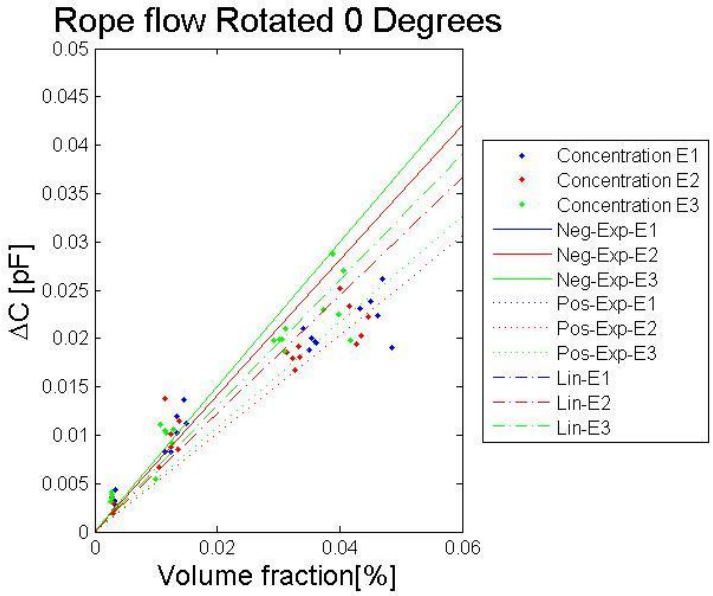

Figure 42: Curve Generation rope flow

The results showed in figure 42 indicates that the fit of a positive exponential or linear function as shown in equations [25 and 26] will produce a better fit than negative curve for the third and fourth set of experimental results. On the other hand the first and second sets (where sets refer to data bundles representative of different flow induction nozzles) show a tendency to be larger than the linear and negative exponential functions. The conclusion that the influence of noise on the system, at such a low capacitance reading, may have a significant influence on the results, in the form of measuring a higher capacitance change reading on the specific volume fraction than expected. Although the noise seems to be minimal it contributes in a significant manner when such small changes in capacitance are measured.

As expected the results of the experiments (set 3 to 4) display the characteristics of core flow as shown in paragraph 2.5. and figure 18. Similar to the experiments of Irons and Chang the introduction of rope or core flow caused a fraction curve representing a shape similar to a positive exponential curve.

The results also indicate that a visible difference occur between each of the three concentration electrodes. The difference in capacitance measurement can be explained by noting that the calibration capacitance of the electrodes differ (E1 tends to have a higher capacitance when filled with sand) and by the time the rope flow reaches electrode 3 (which is downstream of the other electrodes E1 and E2) it has dispersed more resulting in a homogeneous flow regime which according to theory should have a linear volume fraction to change in capacitance, and is also the case for the conducted experiments.

Stratified Flow

The stratified flow experimental procedure followed was as follows:

1. Attached the applicable flow nozzle according to previous experiments (increasing stratified region shown in figure 43).
2. Conduct the experiment 5 times to increase reliability.
3. Rotate the nozzle 22.5° to change material position with regards to the electrode positions.
4. Repeat steps 1 to 3 until a 90° rotation of material position with regards to electrode position have been achieved.
5. Proceed to the next nozzle size to simulate an increase in the volumetric fraction.

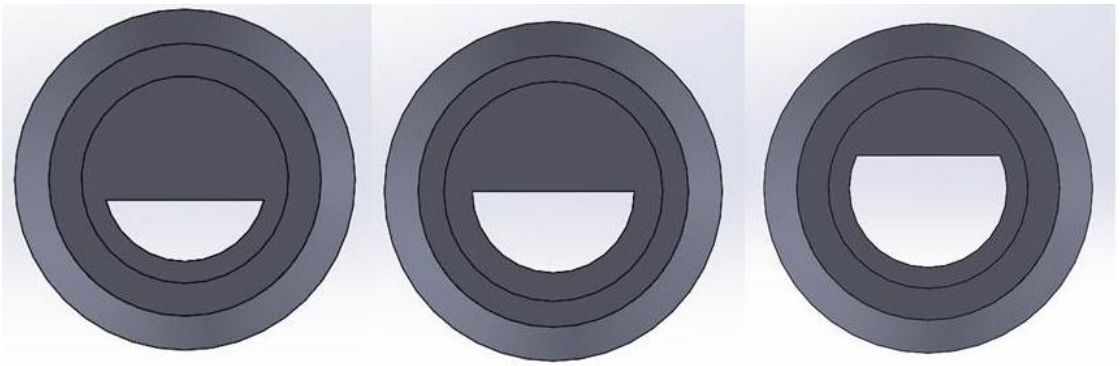

Figure 43: Nozzles for stratified flow

As expected the results varied for each rotation with regards to the electrode position and is shown in figures 44 to 50 .

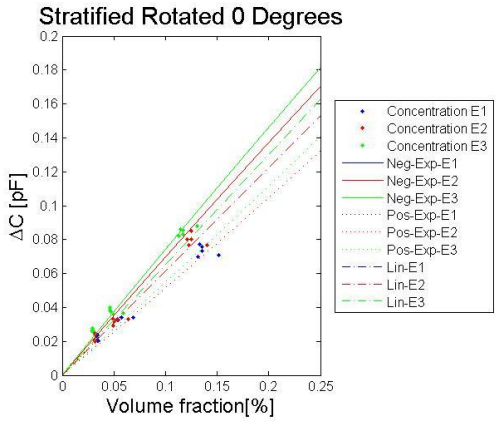

Figure 44: Stratified flow 0 °

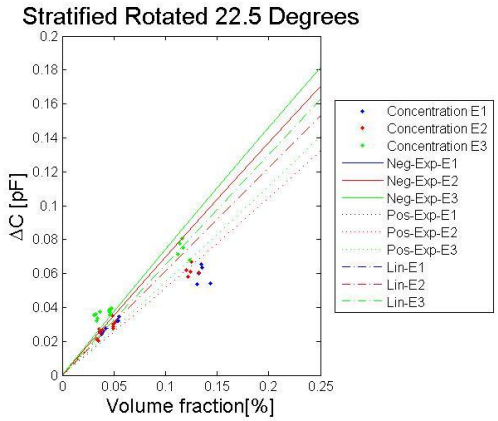

Figure 45: Stratified flow 22.5 °

The idea of evaluating different positions of flow with regards to the position of the concentration electrodes are based on proving that for the same volume fraction different changes in capacitance would be observed. This visible change is due to the sensitivity fields of each electrode being shifted according to the placement around the circumference of the pipe as discussed in paragraph 3.2.1.

The concept of plate sensitivity is clear when analysing figures 44 and 45, when taking the first two cluster of each experiment into consideration one will see that the capacitance change for concentration

electrode 1 and 3 increases probably because more solid material is present in the sensitive region of the electrode pairs due to the 22.5° degree shift.

Figure 45 indicates that the 3 clusters of data can be related as majority of the points fall on the same fitting line, for instance for all 3 instances electrode 3 shows a negative exponential function would fit the best, where positive and linear fit would be viable for electrode 1 and 2. In contrary to figure 45 cluster 3 moves downward for all 3 electrode pairs where in cluster 1 the capacitance change for electrode 3 increase. This results in fraction curves for each cluster set.

Figure 46: Flow rotated 0°

Figure 47: Flow rotated 22.5°

Figure 48: Flow rotated 90°

The phenomena can be explained by analysing figures 46 to 48 where the same angle is use for variable flow regimes, in these figures the changes in nozzle size affect the capacitance measurements in terms of solids falling within or outside of an electrodes sensitive field. To explain this concept further, all three solid distributions fall on the edge of the left and right electrodes top sensitive regions for figure 46, where only 2 of the distributions cover the same region in figure 47 resulting in a lower capacitance reading for the same solid distribution (smallest distribution or faded brown), and volume fraction. Then when looking at figure 46 for the same small distribution no material are situated at most sensitive regions with the implication that the lowest capacitance measurements would be made for the same nozzle and solid density.

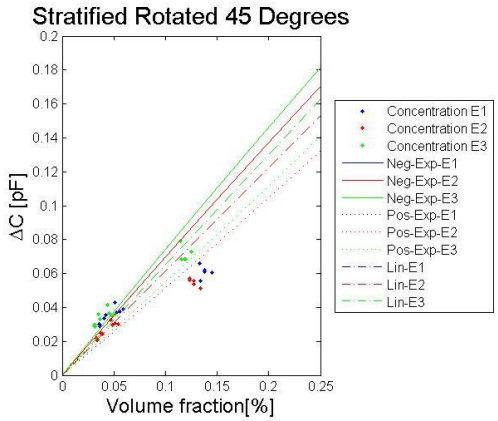

Figure 49: Stratified flow 45°

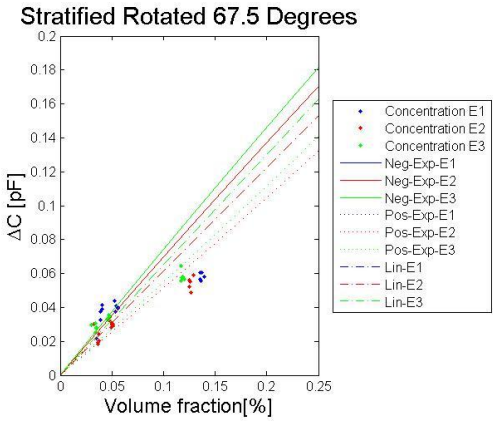

Figure 50: Stratified flow 67.5 °

When the solid geometry is further rotated (45° or 67.5°) it is moved into a sensitive region of the electrode 1 resulting in a slightly higher capacitance reading than for the 0° - 22.5° cases. Electrode 2 and 3 show a decrease in capacitance indicating that the solid material is situated further from the sensitive areas than the 0° - 22.5° cases. Again the characteristics change slightly with the third cluster of tests where all cases are shown to be in a less sensitive area except for electrode 3 at an angle of 45° that results in a closer proximity to the linear approximation this fit then fades as the flow is shifted to 67.5° resulting in a fit that is better captured the negative exponential.

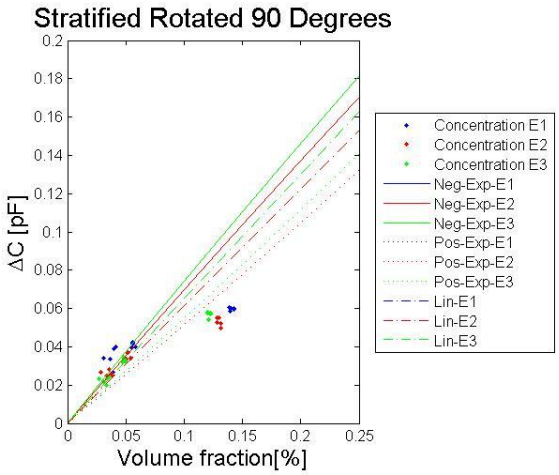

Figure 51: Stratified flow 90 °

It is also clear that the last (third) cluster of data points, corresponding to the largest volume fraction is significantly lower for electrode 3 at 90° and will be most likely be due to the movement of solids out of sensitive regions as the nozzles are rotated. The opposite can be used to explain the increase in capacitance for electrode 1 in cluster 1 and 3 that indicates a movement of solids into a more sensitive region of the electrodes.

In conclusion it can be seen that the connection of clusters through rotation cannot be directly linked due to the sensitivity fields of electrodes and how the solid distribution falls within these sensitivity fields. The use of different size nozzles to induce a variation in volume fraction also only influences the capacitance measurement within a certain margin. In order to achieve a better representation of the fraction curves the volumetric density of the solids within the induced shape should be changed (refer to figure 52 for more clarity). There was a limit to this as the induced flow density could not be adjusted to required shape since the experiments were done by means of the gravity chute.

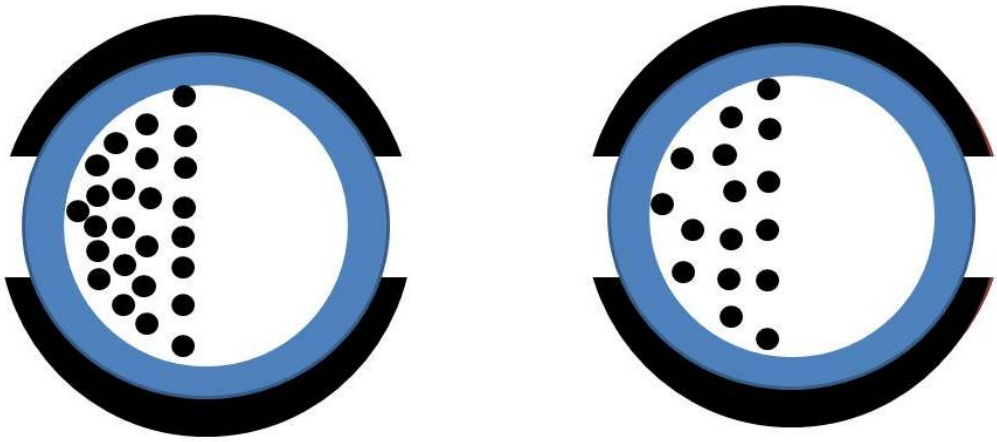

Figure 52: Variation in concentration for a fixed solid volume

Therefore an optimized equation would be calculated for each flow nozzle instead of using all three clusters of data as it is clear from most of the tests that the effect of variation in volumetric concentration according to the solid volume and position of this solid volume would cause a problem in terms of determining an optimal equation. This due to the fact that each data cluster is representative of a different variation in that specific regime. This will lead to the determination of an optimal fraction curve for each nozzle size. This comes as the assumption that a variation in the optimal fraction curve would change as solid volume fraction changes in terms of the actual volume occupied by the solid material.

Annular Flow

The same procedure was used for the annular flow regime experiments as explained for the rope experiments

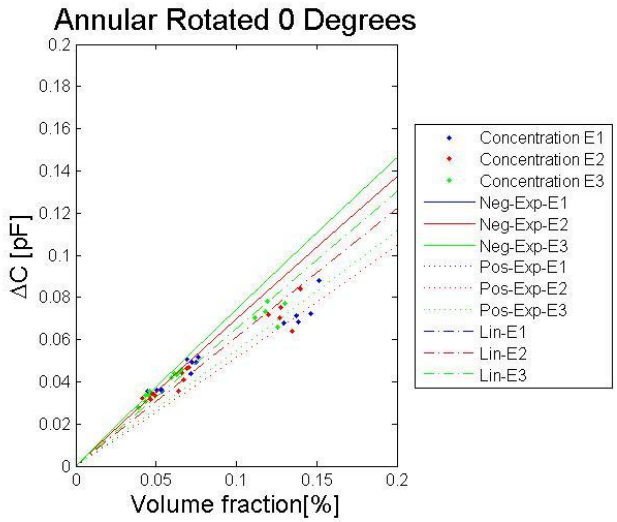

Figure 53: Fraction curve Annular flow

The annular flow regime experiments were conducted over a much larger fraction range than the rope flow experiments and proved to better fit a negative exponential function than a positive power function. This result is as expected as the curve of Irons and Chang show similar results for annular flow. Similar to the previous regime experiments the influence of actual volume that solids occupy and their corresponding volumetric density would influence the actual optimal curve. With this said it is clear that the optimal curve for cluster 1 and 2 would be a negative exponential function where cluster 3 shows a better resemblance to the positive exponential function and can be rather contradictory to the curve generated by Irons and Chang.

The large difference in change in capacitance for cluster 3 is a good indication that probable miss alignment of flow system occurred resulting in flow either simulating flow circumstance closer to homogenous or stratified flow regimes. The representation of other flow regimes will be taken into consideration when determining the optimal fraction curve as the inclusion of such data points will only result in large scale errors.

Auger fed system

In addition to the induced flow regimes that have a constant flow pattern an investigation was done into the effect of having a periodic feeding system. The problem with using a system without a constant flow regime is that the relationship of volume fraction to capacitance is unknown and might be a combination of multiple flow regimes as the wave or slug passes through. The flow will also result in an unstable reaction of the electrodes as the distribution and concentration will change constantly. Resulting in a capacitance reading that changes rapidly as the material flows through the control volume.

One can see from figure 54 that the reaction of electrodes are considerably different from a linear assumption as the fraction to capacitance of all 3 concentration electrodes were more related to an Negative exponential due to an overreaction in capacitive change caused by the presence of solids within the most sensitive regions of the electrodes. The variation in electrode 3 indicates that some of the conveyed material fell on the border of the electrodes most sensitive regions. The results are similar to the findings of the annular regime experiments and would overestimate the mass conveyed caused by the rapid change in capacitance.

The effect of overestimation can be minimised by means of using a calibration curve that represents a lower concentration reading for the same capacitance change, similar to the generated curve of the annular flow regime. It is expected that this method will not be as accurate and reliable as the flow specific experiments due to the inconsistent flow regime but would still prove to be an improvement on the actual estimated conveyed solids.

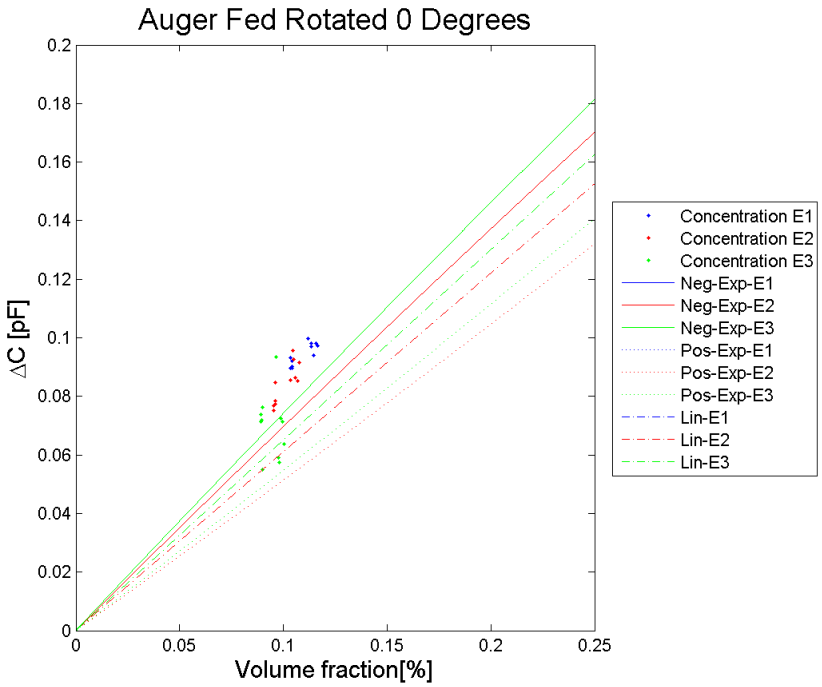

Figure 54: Auger fed experiments

Curve Optimization

As described in the previous paragraph the use of an optimization method was required to determine the equations that will fit each tested flow regime the best, as these equations will be used as means of compensation for circumstances where flow regimes are not fully homogeneous. Continuing from the previous section a base equation was used as governing function for the electrodes, and was chosen in such a manner that it can be used as a positive or negative exponential equation and is shown in equation 30. Where $w(1-4)$ is representative of constants that will determine the shape of the assumed regime dependent curve.

$$\emptyset(\Delta C) = w(1)\left(w(2)^{w(3)\times\Delta C} + w(4)\right) \quad [30]$$

The process of optimization was done by means of using fmincon.m that focuses on the optimization of problems that are constrained by certain properties, as is the case of the investigated problems which all have a maximum and minimum capacitance change value. The choice of using a constrained method was based on the knowledge that the change in capacitance without any solid material present in the system should be equal to zero and the full loaded system (contains a volume fraction of 1) should be equal to the calibrated values for each electrode, resulting in a minimum and maximum value for each electrode curve. Equations 31 to 32 show how these equalities were chosen and set.

$$\emptyset_{start} = w(1)\left(w(2)^{w(3)\times 0} + w(4)\right) = 0 \quad [31]$$

$$\emptyset_{end} = w(1)\left(w(2)^{w(3)\times Cal_{change}} + w(4)\right) = 1 \quad [32]$$

The line of best fit was determined for each of flow regimes and their associated test sets by means of minimizing the error between the actual volume fraction (obtained through experiments) and the anticipated volume fraction.

Rope flow

The fraction curves generated illustrates (figure 55 to 57) the conclusion made earlier that for the two smaller diameter rope flow regimes (cluster 1 and 2 from figure 42) the noise overpowers the signal itself and would cause an incorrect interpretation by representing a fraction curve belonging either a stratified or annular regime. This conclusion further emphasizes why the decision was made to remove these data sets as viable information for characterization of the rope flow regime

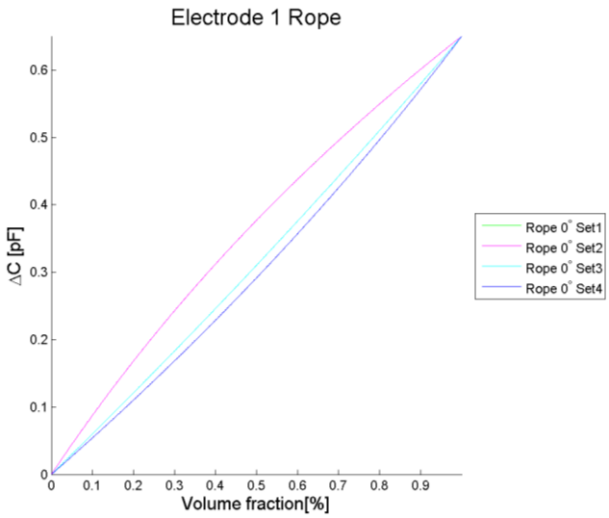

Figure 55: Fraction curves rope flow electrode 1

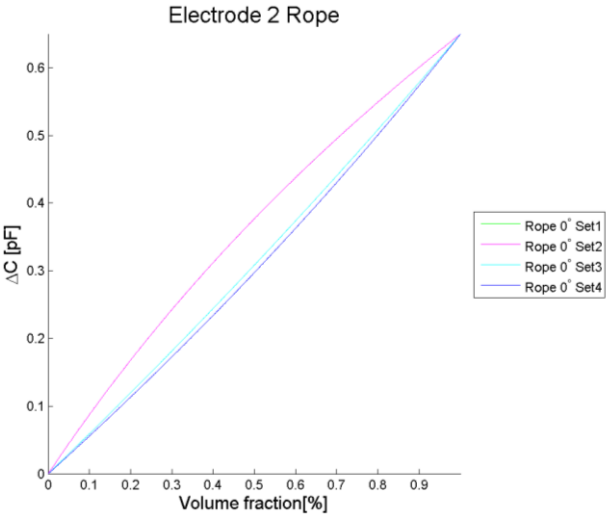

Figure 56: Fraction curves rope flow electrode 2

When analysing set 4 (representing the largest nozzle diameter) one can see that the further downstream the electrodes, the more dispersed the regime becomes and the closer the fraction curve becomes representative of a homogenous flow regime. refer to the shift of set 4 in figures 55 to 57 from curved to almost linear, emphasizing the dependency of capacitance change with regard to variable flow regimes. Table 7 and 8 show how the optimal curves differ for each of the data sets according to their nozzle sizes. This shows the tendency of data sets 1 and 2 to be seen as a different flow regime who's fraction curves are not representative of rope flow but would be more representative of annular or homogeneous flow regimes.

Table 7: Optimal parameters set (1 and 2) for rope flow

	Set 1				Set 2			
Electrode	w(1)	w(2)	w(3)	w(4)	w(1)	w(2)	w(3)	w(4)
1	1.0941	2.4391	1.1936	-1.0941	1.0943	2.439	1.1935	-1.0943
2	1.0942	2.4389	1.1936	-1.0942	1.0942	2.439	1.1935	-1.0942
3	1.1521	2.0535	1.336	-1.1521	1.1091	2.2389	1.2268	-1.1091

Table 8: Optimal parameters (set 3 and 4) for rope flow

	Set 3				Set 4			
Electrode	w(1)	w(2)	w(3)	w(4)	w(1)	w(2)	w(3)	w(4)
1	-6.0341	526.91	-0.0474	6.0341	-2.9449	5.7635	-0.38829	2.9449
2	-5.3996	450.76	-0.05494	5.3996	-3.4532	18.604	-0.19173	3.4532
3	-11.771	308.55	-0.02383	11.771	-8.9951	66.693	-0.04317	8.9951

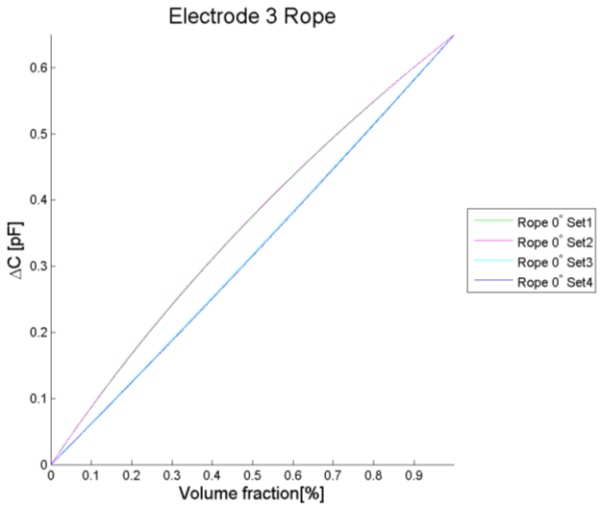

Figure 57: Fraction curves Rope flow electrode 3

Stratified flow

The variation in optimal equations for each cluster during stratified flow tends to be much larger than with rope flow and should be as the material is rotated into as well as out of the sensitive regions of the electrode as shown in figures 46 to 48.

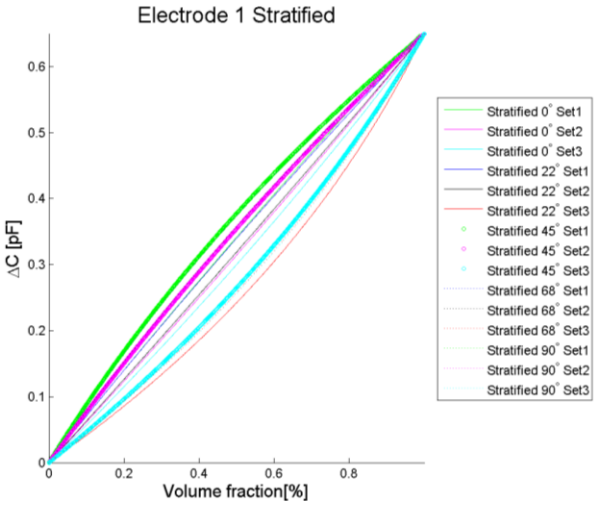

Figure 58: Fraction curves stratified flow electrode 1

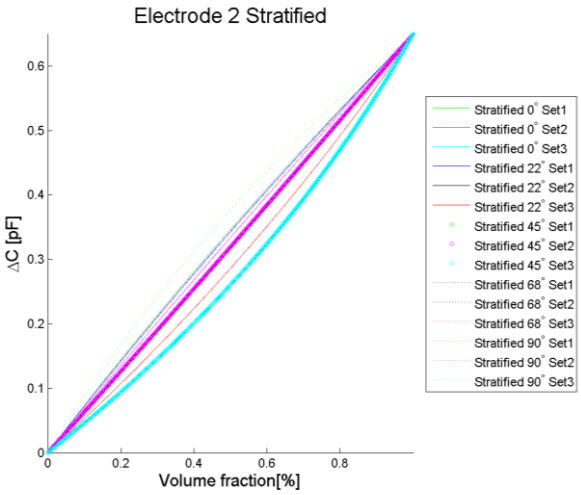

Figure 59: Fraction curves stratified flow electrode 2

Finding generalised equations that can simulate the effects of stratified flow would be challenging as the relationship between the materials position and electrodes sensitivity field should be known currently the method would require a more in depth research into the capacitors sensitivity field and lies outside of the current scope of work.

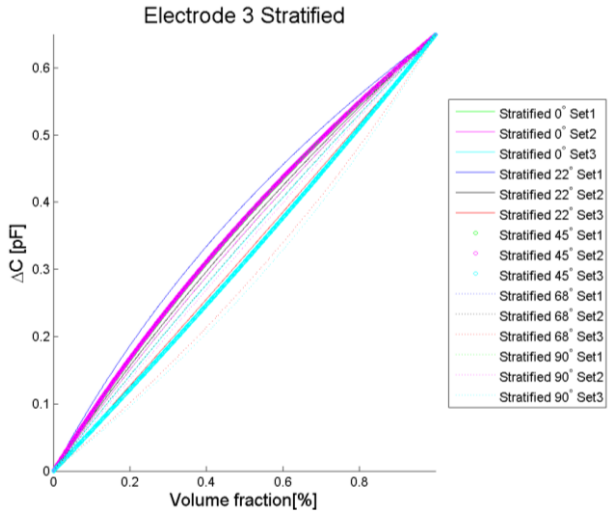

Figure 60: Fraction curves stratified flow electrode 3

Similar to rope flow the magnitude of deviation from a linear approximation fades when the material moves further down the gravity chute resulting in a more linear curvature due to the dispersion of material. This characteristic results in a curve selection that is unique to each conveying system, linking the selection not only to the actual flow regime but to other characteristics like dispersion. From this it is clear that if the decision is made to create generalised equations for each flow regime these equations would be linked to the electrode pair rather than creating a set of equations for all of the electrodes.

Annular flow

Figures 61 to 63 illustrates the statement that for set 3, the experiments' induced regime tends to be very close to a homogeneous regime. The phenomena can be explained by knowing that dispersion of particles will commence to the centre of the pipe centre, which is less dense that the circumference of the pipe.

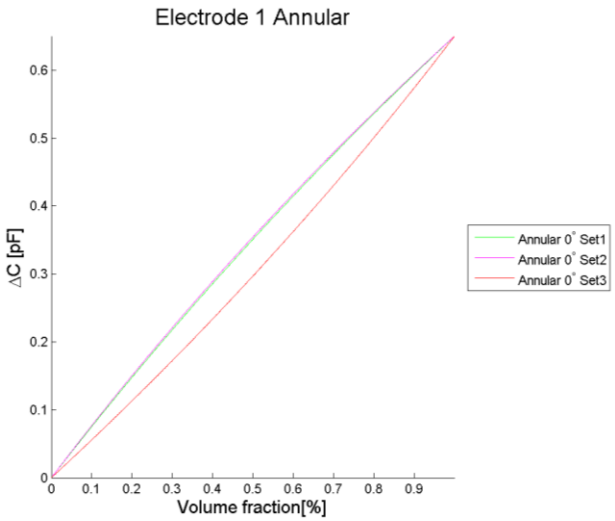

Figure 61: Fraction curves annular flow electrode 1

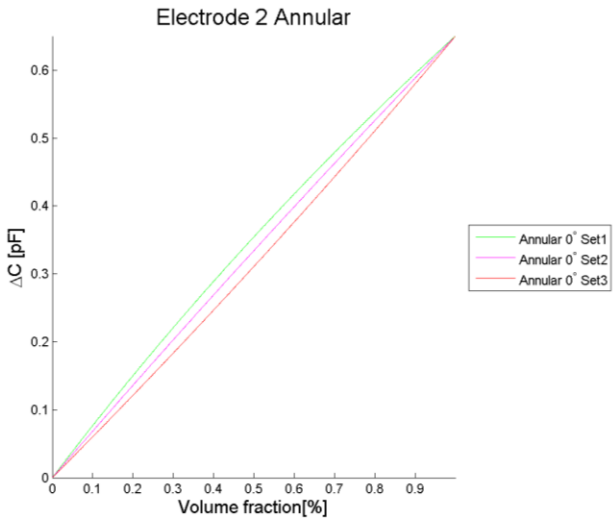

Figure 62: Fraction curves annular flow electrode 2

Similar to all the previous regime analysis the fraction curves for all flow sets tend to linearize more due to dispersion, as the solid material move downwards from electrode pair 1 to 3.

Table 9: Optimal parameters (set 1 and 2) for annular flow

	Set 1				Set 2			
Electrode	w(1)	w(2)	w(3)	w(4)	w(1)	w(2)	w(3)	w(4)
1	2.6342	8.4251	0.24753	-2.6342	2.2762	6.8558	0.31006	-2.2762
2	2.2911	7.1008	0.30277	-2.2911	8.3092	1.9081	0.28834	-8.3092
3	2.2307	5.4086	0.33755	-2.2307	5.6277	1.6963	0.47618	-5.6277

Table 10: Optimal parameters (set 3) for annular flow

	Set 3			
Electrode	w(1)	w(2)	w(3)	w(4)
1	-3.4051	30.87	-0.16618	3.4051
2	-6.2681	75.959	-0.0658	6.2681
3	-6.3554	75.434	-0.06092	6.3554

In general one can see that the closer to homogeneous flow regime the more variation in the optimized variable occurs. The optimal parameter for set 3 also differs significantly from parameters of set 1 and 2 suggesting that the flow cannot be associated with annular flow as it does not poses the same characteristics (refer to table 9 and 10).

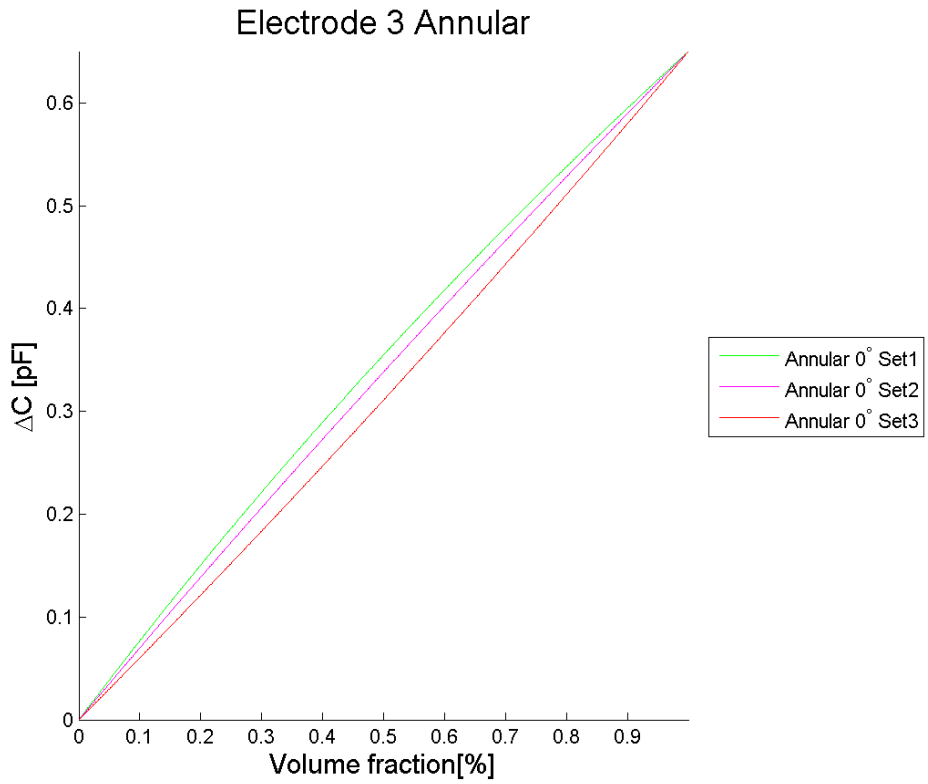

Figure 63: Fraction curves annular flow electrode 3

Auger fed flow

An investigation into the reaction of systems fed by means of an auger showed that the reaction of electrodes resembled a fraction curve that would give a lower fraction estimation towards the same capacitance measurement for the linear assumption. Similar to the previous 3 cases the readings of electrode 3 seems to differ slightly from the other 2 electrode pair readings as factors such as dispersion and electrode position would have an influence resulting in an representation that would lead to an approximation that is more representative of an linear approximation.

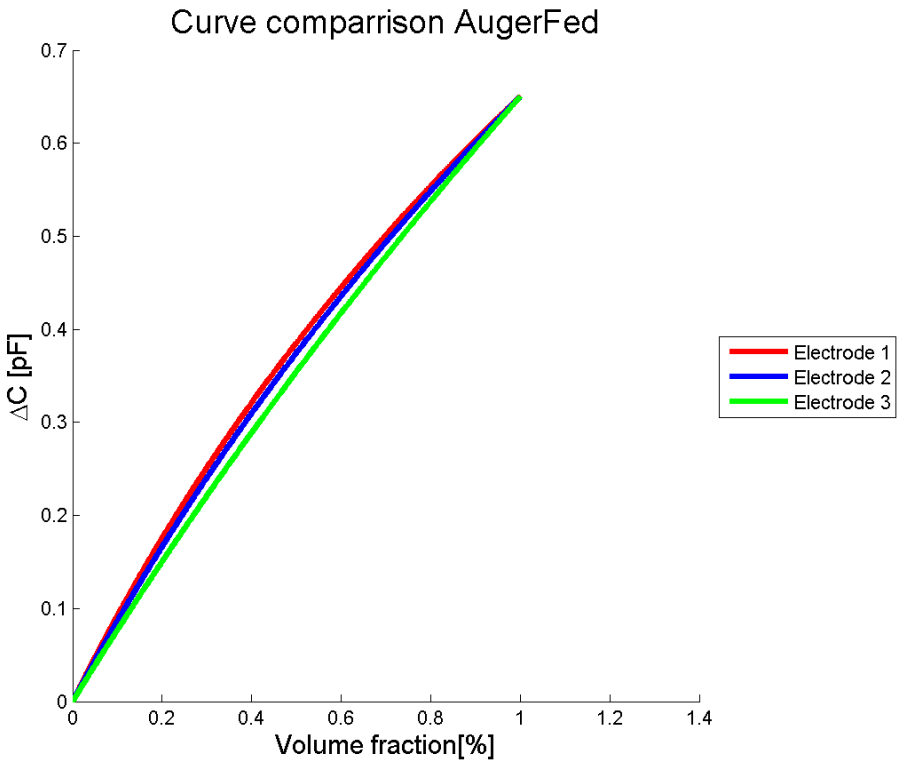

Figure 64: Fraction curve for an auger fed system

The resultant fraction curve shows that in an overall view the flow produces characteristics similar to that of a constant annular flow regime. The phenomena can be explained in light of the large fluctuation in capacitance signal as waves flow through the control volume resulting to a overestimation of solid concentration but is not only limited to the fluctuation and can be caused by solid distribution and relative electrode positioning as well.

4.2.2. Regime Identification

The implementation of a successful method to determine the actual flow regime experienced will aid the improvement of flow regime sensitivity of capacitive sensor by using the curves suggested in paragraph 4.2.1 to calculate the actual mass flow rate. In general the classification of types of flow regimes were characterised into two methods namely:

- Support vector machines.
- Decision tree classification based on data properties.

Support vector Machine classification

Bishop states in his book that the use of support vector machines is an increasingly popular method for classification of data sets (Bishop 2006). SVM or support vector machines are optimization based functions that aim to maximize the margin between 2 data points by means of using a surface. Bhuvaneswari and Kumar (Bhuvaneswari & Kumar 2013) states that support vector machines can in broad be used for the classification of 3 types of data sets namely:

1. Linearly separable data, which refers to data sets that can be separated by a linear line without any misclassification.
2. Linearly inseparable refers to data that contain errors like noise that could lead to misclassification. The use of a slack variable that represent the error of misclassification is then used as a compensation for misclassified data points.
3. Non-linearly separable refers to data points that are not able to be linearly separated but can be separated by means of using a higher dimensional mapping method as shown in figure 65. Bhuvaneswari and Kumar also explains that the type of kernel functions determine the mapping function.

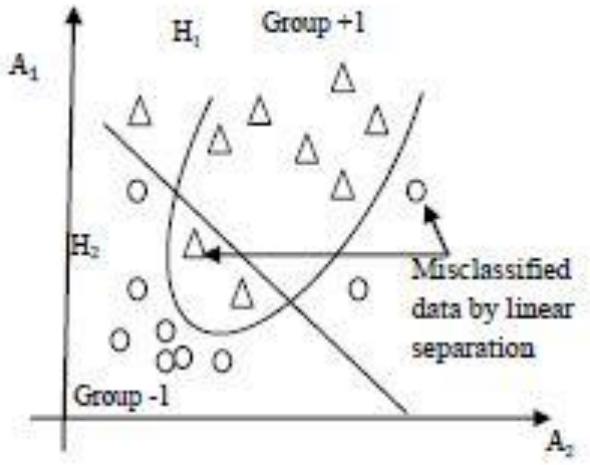

Figure 65: Non-linear data separation through the use of kernel functions (Bhuvaneswari & Kumar 2013)

Bishop explains this by using linearly separable data as explanation. In figure 66 the margin shown (distance between the red line and the blue lines) is used to define the decision boundary and is equal to the perpendicular distance between the decision boundary and the closest data points.

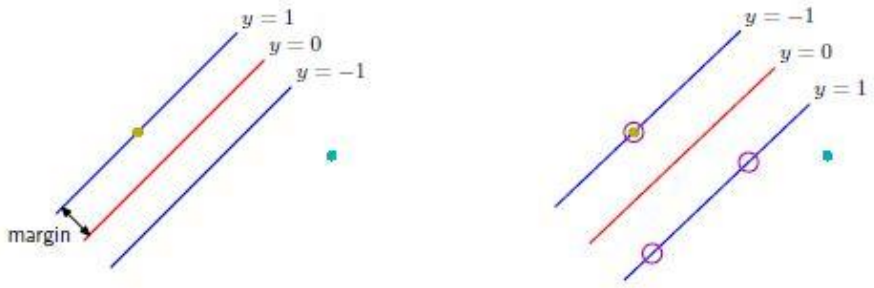

Figure 66: SVM on Linearly separable data(Bishop 2006)

.

The data points closest to the decision surface are then defined as the support vectors and is indicated in figure 66 as purple circles. As discussed earlier the margin is optimized resulting in a decision boundary that divides the data set into two classes. The use of a support vector machine for classification of data that is not linearly separable is also possible and can be seen in figure 67 where the use of a kernel function enabled the separation of 2 classes that were not linearly separable.

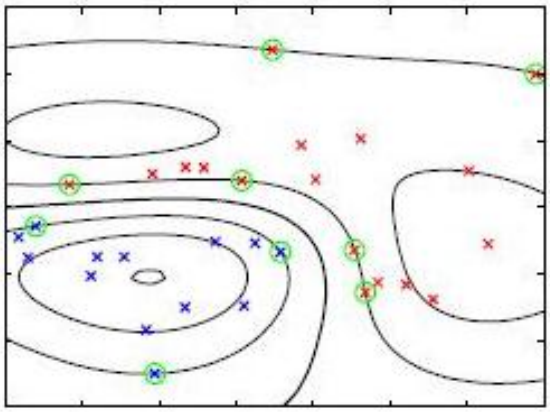

Figure 67: SVM on non-linearly separable data (Bishop 2006)

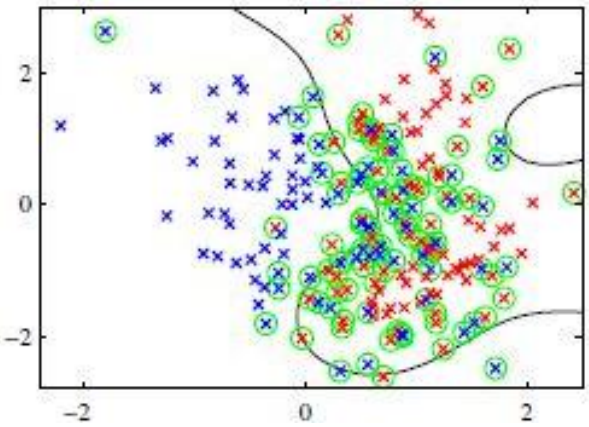

Figure 68: SVM on non-Linearly separable data with interfering data points (Bishop 2006)

Flow regime identification is done by means of using support vector machines as it will help significantly in identifying the actual flow regime present in the system where simple user defined cut of values are not easily defined. The properties that are used for input into the SVM's are as follows:

1. Correlation coefficient of the capacitive change measured for each electrode. The use of correlation would help identify whether the solid material present in the measurement volume is evenly distributed over the most sensitive regions of the electrode pairs. Where a high

correlation coefficient for all 3 electrodes would be representative of a flow regime where the solid distributions are similarly spreaded over the sensitive regions of all three electrode pair.

2. The change in capacitance between electrode 1 and 2, 2 and 3, 1 and 3 will indicate the distribution of material with regards to the sensitive regions. This measurement can be used in a similar fashion than the correlation coefficient but with a difference in the form of having a measurement directly related to the actual capacitance measurement. The difference is showed as Diff in figures 69 and 70.
3. The standard deviation of each of the raw concentration signals. The concept of using standard deviation is based on the fact the standard deviation is representative of the reactance of electrodes to material present in the measurement volume. A variation in position and shape will cause an increase in variation of data.
4. Percentage Diff was also added to establish how big the difference between electrodes where with regards to the maximum capacitive measurement of each electrode this will indicate to what degree the measurements differ from each other showing if the electrode difference is high with regards to actual measurement or if the difference is only marginal.

The basis for making these decisions can be seen in figures 69 and 70 where a comparison is made between the properties of each flow regime.

In addition to these properties above the maximum, minimum and average values for the properties will also be added to gain even more insight on how these flow regimes differ from each other. These properties was then used as inputs to a support vector machine program that used 60% of the data to train the program and 40% to test the program.

During the investigation using support vector machines the student found that the program found it hard to establish a difference between rope and annular flow but was capable of establish a difference between whether the flow was stratified or not. Meaning that a decision tree can be created into which the characteristics are used to identify firstly if the flow is stratified and auger fed or rope and Annular. if the data wasn’t classified as stratified or auger fed the characteristics will be fed into a similar SVM with the difference that the training and testing data used will only be of that of rope and annular flow regimes.

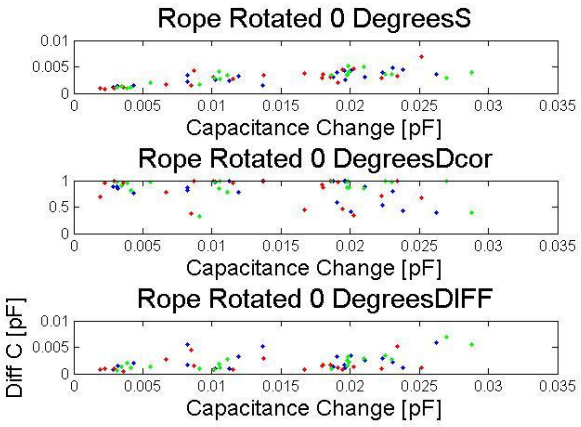

Figure 69: Statistics Rope flow

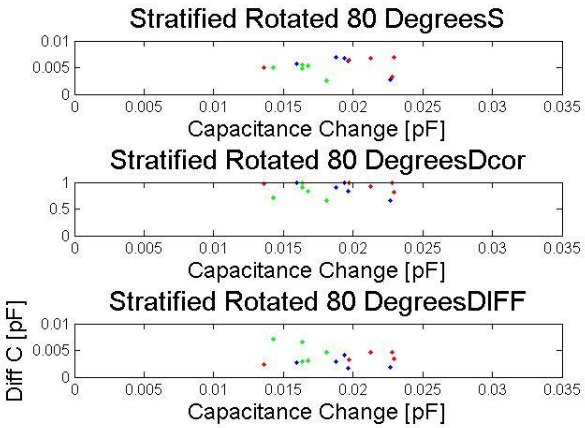

Figure 70: Statistics Stratified Flow 280 Degrees

The structure of the decision tree used can be seen in figure 71 and the associated properties used for the SVM's in tables 11 and 12.

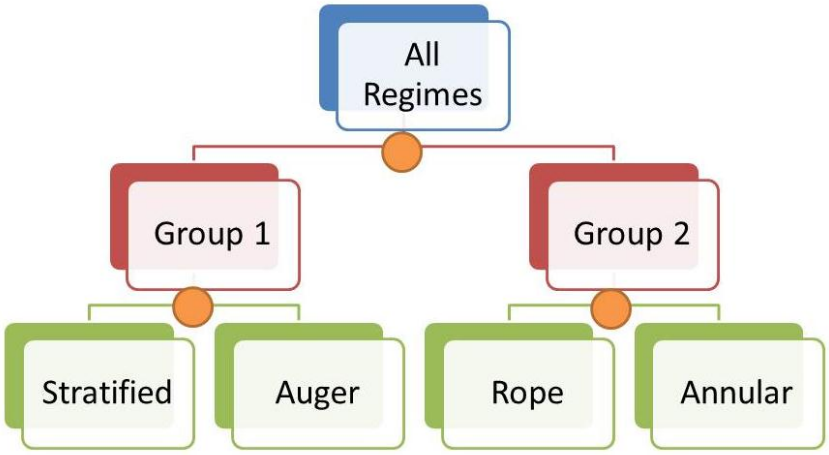

Figure 71: Decision tree hierarchy

Group 1 and 2 separation

Table 11 indicates what information was used to determine whether the flow was classified as either stratified/auger or rope/annular. The property that governed the choice for determining what characteristics to use for this decision was the fact that stratified flow or an auger fed regime is not necessarily evenly spread over all the sensitive regions for all 3 concentration electrode pairs. Whereas for annular and rope flow these distributions will most probably have similar reactions for all 3 electrodes as the solids are most likely concentrated at the centre or the circumference of the pipe.

Table 11: Properties for group 1 and 2 separation

Property	Min	Max	Average	Individual
Std. Dev.		√		√
Diff		√		
Cor.	√	√		
% Diff		√	√	

When using the specified characteristics from table 11 the program was able to identify whether all 43 test sets were group 1 or 2 when a training set of 54 data sets were used (giving a ratio of 44% of data used for testing and 56% of data used for training). The use of the properties as specified in table 13 led to a 100 % accuracy with regards to separation of group 1 and 2 and is shown in figure 72 where the accuracy of the SVM was plotted in terms of a grid search over a variety of values for gamma and cost.

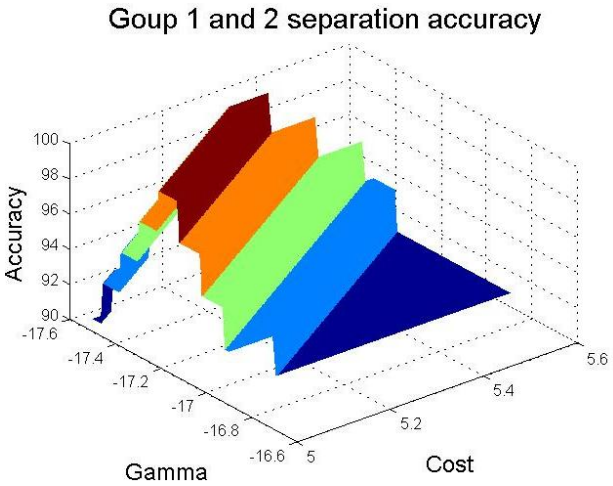

Figure 72: Accuracy for identifying group 1 regimes

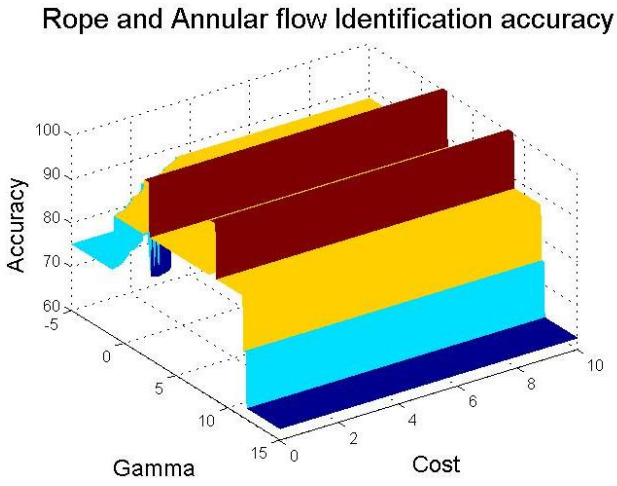

Figure 73: Accuracy for identifying group 2 regimes

Group 2 Separation

Table 14 indicates what information was used to determine whether the flow was rope or annular. It is anticipated that difference in the respective capacitance measurements for each electrode pair will be different for annular and rope as the bulk of solid material for rope flow falls in the less sensitive regions of the electrodes and if the regime deviates from the centre it will cause a larger change in the electrode

measurements as the deviation will occur in a more sensitive area (refer to figure 25). The opposite is true for annular flow as any deviation of solids will occur to the centre of the pipe into the less sensitive regions, as this results in solids moving into sections further away from the electrodes, that in effect results in smaller capacitance changes for the same volume fraction. The use of input data as chosen in table 12 led to the positive identification of all flow cases within the rope and annular group. A total of 20 data sets were used for the identification (10 sets for each flow regime), of which 40% or 8 sets were used in testing and the remainder for training of the SVM.

Table 12: Properties for rope or annular decision

Property	Min	Max	Average	Individual
Std. Dev.				
Diff		√	√	
Cor.	√	√	√	
% Diff		√	√	

Separation of group 1

The methods stated above can be used for systems where the data sets are corresponding to a non-periodic flow regime as the properties used show minimal resemblance of the periodicity associated with the flow regime. The periodicity of slugs plugs waves will cause a change in the capacitance during the flow period which is significantly different from the type of variation seen for stratified flow (Figure 74). The occurrences of these drastic variation in capacitance measurements would be seen as result of small air gaps passing through the system dividing the high density clouds or ‘’slugs’’ which in return result in large changes in the capacitance measurement and would be a property of the type of conveying system as discussed in paragraph 2.

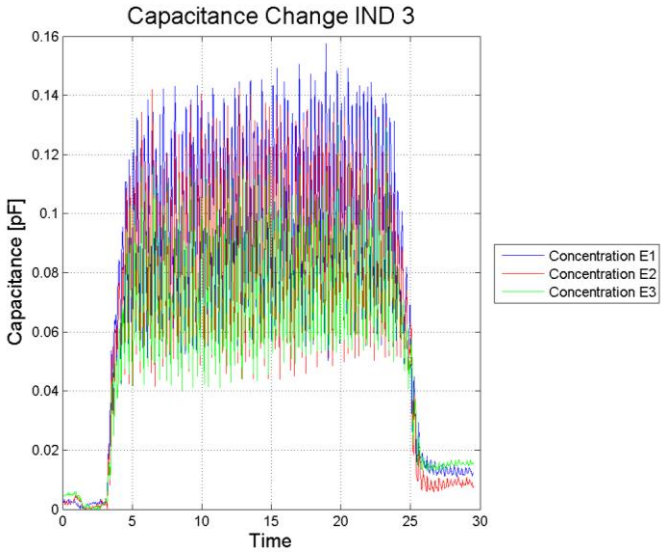

Figure 74: Drastic changes in capacitance during dune conveying

The use of a frequency analysis technique was previously used by Zhang (Zhang et al. 2012) to distinguish between rope and stratified, with the knowledge that the auger fed system will have a form of periodicity as explained earlier the properties of each data set in the frequency domain can be used as means of classification between auger and stratified flow.

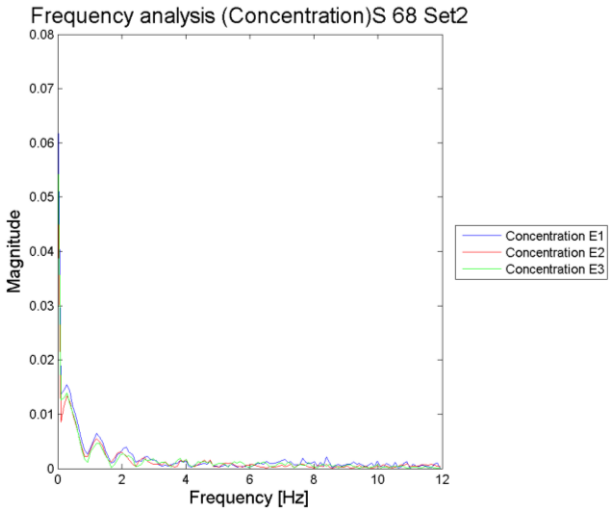

Figure 75: Frequency analysis stratified flow (concentration)

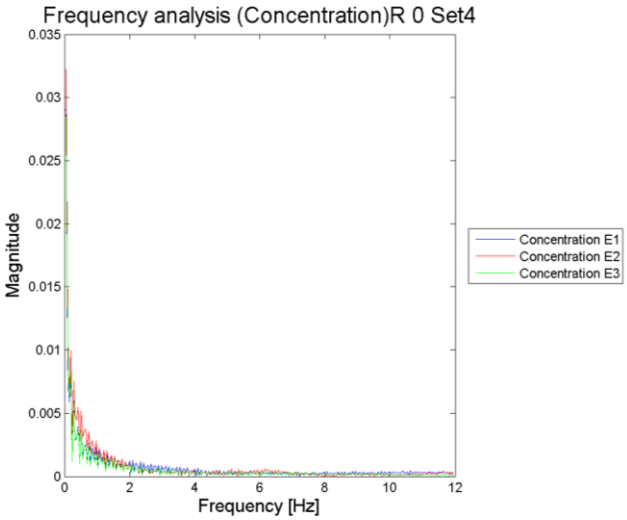

Figure 76:: Frequency analysis rope flow (concentration)

The proposed frequency analysis accompanied with the 5 electrode setup has the advantage that both the velocity and concentration electrodes could aid in the investigation of possible periodicity. The velocity electrodes sampling frequency is also significantly higher than the concentration electrodes' sampling frequency enabling evaluation over a larger frequency range for systems that are of such nature that the slugs or plugs move faster than measurable with the concentration electrodes. The use

of individual electrodes supplies 5 separate sets of data that can be used for identification adding certainty that the correct identification would be made.

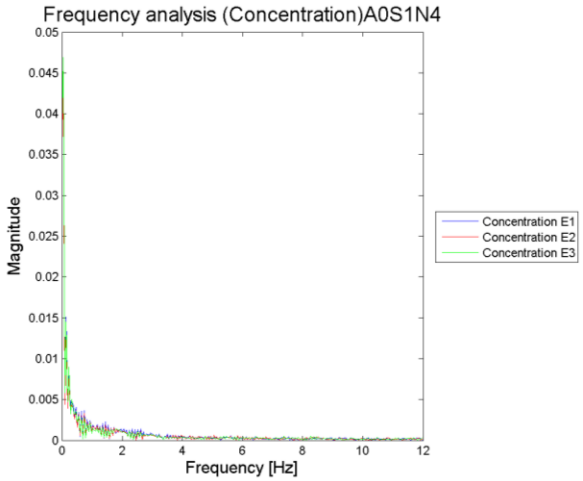

Figure 77: Frequency analysis annular flow (concentration)

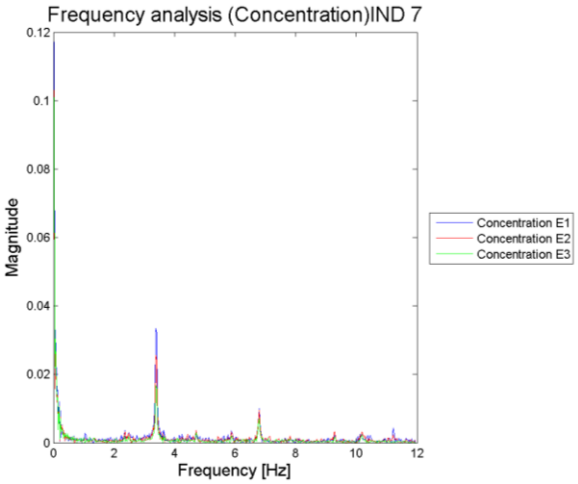

Figure 78: Frequency analysis auger (concentration)

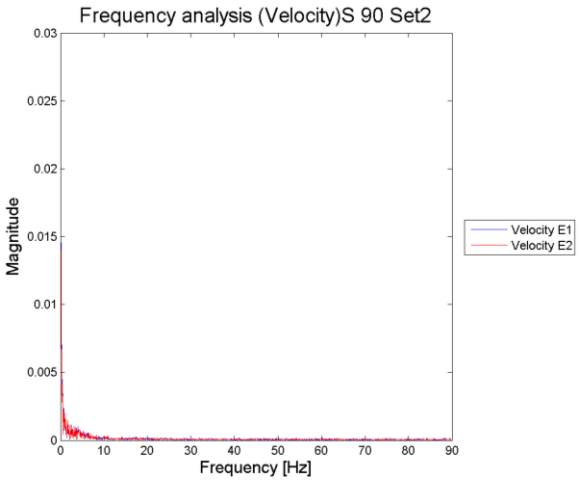

Figure 79: Frequency analysis stratified flow (velocity)

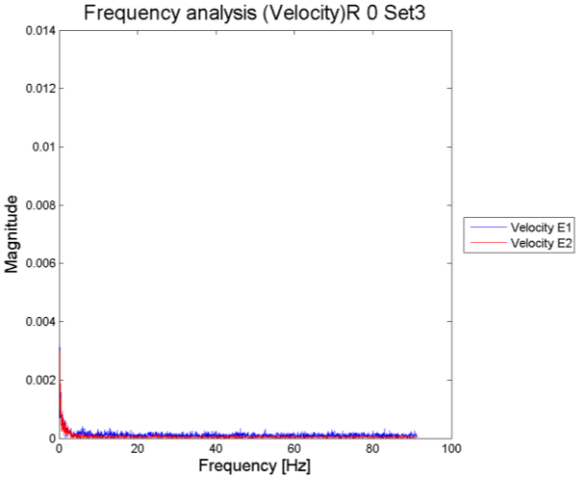

Figure 80: Frequency analysis rope flow (velocity)

When considering figure 75 to 82 one can clearly differentiate between periodic and non-periodic flow by looking at the peaks that are visible at just below 4 Hz and about 7 Hz these frequencies are representative of the frequency of slugs or plugs of material flowing through the system. If these values can be extracted and placed into a SVM or classification system, it can lead to the identification an additional flow regime in terms of periodic flow that also occurs due to a system characteristic such as the feeding techniques (refer to paragraph 2.1.2).

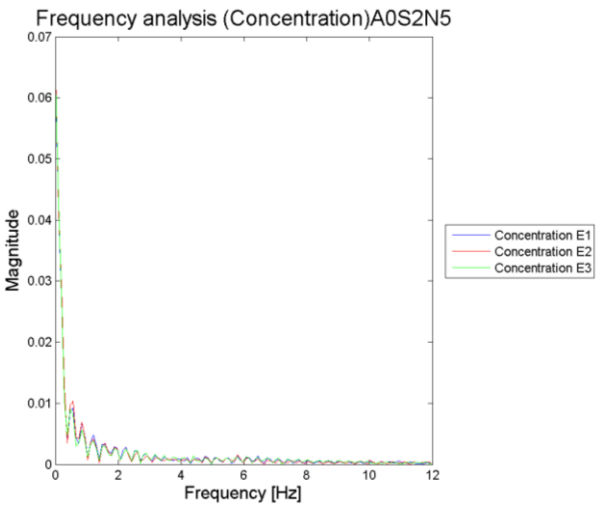

Figure 81: Frequency analysis annular flow (velocity)

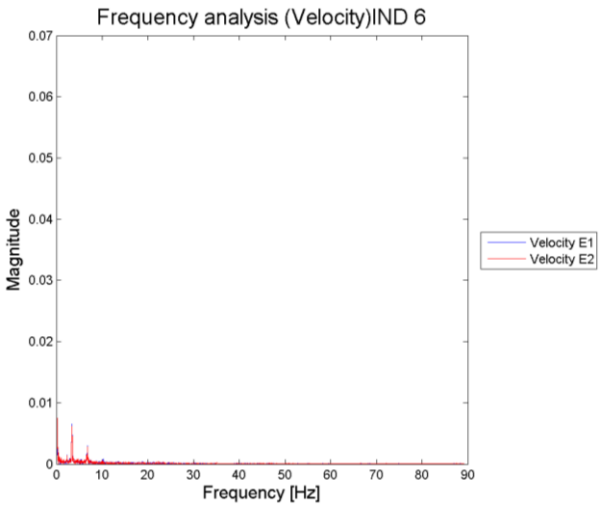

Figure 82: Frequency analysis auger fed (velocity)

The problem of using this feature is that the signal needs to be altered into a form that can be used by either a SVM or decision tree in terms of a value representing the frequencies with the highest magnitude. Li et al. (Li et al. 2013) uses an energy method accompanied with wavelet decomposition in order to manipulate the data into a format that is usable as an input for a SVM to analyse vibration signals of conveyer belts. The authors use the method in order to determine whether these conveying systems contain any faults. In order to identify the faults within the system the researchers divide the frequency analysis into a predetermined number of wavelets. The energy of these wavelets is then evaluated (equation 33) in order to establish what percentage of the energy each envelope represents. The energy of the envelopes can then be used as input into the SVM or decision tree to determine if any faults are present in the system.

$$E_{bin} = \sum_{i=f_{bin\_start}}^{f_{bin\_end}} |Mag|_i^2 \quad [33]$$

$$\%E_{bin} = \frac{E_{bin}}{\sum_{fstart}^{fend} E_{bin}}(100) \quad [34]$$

Instead of using these energies of an indication as a fault within the system, the present work aims to use the energy of each wavelet packet to identify if there is any periodicity in the conveying system with regards to the amount of solids flowing through the control volume.

The concept of decomposing the signal into wavelets is shown in 83 and 84. From the images it is clear that the separation of these signals into wavelet would result in the identification of a periodic frequency component if the correct amount of bins is chosen for instance if the number of wavelets was chosen to be 8 for the concentration electrodes the peaks corresponding to the frequency of material

moving through the control volume will fall into different bins resulting in a variation of the energy distribution (showed in figure 84 and 86).

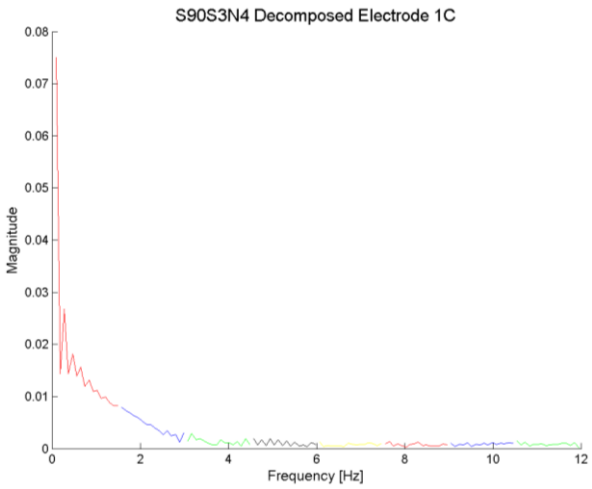

Figure 83: Decomposed wavelet analysis for velocity electrodes

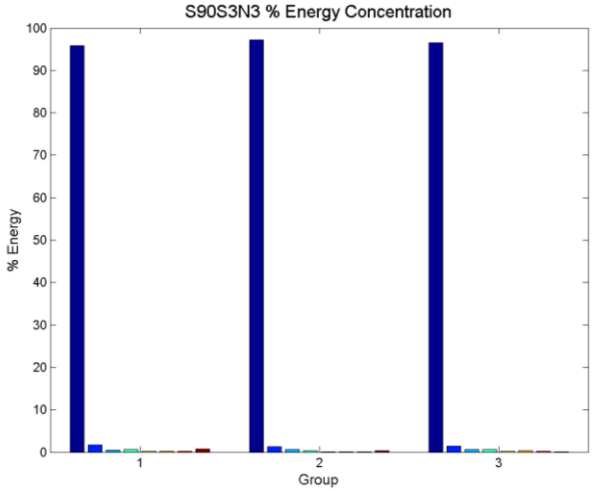

Figure 84 :Energy distribution for velocity electrodes

The clear difference in the energy distributions between figures 84 and 86 shows that the classification of flow between periodic and non–periodic would not be hard to establish as the largest difference would be observed in the 3rd energy bin that now represents more than 10% of the total energy. The only problem with the method is that the occurrence of cases where the energy of the data sets are more distributed of over the 4 bins resulting in energy distributions that will be hard to differentiate.

When considering figures 84 and 86 one can see that the majority of energy for both flow regimes are situated in the 1st bin. If the bin was removed and the percentage energy recalculated it would have result in a distribution where the difference between the flow regimes are emphasized and would result in a simpler classification.

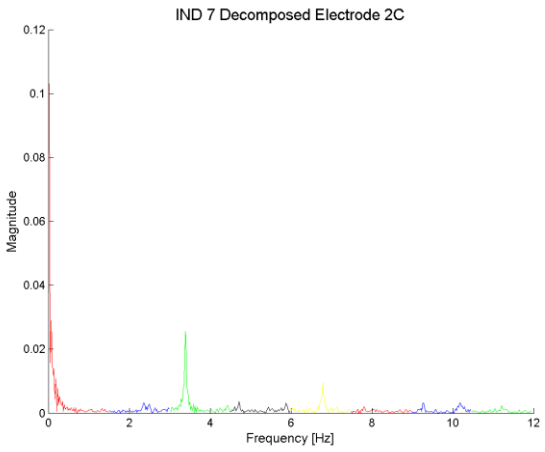

Figure 85: Decomposed wavelet analysis (concentration)

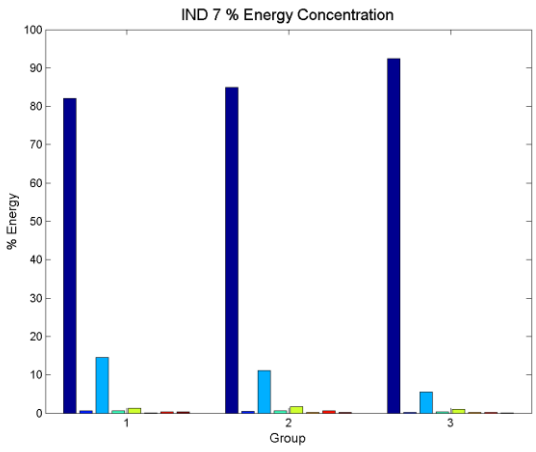

Figure 86:Energy distribution for velocity electrodes

The use of a band pass filter was seen as applicable due to the ability to remove unusable or unsuitable data that would lead to additional emphasis on data that would be more applicable to the specific conveying system when some of the conveying properties are known such as the region of flow periodicity in the frequency domain as well as the .range of frequency content. If the range is known, the low pass filter can be used to remove any high frequency content that are inapplicable as well as the removal of unusable low frequency content.

- High pass filter $H_h(s)$ equation 35.
- Low pass filter $H_l(s)$ equation 36.
- Band pass filter $H_b(s)$ equation 37.

These filters can be written as: (Rimell et al. 2015)

$$H_h(s) = \frac{s^2}{s^2 + \frac{\omega_1}{Q_1} + \omega_1^2} \quad [35]$$

$$H_l(s) = \frac{{\omega_2}^2}{s^2 + \frac{\omega_2}{Q_2} + \omega_2^2} \quad [36]$$

$$H_b = H_h(s) \times H_l(s) \quad [37]$$

The function also required the coefficients ω_1, Q_1,Q_2,ω_2 . These values can be obtained from table 13 in Rimmel and Mansfield, where $\omega_n = f_n \times 2\pi$

Coefficients	Value
f_1	2
f_2	25
Q_1	0.7071
Q_2	0.7071

Table 13 : Filtering coefficients

The function whfilter.m was written by setting up the equations for the three separate filters in the laplace domain by writing them in terms of **s** as shown in equations 35 to 37.The convolution function (conv) was used to place the numerator and enumerator of each of the equations 35-37. There after the filts.m function of matlab was used to set up a filter in the frequency domain. The values for each of the coefficients were then defined based on the known system characteristics.

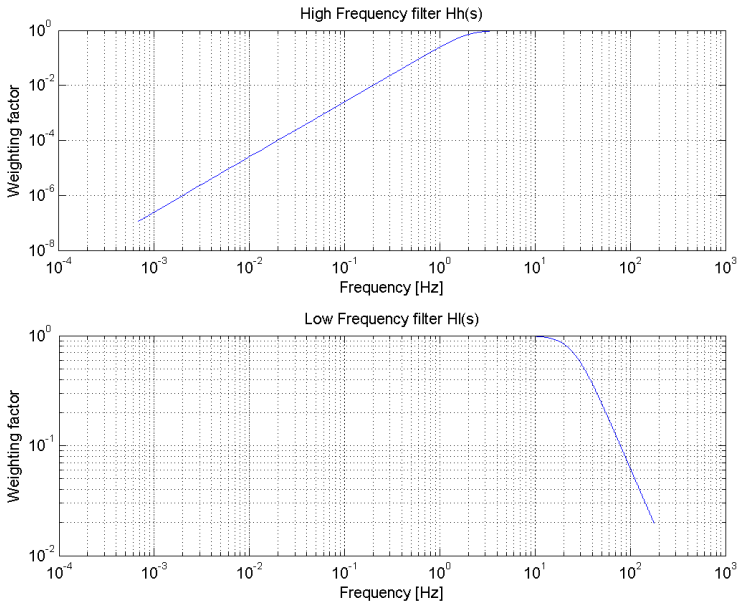

Figure 87: High and low pass filter

After the definition of each filter was done the two filters were multiplied with each other to form the final band pass filter seen in figure 88 and equation 37. The range of the filter was pre-defined to range from 0 to the sampling frequency determined from the data set.

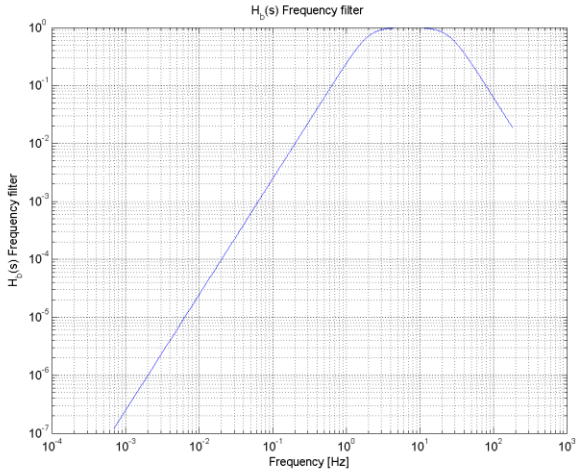

Figure 88: Band pass filter

The results obtained show that the low pass filter reduces the influence observed by higher frequencies where the high pass filter reduces the influence observed by low frequencies resulting in an increased emphasis on bins that are considered valuable for the classification. The effect of applying the band pass filter to concentration electrodes can be seen in figures 89 and 90 that indicates how the emphasis of the data have been shifted to the bins that are seen as valuable to the evaluation, which in the case of the auger fed system would be energy bins 5 and 10.

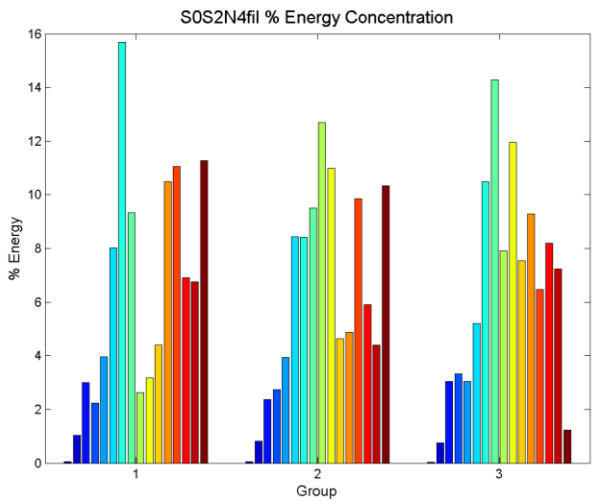

Figure 89: Filtered energy distribution (stratified concentration)

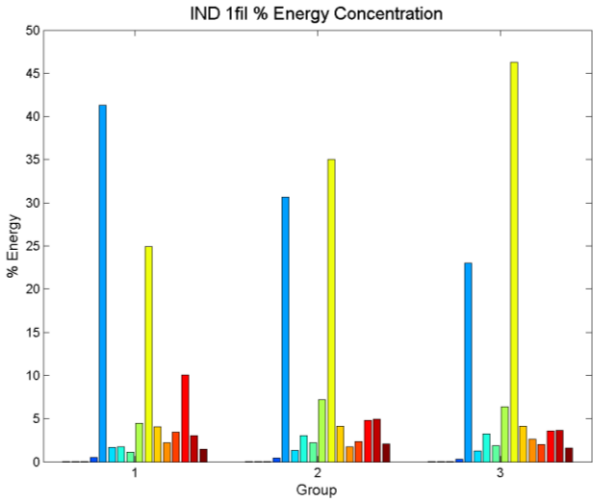

Figure 90: Filtered energy distribution (auger Fed concentration)

The analysis of the energy contained in bins 5 and 10 would provide information whether the flow contains periodicity specifically within the 3.5 and 7 Hz range. If the energy of these 2 bands would be summed it would provide the bulk of the energy of the whole system. A decision tree can then be crated in terms of the energy contained in these 2 bands that would be reflective of whether the flow can be classified as a periodic flow system.

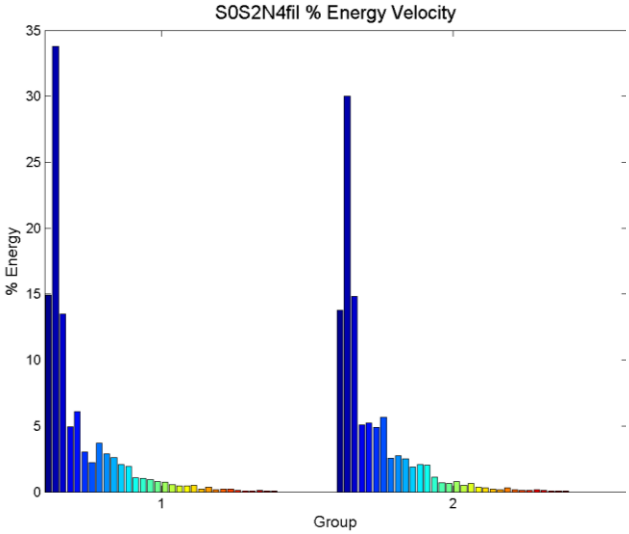

Figure 91: Filtered energy distribution (stratified velocity)

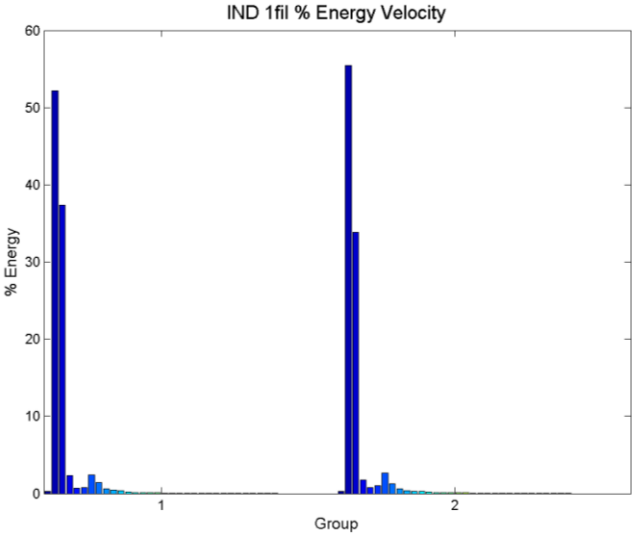

Figure 92: Filtered energy distribution (Auger fed velocity)

Similar to the energy distribution of the concentration electrodes the bulk of energy can still be seen in the first few energy bands of the distributions with the difference that the energy for stratified flow regimes are more evenly distributed over the rest of the energy bands when compared with the Auger fed experiments. For the periodic experiment more than 80% of the energy is situated in bands 2 and 3 (corresponds to bands that contain the 3.5 and 7 Hz components). The analysis for all electrodes over all

stratified flow and auger fed systems showed that the data could be separated by means of a constant benchmark or cut-off value as shown in figures 93 and 94.

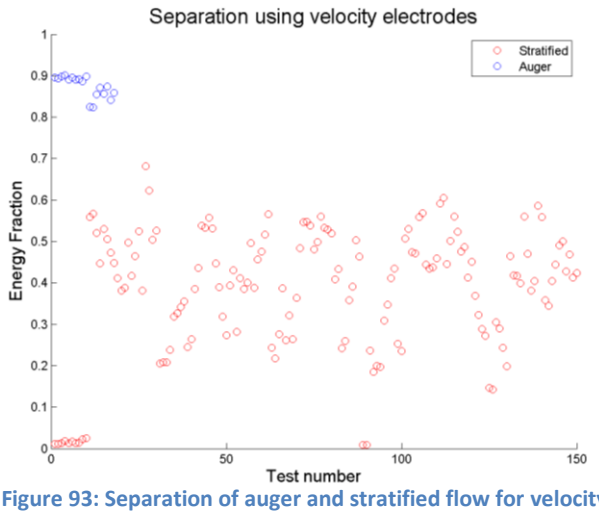

Figure 93: Separation of auger and stratified flow for velocity electrodes

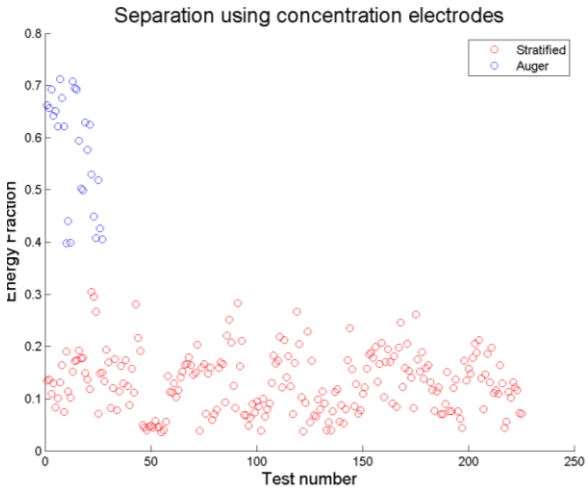

Figure 94: Separation of auger and stratified flow for concentration electrodes

From the above the following constraints can be used in terms of guidelines for determining whether the flow is stratified or periodically based.

The conditions were seen as viable as 255 data sets have been used for the concentration electrodes and 170 sets for the velocity electrodes. The constraints for separation of the data are seen in equations 38 to 39.

$$E_{V2} + E_{V3} \geq 0.7528 \quad [38]$$

$$E_{C5} + E_{C10} \geq 0.3515 \quad [39]$$

The separation value was determined by means of using the average value between the minimum and maximum values of the auger fed and stratified experiments as it would provide the value with the least chance of incorrect classification. The proposed classification method had the advantage that none of the datasets were classified wrongly and that it is of simple nature.

4.3. Concentration calculation

The concentration calculation will be done by using the change in capacitance from the experimental data and comparing it to the prescribed concentration curve (as identified in paragraph 4.2). The actual volumetric concentration will then be determined via interpolation of the experimental capacitance change on the prescribed curve as shown in figure 95. Note that interpolation done on figure 95 is purely done for illustrative reasons.

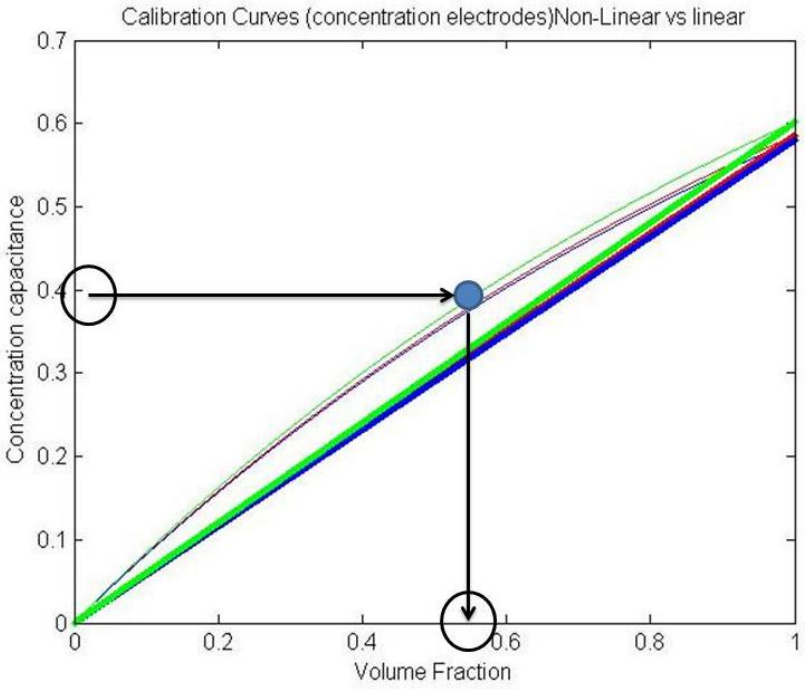

Figure 95: Interpolation

The interpolated concentration value (figure 95) will then be representative of flow compensated system where the type of flow is considered and more representative of the capacitive measurement with regards to induced flow regime.

4.4 Velocity calculation

4.4.1. Cross correlation velocity

The particle velocity has been analysed in terms of two methods namely an instantaneous velocity method and an adjusted cross correlation method. The instantaneous method uses the velocity electrodes concentration data and then compares it with the second electrodes' data by means of identifying the maximum reading in a specified region and then comparing the index of the specified maximum with the index of the other velocity electrodes maximum in the same specified index range just shifted on one index (prevents the estimation of a velocity of ∞). The velocity is calculated by means of using the change of indices dividing it with the sample frequency to find the transit time. If the distance between the electrodes is then divided by the transit time it would provide an estimation of the particle velocity (shown in equation 40).

$$v = \frac{d}{\tau} \quad [40]$$

$$\tau = \frac{index_2 - index_1}{SF_v} \quad [41]$$

The velocity vector is then interpolated to have points according to the concentration vector. This enables the multiplication of vectors to be done later on. This method uses an instantaneous velocity method rather than the assumption of the velocity remaining constant as in previous journal articles.

The second approximation is to use a normalised cross correlation function as prescribed by (Sen et al. 2000) where the upstream data signal is compared with the downstream signal by means of taking the capacitance value and comparing it with a number of points in the downstream signal in the form of a normalisation function which is shown in equation 42.

$$R_{V1-V2}(j) = \frac{2\sum_{n=0}^{N-j} C_{v1}(n) \times C_{v2}(n+j)}{\sum_{n=0}^{N-j} C_{v1}(n) \times C_{v1}(n) + \sum_{n=0}^{N-j} C_{v2}(n+j) \times C_{v2}(n+j)} \quad [42]$$

For the equation stated above it is important take into consideration the size of N as it represents the amount of data used as sample for the calculation of the cross correlation coefficient and should be chosen at the right length in order to eliminated the effects of noise and also to neglect the effect of the next 'wave' passing. In equation 42 C_{v1} and C_{v2} represent the upstream and downstream capacitance measurements from the velocity electrodes. The equation compares the upstream signal with the downstream signal by shifting the downstream signal an index at a time.

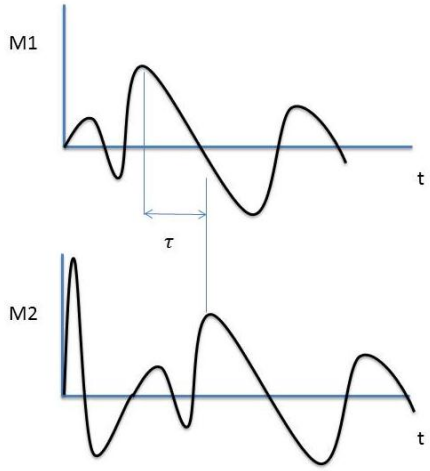

Figure 96: flow velocity identification

The velocity is then also calculated in terms of change of indices and distance travelled between the different velocity electrodes. The velocity is then chosen to be constant throughout the evaluation period. Figure 97 illustrates a general output that can be expected a normalised cross correlation curve.

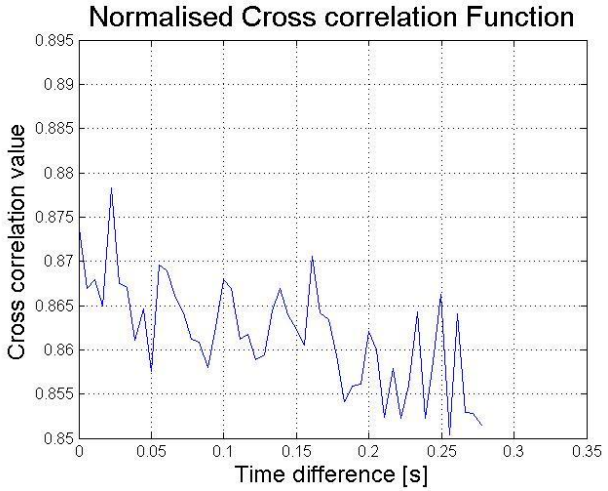

Figure 97: Normalised cross correlation curve

For the research done there are problems in accessing the velocity using all the above stated methods due to the fact that the use of an high sample rate will result in an low resolution in the velocity electrode capacitance measurements leading to the reduction in ability to measure small changes in capacitance due to small position and densities changes associated with waves moving through the sensing system. The problem can be rectified by means of increasing the sample rate and also increasing the distance between the electrodes slightly, both of the above stated solutions will provide a better solution in terms of the resolution of the measurable velocities.

For some of the cases where a flow regime was induced into the system the cross correlation method was not successful in determining the actual velocity as the induced flow regime resulted in minor waves flowing through the system. The lack of a wave effect caused insignificant capacitive change measurements that proved difficult to track between the two velocity electrode pairs due to the associated tow resolution of the SVM at high frequencies.

4.4.2 Velocity verification

Difficulties were encountered in measuring the actual solid velocity as no waves where induced in the flow. The absence of waves resulted in the false identification of waves when small amounts of sand represented turbulent flow away from the main stream of particles. The lack of waves also meant that no significant change in capacitance can be identified when the stream passes through the velocity electrodes.

The use of the high speed cameras enabled the investigation of wave formation as well as the verification of particle velocity by means of using wave displacement accompanied by image sample rate.

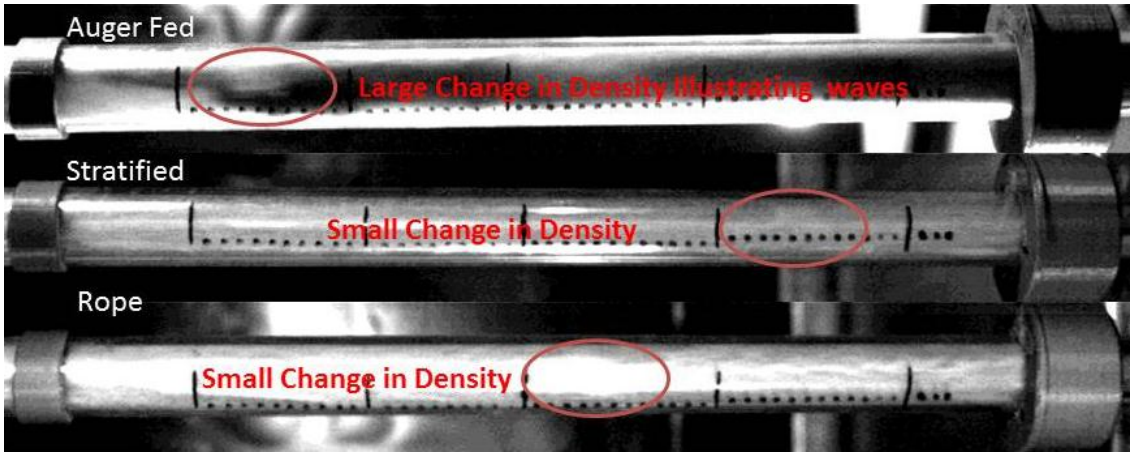

Figure 98: Difference in flow regimes

In order to validate the actual solid velocity a high speed camera was used to determine the instantaneous velocity as the particles passed through the middle of each electrode. This investigation would provide additional information regarding the actual induced flow pattern at each electrode as well as the formation of clouds.

The velocity can be calculated by means of using the displacement of the first cloud and dividing it by the time taken for a separate frame as shown in equation 43. The concept is also showed in figure 99.

$$V = \frac{\text{Distance travelled}}{\text{Time taken for each frame}} \quad [43]$$

The time taken for transmission is calculated in terms picture frames where the frame rate is known to be 420 frames per second leading to the time taken calculation to be as illustrated in equation 44.

$$\text{Time taken for each frame} = \frac{(\text{Frame difference})}{(\text{Frame Rate})} \quad [44]$$

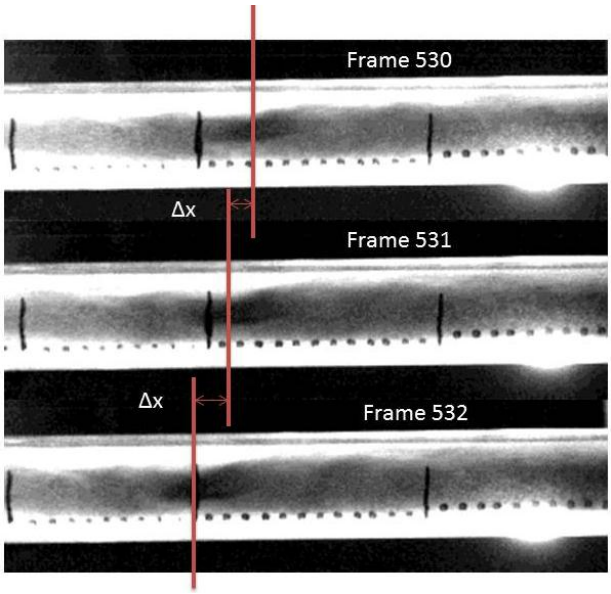

Figure 99: Wave velocity

The results for the high speed camera test are shown in table 14. The overall speed of all the electrodes are very closely related to the assumed solid velocity due to gravity. This validates the use of the assumption that the velocity due to gravity can be used for calculating the velocity during the regime induced experiments where the capacitive velocity electrodes would not be able to identify the passing of waves through the control volume as explained earlier.

Table 14: High speed camera results

Accuracy Analysis	Estimated	Rope Small	Rope Medium	Rope Large	Rope X Large	Strat Small	Strat Medium	Strat Large
Electrode 1	2.69	2.52	2.66	2.52	2.52	2.59	2.59	2.66
Electrode 2	2.92	3.01	3.01	3.01	3.01	2.94	3.15	3.08
Electrode 3	3.13	3.5	3.57	3.57	3.36	3.36	3.57	3.43

The velocity verification through high speed cameras also showed that the statement made in Chapter 3.1 that the use of an auger would simulate passing waves as each vane passes through the opening of the piping system causing a change flow density.

4.5 Calculation of mass flow rate

The mass flow rate is then calculated using the properties specified in the previous sections by means of using the volume fraction and particle velocity in conjunction with equation 1. The average fraction between the concentration electrodes is then used as a representation of the mass flow rate. It should be noted that all the concentrations were calculated for each individual data point using the optimized equations generated from section 4.1 in terms of the flow regime present.

The total mass conveyed is then calculated by using each measurement from the instantaneous flow rate (figure 101) and multiplying it with the time interval between that measurement and the previous measurement to get the amount of solids transferred for each time interval. The cumulative sum of this value's was then used to calculate the mass conveyed for the full time period (figure 102).

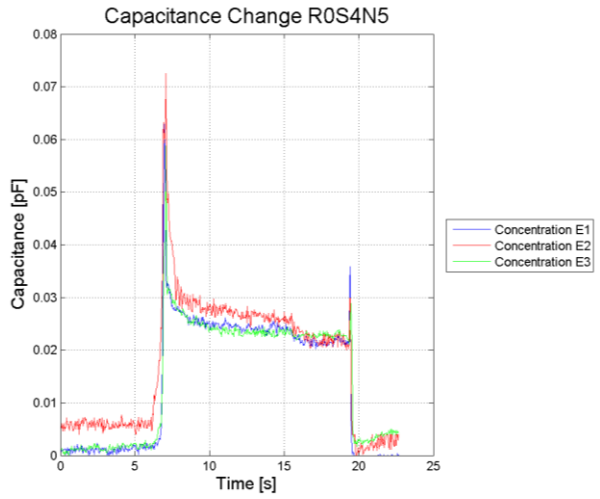

Figure 100: Capacitance change

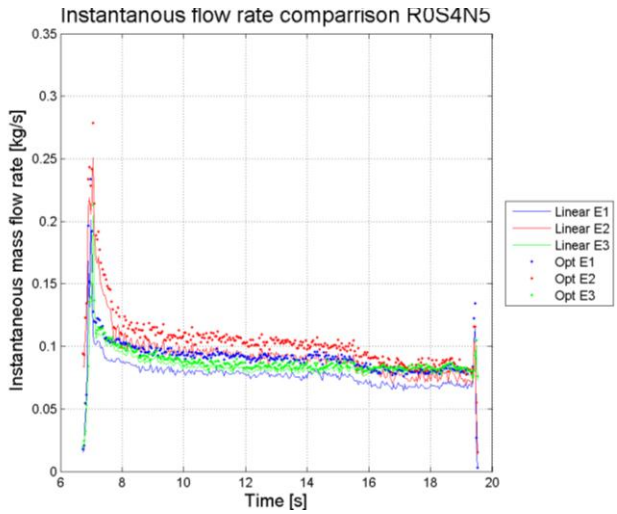

Figure 101: Instantaneous flow rate

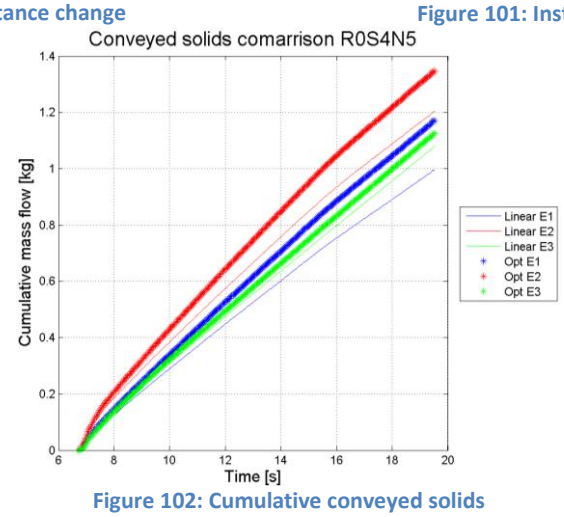

Figure 102: Cumulative conveyed solids

As means of validation, the actual mass conveyed was measured by weighing the collection bin before and after the conduction of the experiment. The difference in the mass conveyed can then be used to evaluate the accuracy of the ensuring unit in terms of error made. The equation for determining the error of measurement can be seen in equation [45]

$$\%\text{error} = \frac{\text{Estimated-Actual}}{\text{Actual}} \quad [45]$$

The inclusion of a sensor calibration factor that might serve as a handy tool in systems where constants, such as the velocity, bulk density and distance between electrodes were not estimated accurate. The meter factor will upon calibration aid as a compensator for measurement errors made during the manufacturing stage and would greatly improve sensing accuracy caused by inaccurate approximations. Equation 46 illustrates how the individual meter factor can be calculated.

$$\text{Meter factor} = \frac{\text{Actual ash conveyed}}{\text{Sesnsor Estimation}} \quad [46]$$

The use of the meter factor was not implemented into the measurement program but could be implemented for systems where errors occur in the estimation of the assumed constants.

5.1 Specific flow induced experiments

This paragraph covers the experiments done for flow regimes that have been purposefully induced into the system in order to determine if the procedure followed in the research led to a better approximation of the flow rate than when a non-linear volume fraction curve has been used.

The approximations of the mass flow rate required a few assumptions that were required to calculate the total mass conveyed, and they are as follows:

1. The use of gravity for the velocity estimation would be appropriate as the lack of variation in induced flow regimes volume fraction would lead to an inaccurate approximation.
2. The optimal equation for the fraction curve can be used regardless if the equation can be determined with the known data properties.
3. The use of the data sets used for calibration of the volume fraction curves can be used for the evaluation of the methods accuracy.
4. The use of a combination of all 3 electrode pair's conveyed mass measurement, by means of using an average measurement, would be a viable measurement technique.

5.1.1 Using optimal curve

Rope flow

The investigation into the rope flow induced experiments proved that the optimization and identification method would have resulted in a slightly lower error over the 10 data sets with an average error of 6.54% against an average error of 10.05% for a linear estimation.

The difference in the % error made is small and may seem insignificant but can be explained by the close relationship of rope flow to homogeneous flow for such a small control volume.

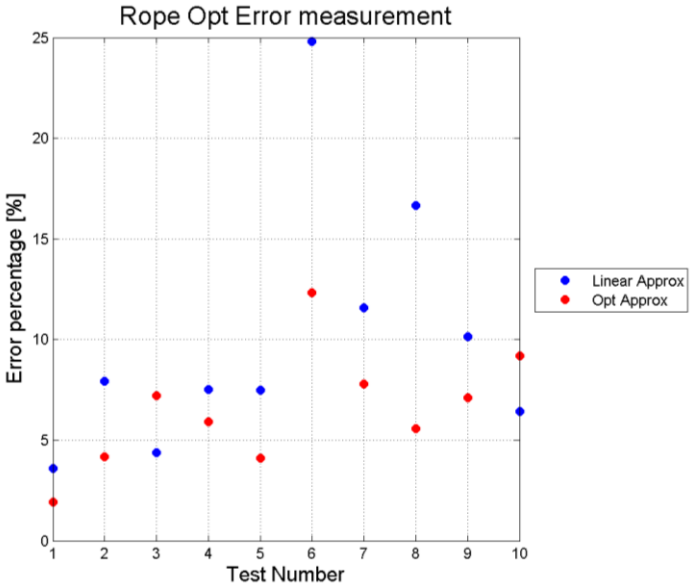

Figure 103: Error estimation optimised vs. linear estimation (rope)

Figure 103 shows the individual errors for each of the ten rope experiments. It also emphasizes the improvement in estimation as it provided better results for 8 out of the 10 experiments. The largest error made for the optimized curve experiments was 12.34% that can be seen as a significant improvement to the 24.82% error of the linear approach.

Stratified flow

As expected the optimised fraction curves causes large scale improvements from the linear approximation due to the compensation for solid material falling inside or out of sensitive regions of the electrodes as explained in section 4.2.

Figure 104 shows the scale of improvement by indicating that the maximum error for the optimization method was only 24.26% compared to 58.14% for the linear approximation. The only problem with this estimation is that the larger variation in the optimal curves (refer to figures 58 to 60) exist due to the non-homogeneous distribution of solids over the most sensitive regions of the electrodes (refer to paragraph 4.2 and figures 46 to 48). The larger variation in optimal equations will also decrease the efficiency of using a general fraction curve to use for stratified flow regimes. The optimization method decreased the mean error from 19.41% to 5.02%.

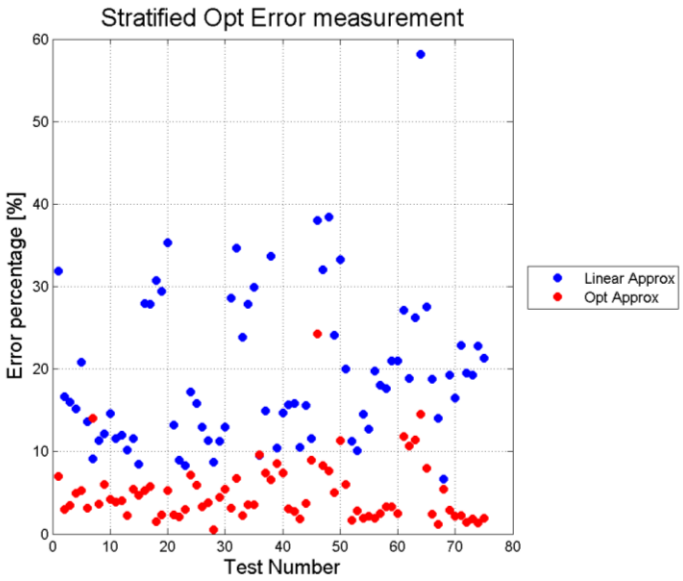

Figure 104: Error estimation optimised vs. linear (Stratified)

Annular flow

In general the occurrence of the annular flow regime would result in an overestimation of mass conveyed through the system due to the bulk of the solids being distributed over all the most sensitive regions of the electrodes. The smaller the inside section where no material is present the closer the fraction curve will be to that of a linear approximation (refer to paragraph 4.2 and figures 61 to 63). The above stated can also be seen in figure 105 where the % error for the linear approximation decreases as the diameter of the empty region decrease (inside diameter decreases as test number increases).

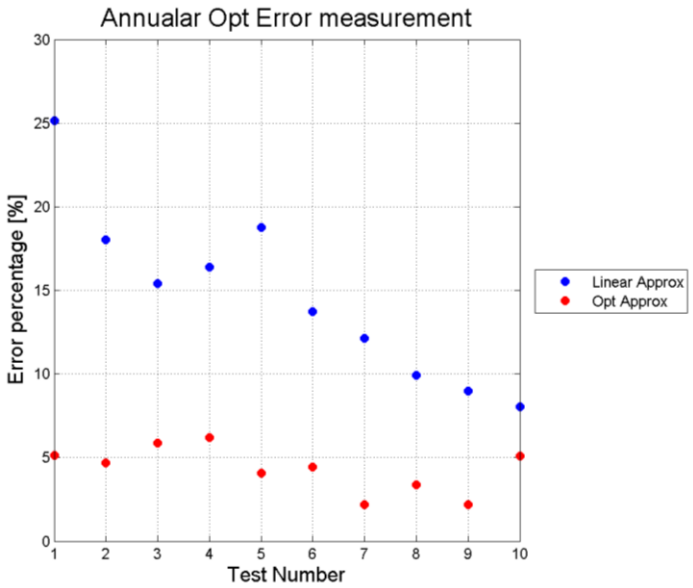

Figure 105: Error estimation optimised vs. linear (Annular)

The figure also shows the improvement that can be achieved if the correct fraction to capacitance curve could be determined. The approximation enables an improvement for overall percentage error from 14.66% to 4.33%. It also decreases the maximum error from 25.14% to 6.20%. The result again emphasises how the correct identification of the flow regime could lead to an improvement of the measurement of conveyed mass.

Auger induced flow

The auger fed experiments were conducted over using the experimental setup proposed in paragraph 3.1 consisting out of an auger feeding system coupled to a hopper. For the experiment the rotational speed of the motor was kept constant. The test was conducted 11 times and both the concentration and velocity electrodes were active during the experiments as they were used for the regime identification of auger fed systems.

Similar to stratified flow the analysis serve as a significant improvement as the tested group showed a mean error of 5.00% where the linear approximation showed a mean error of 32.57%. The proposed method also reduced the largest error from 44.73% to 9.26% which is a significant improvement from a system where no identification and compensation could have been done.

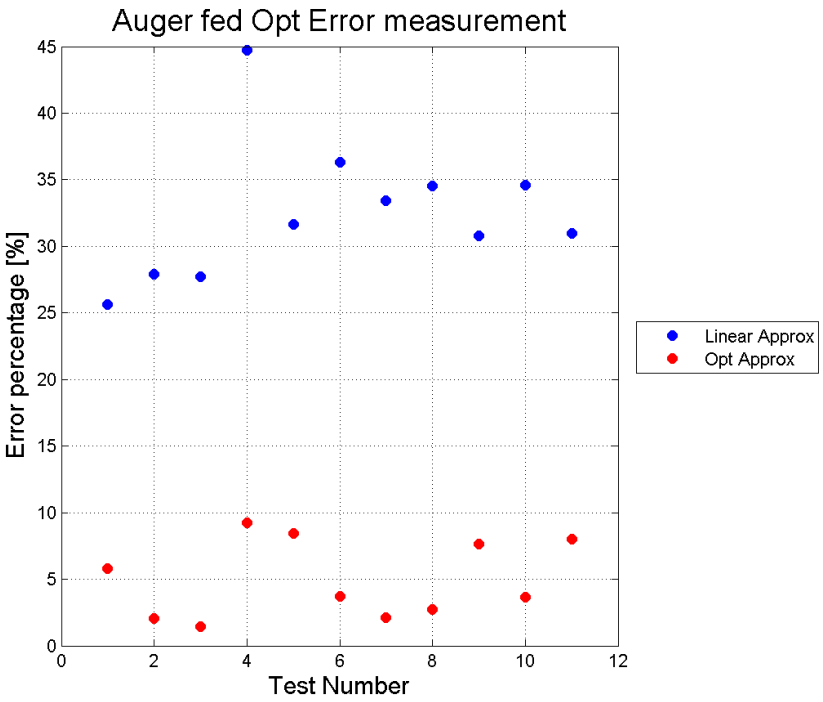

Figure 106: Error estimation optimised vs. linear (Auger fed)

The curves fitted in terms of an optimal fit are similar to the curves that are to be used in terms the generalised curves as they were not separated into smaller groups that form more case specific flow regimes but rather represented an auger fed system where the auger rotational speed have been kept constant.

The proposed systems then enables the correct identification of the systems current flow regime it also supplies accurate estimations with regard to the measured mass conveyed over each test period.

5.1.1 Using general curves

A general curve analysis was done due to the lack of determining an optimal curve for the flow actually present in the system reducing the applicability and usability of the method used thus far. The determination of a general equation would be seen as viable through simulations before installation in industrial systems.

The aim of the use of generalised equations is not to provide a case specific curve but rather to provide an improved approximation when certain flow regimes are present in a conveying system.

The use of individual equations for each electrode pair would be fitting as the dimensions and fixation properties of the electrodes are not exactly the same. The test loop also had implications in terms of using individual equations as the usage of a gravity fed system would result in more dispersion of solids trough the conveying system.

Rope flow

For the rope flow regime the choice was made to use the equations for the results corresponding to the nozzle with the third biggest inlet diameter. The decision is based on the nozzle representing an average rope regime for the range of evaluated rope flows.

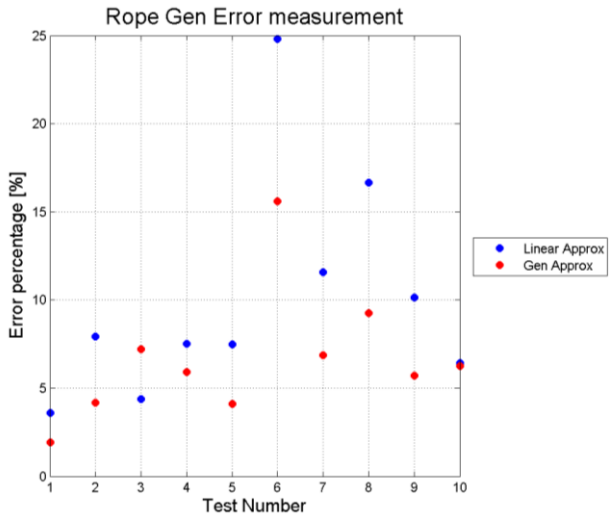

Figure 107: Rope flow estimation using general estimation

The use of the general equation resulted in an improvement on the on the error made and reduced the average error over the tests to 6.71 %. The general approximation shows an improvement from the optimal equation sets for some of the test. These slight improvements can be seen in figure 107 that shares very close resemblance to figure 103 with the only visible difference occurring in test 10 that yields a closer approximation than the optimal curve set. The largest error of 16.61% serves as an improvement from 24.82% but would not be accepted as good practice in industry.

The differences observed can be explained by viewing the actual data and the data used for the evaluation of the fraction curves (figure 40). The removal of peaks when determining the optimal

equation results in a fit that disregards the peak or outliers within the data set. The evaluation of the flow regimes with the peaks resulted in a slight over estimation as the flow is not representative of rope flow regime throughout the period of stabilisation (duration where peaks were observed). The use of an equation set that has a slightly more linear geometry will then inherently compensate for the for the peaks by having a lower estimation of the volume fraction than the optimal equation set (which had a more curved geometry).

Although a unintentional improvement is made the conclusion cannot be made that the use of a general equation would be an improvement from the optimal method but rather show that the use of a general set of equations will still serve as an improved approximation with regards to an linear estimation.

Stratified flow

The stratified flow regime poses a difficulty in the assignment of either a positive or negative exponential as the properties measured to date have not proven to be a viable source to provide information that could lead to correct curve allocation. The problem can be evaded by means of placing the sensors on a section of the conveying system where the position of stratified flow can be determined this will lead to the correct identification of the type of curve to allocate.

In contrasts to the general equation tests for the rope flow regimes the mean accuracy drops from an error of 5.02% to 9.42%. Although the error is still large it is a significant improvement from the linear estimation that had a mean error of 19.41%. The largest error had an increase to 26.58% but is still significantly smaller than the 58.14% of the linear estimation. The conclusion can then be made that the use of a general equation with a stratified flow regime would result in an estimation that would not represent a viable and accurate mass flow measurement for all cases of stratified flow.

The lack of knowledge of the orientation of the stratified flow might also lead to large scale errors due to lack of knowledge regarding the nature of the fraction curve's equation (positive or negative).

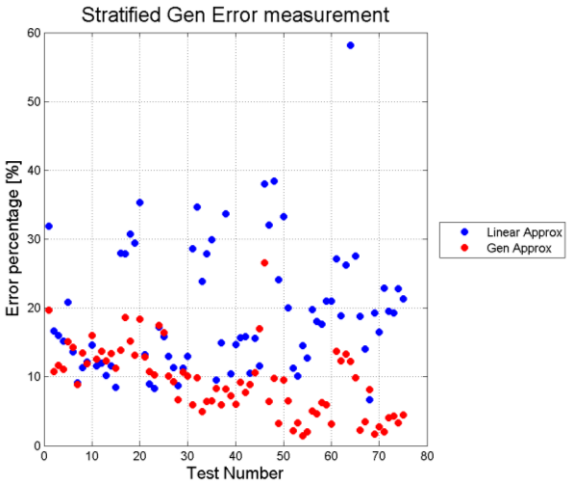

Figure 108: Stratified flow estimation using general estimation

Annular Flow

As with the rope flow the decision was made to use the middle set of tests' optimal equations as it would provide the best representation of the annular flow regime (the set refers to the second data cluster 2 on figure 54, which is also caused by annular nozzle 2).

Similar to the stratified case for generalised equations the mean error increased slightly (from 4.33 % to 4.53%) but still has a significant improvement from the linear assumption (14.66%) as visible in figure 82. The tests also show that the maximum error will be smaller than 10% (8.75%) that would be regarded as viable for industrial use.

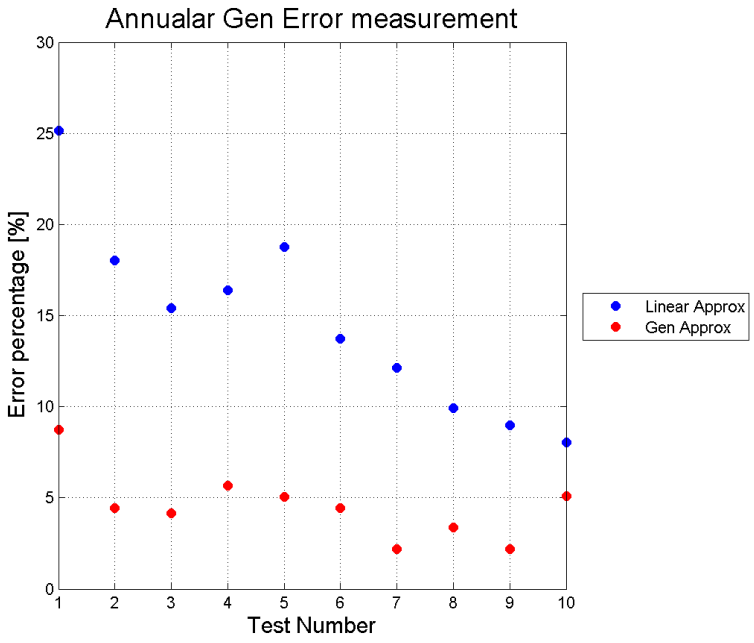

Figure 109: Stratified flow estimation using general estimation

6. Conclusion and recommendations

The use of a calibration technique for systems where non homogeneous flow regimes are present would serve as a good base for the improvement on errors made by concave plate capacitors due to the loss of their linearity property. It would also be wise to use the procedure used in the dissertation for training the support vector machine in order to identify the correct flow regime present in flow volume.

The prescribed process also decreases the error made with regards to a linear approximation for both the optimal and the general equation sets. The proposed system also allows the user to identify the correct flow regime 100% of the time, allowing a much broader understanding of the flow regime actually present in the flow volume and would cause an improvement of the flow rate measured for systems where annular, rope, stratified and auger fed flow regimes are present. The method also provides accurate and usable results for rope and annular flow regimes regardless of the rotation and position of the sensors within a pneumatic environment.

The technique is still lacking with regards to the identification of a fixed set of general equations for stratified flow due to the variation of the optimal curves as solid material move in and out of the sensitive regions of the electrodes. This concept is illustrated by figure 108 that shows how the reaction of electrodes changes with regards to rotation of the solid distribution. The problem could in principle be rectified easily by means of placing the sensor unit in a section of the system where the position of the solid distribution would be constant with regards to the senor unit, but this is not always possible in an industrial environment due to environmental and space constraints.

In conclusion the prescribed method and procedure will aid in the improvement of solid flow measurements made within a pneumatic environment and stands as a better approximation than assuming the electrode pairs will have a linear reaction to solid material distributed in a non-homogeneous manner.

The proposed method of identification also allows the user to positively distinguish between four types of flow regimes namely rope, annular, stratified and auger fed flow regimes. The positive identification of these flow regimes has the implication that for a system where flowing conditions are unknown an improvement of mass flow measurement can be made by means of using pre-calibrated curves representative of flow regimes that are expected within these conveying systems. The predicted flow regimes should be determined in terms of sensor location and system characteristics as prescribed in paragraph 2.1.

Applications

The proposed methodology and sensor setup would have a wide variety of applications not only in ash management plants in power stations, but would be able to operate in supply lines for food chains that also require a nonintrusive method of determining the amount of solids conveyed. The method would also allow for a variety of flow regimes and still achieve acceptable accuracies.

Recommendations

In order to have the system fully functional and accurate for all the flow regimes the following improvements are required:

1. Further improvement of stratified flow regimes in terms of rotational position that would result in correct identification of fraction curves with regard to solid position in electrode sensitivity fields.
2. Improvement in terms of fraction curves for auger fed systems by either applying a sensor factor as done by Shao et al. (Shao et al. 2000) or either by means of doing large numbers of experiments to determine a fraction curve representative of a ranging fraction to capacitance curve.
3. Improvement in terms of evaluation module of capacitance sensor in the following manners:
    a. Improved resolution for a higher sampling frequency in order to enable measurement of solid velocity, that will enable the measurement of solid velocity using capacitive sensors for not only slow moving systems but for high speed systems as well.
    b. The improvement of software in order to enable the simultaneous start of both the velocity and concentration electrode pairs decreasing the chance of errors seeping into the system. This can be done by means of enabling multiple module use for one graphical user interface with the functionality to measure more than four channels at different sampling rates.

Bibliography

Abdul Rahim, R. & Green, R.G., 1998. Optical-fibre sensor for process tomography. *Control Engineering Practice*, 6(11), pp.1365–1371.

Abouelwafa, M.S. a. & Kendall, E.J.M., 1980. The Use of Capacitance Sensors for Phase Percentage Determination in Multiphase Pipelines. *IEEE Transactions on Instrumentation and Measurement*, 29(1), pp.24–27.

Arakaki, C. et al., 2006. Non-Intrusive mass flow measurements in pneumatic transport. In *CHoPS*. Telemark University College Kjølnes Ring 56, Porsgrunn, N-3901, NORWAY.

Arakaki, C., Ratnayake, C. & Halstensen, M., 2009. Online prediction of mass flow rate of solids in dilute phase pneumatic conveying systems using multivariate calibration. *Powder Technology*, 195, pp.113–118.

Arko, A. et al., 1999. Development of electrical capacitance tomography for solids mass flow measurement and control of pneumatic conveying systems. *1st World Congress on Industrial Process Tomography*, pp.140–146. Available at: http://www.vcipt.org.uk/pdfs/wcipt1/a2_7.pdf.

Aslam, M.Z. & Tang, T.B., 2014. A High Resolution Capacitive Sensing System for the Measurement of Water Content in Crude Oil. *Sensors*, (14), pp.11351–11361.

Barratt, I.R. et al., 2000. Mass flow measurement of pneumatically conveyed solids using radiometric sensors. *Flow measurement and instrumentation*, 11, pp.223–235.

Beck, M.S., Green, R.G. & Thorn, R., 1987. Non-intrusive measurement of solids mass flow in pneumatic conveing. *Phys. E: Sci. Instrum*, 20, pp.835–840.

Bhuvaneswari, P. & Kumar, J.S., 2013. Support Vector Machine Technique for EEG Signals. , 63(13), pp.1–5.

Bishop, C., 2006. *Pattern Recognition and Machine Learning*, New York.

Das, S., Sarkar, T.S. & Chakraborty, B., 2014. A Semi-Cylindrical Capacitive Sensor Used for Soil Moisture Measurement. , 8(1), pp.160–165.

Geraets, J.J.M. & Borst, J.C., 1988. A capacitance sensor for two-phase void fraction measurement and flow pattern identification. *International Journal of Multiphase Flow*, 14(3), pp.305–320.

Hu, H.L., Xu, T.M. & Hui, S.E., 2006. A novel capacitive system for the concentration measurement of pneumatically conveyed pulverized fuel at power stations. *Flow measurement and instrumentation*, 17(2), pp.87–92.

Huang, S.M. et al., 1988. Electronic transducers for industrial measurement of low value capacitances. *Journal of Physics E: Scientific Instruments*, 21(3), pp.242–250.

Irons, G.A. & Chang, J.S., 1982. Particle fraction and velocity Measurement in gas-powder streams by capacitance transducers. *Int. J. Multiphase Flow*, 9(3), pp.289–297.

King, J.D. & Rollwitz, W. l., 1983. Magnetic resonance measurement of flowing coal. *ISA Trans.*, 22, pp.69–76.

Konrad, K., 1986. Dense-Phase Pneumatic conveying: A Review. *Powder Technology*, 49, pp.1–35.

Li, W. et al., 2013. Design of online monitoring and fault diagnosis system for belt conveyors based on wavelet packet decomposition and support vector machine. *Advances in Mechanical Engineering*, 2013. Available at: http://www.scopus.com/inward/record.url?eid=2-s2.0-84878734589&partnerID=40&md5=b2a02debb5b401fb07fc133586d0cbaf.

Masuda, H., Matsusaka, S. & Nagatani, S., 1994. Measurements of powder flow rate in gas-solids pipe flow based on the static electrification of particles. *Amphibia-Reptilia*, 5(3), pp.241–254.

Mills, D., 2004. *Pneumatic Conveying Design Guide* 2nd ed. E. Butterworth-Heinemann, ed., Elsevier.

Rimell, A.N., Mansfield, N.J. & Paddan, G.S., 2015. Design of digital filters for frequency weightings (A and C) required for risk assessments of workers exposed to noise. *Industrial health*, 53(1), pp.21–27.

Sen, S. et al., 2000. PC-based gas-solids two-phase mass flowmeter for pneumatically conveying systems. *Flow Measurement and Instrumentation*, 11(3), pp.205–212.

Shao, F., Lu, Z. & Wu, E., 2000. Study and industrial evaluation of mass flow measurement of pulverized coal for iron-making production. *Flow measurement and instrumentation*, 11, pp.159–163.

Sowerby, D.B., Millen, M.J. & Abernethy, D.A., 1991. Online determination of pulverised coal mass flow using ultrasonic technique. *Ultrasonics simposuim*.

Strizzolo, C.N. & Converti, J., 1993. Capacitance Sensors for Measurement of Phase Volume Fraction in Two-Phase Pipelines. *IEEE Transactions on Instrumentation and Measurement*, 42(3), pp.726–729.

Sun, M. et al., 2008. Mass flow measurement of pneumatically conveyed solids using electrical capacitance tomography. *Measurement Science and Technology*, 19(4), p.45503.

Szebeszczyk, J.M., 1994. Application of clamp-on ultrasonic flowmeter for industrial flow measurements. *Flow Measurement and Instrumentation*, 5(2), pp.127–131. Available at: http://www.sciencedirect.com/science/article/pii/0955598694900477.

Terzic, E. et al., 2012. A Neural Network Approach to Fluid Quantity Measurement in Dynamic Environments. Available at: http://link.springer.com/10.1007/978-1-4471-4060-3.

Texas Instruments, 2015. FDC2214 Proximity and Capacitive Touch EVM User ' s. , (October).

Tollefsen, J. & Hammer, E.A., 1998. Capacitance sensor design for reducing errors in phase concentration measurements. *Flow Measurement and Instrumentation*, 9(1), pp.25–32.

Williams, R.A. et al., 1991. Multi-phase flow measurements in powder processing. *Powder Technology*, 66, pp.203–224.

Xie, C. et al., 1989. Mass-flow measurement of solids using electrodynamic and capacitance transducers. *Journal of Physics E Scientific Instruments*, 22, pp.712–719. Available at: http://iopscience.iop.org/0022-3735/22/9/007.

Xie, C.G. et al., 1990. Design of capacitance electrodes for concentration measurement of two-phase flow. *Measurement Science and Technology*, 1(1), pp.65–78. Available at: http://iopscience.iop.org/0957-0233/1/1/012%5Cnhttp://stacks.iop.org/0957-0233/1/i=1/a=012?key=crossref.d46bd0711d11d62c33082e7023ac9fca.

Xu, C. et al., 2008. Velocity measurement of pneumatically conveyed solid particles using an electrostatic sensor. *Measurement Science and Technology*, 19(2), p.24005.

Yan, Y., 1996. Mass flow measurement of bulk solids in pneumatic pipelines. *Measurement, Science and Technology.*, 7, pp.1687–1706.

Yan, Y., Byrne, B. & Coulthard, J., 1995. Sensing field homogeneity in mass flow rate measurement of pneumatically conveyed solids. *Flow Measurement and Instrumentation*, 6(2), pp.115–119.

Zhang, J. et al., 2012. Concentration measurement of biomass/coal/air three-phase flow by integrating electrostatic and capacitive sensors. *Flow Measurement and Instrumentation*, 24, pp.43–49.

Available at: http://dx.doi.org/10.1016/j.flowmeasinst.2012.03.003.

Zheng, Y., Li, Y. & Liu, Q., 2007. Measurement of mass flow rate of particulate solids in gravity chute based on laser sensing array. *Optic and Laser technology*, 39, pp.298–305.

Zheng, Y. & Liu, Q., 2011. Review of techniques for the mass flow rate measurement of pneumatically conveyed solids. *Measurement*, 44, pp.589–604.

Appendix 1: Different sensing techniques

Table 15: Direct Monitoring techniques

Advantages and disadvantages of monitoring techniques (Direct techniques)			
Technique	Advantages	Disadvantages	Accuracies
Thermal Technique (Zheng & Liu 2011)	• Directly measures mass flow rate • Simple setup	• Slow measurement response • Performance influenced by pipe size • Flow regime sensitive (prefers dense phase) • Measurement probe attrition occurs • Requires a fully mixed measurement volume.	• $\pm 10\%$ for 100µm aluminium oxide at max 1 ton/h
Active Charge technique (Yan 1996)	• Directly measures mass flow rate	• Spontaneous combustion of flammable materials. • Limitation in applied voltage. • Length and diameter of pipe used influences accuracy	• 1-2% for 600µm coal (very large pieces)
Passive Charge technique (Masuda et al. 1994)	• Directly measures mass flow rate	• Charge measurement is influenced by original charge. • Measurement requires particles to be fully suspended. • Steady state flow is required.	• 10% for aerosol particles conveyed at 14.4 kg/h.
Particle least squares technique (Arakaki et al. 2009)	• Use of pressure sensors that are readily available. • Predictions can be made at high frequency. • Directly measures mass flow rate	• Changes in system affects accuracies • Calibration of regression model is required. • New and unproven. • Time shifts occur in measurements • Costly in terms of sensors and maintenance	• Less than 10% for particles with a size of 138.19µm conveyed at 4.32 ton/h

Coriolis force technique (Zheng & Liu 2011)	• Directly measures mass flow rate • Does not influence particle flow	• Pressure drops occur over installed area • High wear rate on tubes	• Not published
Gyroscopic Techniques (Beck et al. 1987)	• Directly measures mass flow rate	• Used for gas/liquid measurements	• Not published

Table 16: Indirect Monitoring Techniques (Concentration)

Advantages and disadvantages of monitoring techniques Indirect techniques (particle concentration techniques)			
Capacitive techniques	• Low sensor cost. • Large amount of research have been done • Measurement device has no interference with particle flow • Direct electrical signal output.	• Baseline drift may occur • Low sensitivity if small volume fractions are present. • New and unproven. • Solid build up might occur • Permittivity of conveyed material is required • Slightly dependent on flow regime. • Capacitance can be affected by outside sources	• Error within a 5% range for pulverised coal.
Microwave measurement technique (Arakaki et al. 2006; Yan 1996)	• Can accommodate particles as small as 1µm	• Highly dependent on moisture content • Decomposition of particles might occur	• Not applicable
Radiometric sensoring (Beck et al. 1987; Barratt et al. 2000)	• Measurements are made independent of distribution. • Measurements are made independent of moisture content	• Expensive • Geometrical errors might occur • Administratively inconvenient	• $\pm 2\%$ For Ilmenite powder conveyed at varies velocities.

Laser sensing (Zheng et al. 2007)	• Insensitive to chemical properties of material. • No effect on flow.	• Require a constant and known particle size • Inaccurate during high density situations • Accumulation of particles on sensor	• 1.32% for particles with a size variation from 500-1000µm (very large particle size)
Magnetic resonance techniques (King & Rollwitz 1983)		• Require non-metallic piping • High cost association • Measurements limited to relaxation time	• Plausible but no results published.
Tomography techniques (Sun et al. 2008; Abdul Rahim & Green 1998)	• Provides a visual representation of particle flow.	• Has high computational cost. • Might lead to slow calculations • High sensor costs due to large amount of sensors.	• Error of about 11.3% for sand or 3mm plastic chips (large particle size)

Table 17: Indirect Monitoring Techniques (Concentration)

Advantages and disadvantages of monitoring techniques (Indirect velocity measurements)			
Technique	Advantages	Disadvantages	Accuracies
Doppler measurement techniques (laser)	• Good spatial resolution • No calibration required	• Accuracy dependent on particle concentration • Accumulation of particles on sensor	• Not applicable to dense phase (requires an optical path)
Doppler measurement techniques (microwave)	• No limit in terms of transparency • Simple to use • Low sensor cost	• Dependent on moisture content • Poor spatial resolution	• Not documented
Ultrasonic technique (Sowerby et al. 1991)	• Simple and easy setup	• Particle impingement noise • High attenuation • Acoustic impedance mismatch	• Accurate within 8% when done with pulverised coal at varies velocities.

		• Decrease in accuracies for high velocities	
Cross correlation (Shao et al. 2000)	• Low cost • Accurate	• Response times dependent on computing power.	• 6 % error for particles with a mean size of 200µm
Electrodynamics techniques	• Low cost • Highly sensitive to particle concentration	• Charge (output signal) dependent particle properties	• No accuracies documented
Spatial filtering (general) (Xu et al. 2008)	• Requires no additional sensor	• Particle property dependent • Requires steady flow conditions	• Error ranges between 6 and 16 % for different techniques.

Appendix 2: Code explanation and layout

Code Layout

The programming done can be divided into 3 main codes:

1. Data manipulation as suggested in sparagraph 4.1 by means of Dataditor.m
2. Flow regime compensation, identification and calibration as suggested in paragraph 4.2 by means of CurveGenMaster.m
3. Calculation and evaluation of measured mass flow rate as suggested by paragraphs 4.3 to 4.5 by means of PPVmaster.m.

Explanation of code and their appropriate functions

DataEditor

- Reads all the data as supplied from the GUI and the EVM and converts it to a usable format containing only the required information such as capacitance of the applicable electrodes and their time stamp.
- Writes the edited data into a folder that's ready for use in later programs.

CurveGenMaster

The code runs through all the experiments loading the edited data and then uses the following function to execute their functions:

- Sigman.m takes the edited data and extracts the capacitive change from each electrode, refers to change due to material entering control volume.
- Appsignal.m takes the data from sigman.m and evaluates when material starts to flow within the control volume the data is then cut to only contain the applicable signal. The functions also contain the PeakRemove.m function that removes outliers in the data caused by sudden change in regime.
- ValcVFR.m calculates the theoretical volume fraction for each data set according to the total mass conveyed, solid velocity, solid density, surface area and time conveyed.
- fft_func.m conducts a frequency analysis over the specified electrodes data set and returns the magnitude of each frequency component that can be used as input for the classification of the flow regimes.
- Bandpasfilter.m then puts the frequency analysed data through a band pass filter eliminating all high and low frequency content that limited classification in terms of energy content.
- wavedecomp.m decomposes the frequency content into the specified amount of bins and then calculates the percentage of energy that each bin contains.
- FlowregIN.m then investigates and calculates the properties required for input into the SVM for separation of different flow regimes.
- optcurvefunc.m uses the capacitance change and volume fraction of each data set and finds the optimal fraction curves for the points by means of using fmincon.m function along with the constraints set by the calibration experiments.

- comb.m is then used to condense the data and properties for each nozzles set (corresponding to clusters of data) to single matrices.
- Error_Estimate.m was used as an evaluation function to iteratively determine which type of default curve would represent the fraction data best. By evaluating these parameters the user can then place a guess value for the fraction curve into optcurve.m function. Note the function was only used at an earlier stage of iteration to gain insight into what steps should be taken.
- datacomp.m was used as a function that visually illustrates the properties of the data for each individual flow regime.
- SVMmatrix.m is used to generate the matrix consisting out of the properties defined in FlowregIN.m in s form that is usable as an input into the SVM.
- SVMtest.m is then used to train and evaluate the test data in order to distinguish between either group 1 (Rope and Annular) and group 2 flow regimes. After the first separation is done the SVM is used to distinguish between rope and annular flow within group 1, the function then gives a accuracy for classification as output.
- AugerSep.m is used to distinguish between stratified and Auger fed flow by means of using separation values and the energy of each frequency band.

PVVMaster.m

The code is required to determine what the difference between the sensors estimate and the actual conveyed mass for each test.

- Flowreg.m is used to extract the capacitance data from the edit data as well as fiving the capacitance change data by means of an internal function appsignal.m.
- conCal.m is then used to determine the concentration with regard to the capacitance change according to a linear fraction to capacitance curve.
- OptcurveFraction.m is used to determine the volume fraction according to the optimal fraction curve determined from CurveGenMaster.m .
- GenFractionRope.m, GenFractionAnnular.m and GenstratFraction.m are then used to evaluate the volume fraction according to the generalised fraction curves if a general analysis is chosen.
- DetVelocity.m is used to determine the velocity according to the setting specified by the user. Note for the case of the research only the gravity method was used as explained in paragraph 4.4.
- CalcMFR.m is used to determine the mass flow rate for both the the optimal and linear approximations.
- CalcukateCAL.m is used to calculate the calibration value for each electrode pair as well as determining the error between actual and measured conveyed mass flows.

Additional information of calculations and methods of calculations are supplied in the code itself and the description given in the dissertation.